Nano Research
2019, 12(9): 2093–2125

ISSN 1998-0124 CN 11-5974/O4
https://doi.org/10.1007/s12274-019-2403-y

Review Article

Heterogeneous molecular catalysts for electrocatalytic CO_2 reduction

Nathan Corbin, Joy Zeng, Kindle Williams, and Karthish Manthiram (✉)

Department of Chemical Engineering, Massachusetts Institute of Technology, Cambridge, MA 02139, USA

Received: 18 February 2019 / **Revised:** 29 March 2019 / **Accepted:** 3 April 2019

ABSTRACT

This review provides an overview of the literature regarding heterogeneous molecular catalysts for electrochemical CO_2 reduction (ECR). Fundamental aspects of the science, including aggregation, electrochemical rate laws, and electrode-catalyst electronic coupling, are discussed to provide a solid foundation on which to design experiments and interpret results. Mechanistic aspects of ECR are presented based on electrokinetic and spectroscopic measurements as well as density functional theory (DFT) calculations. Consensus is improving for electrokinetic measurements, but the redox state of the metal center under reaction conditions and DFT reaction pathways lack agreement in the literature. Concerning the tunable aspects of the molecular catalyst, the impacts of the metal center, ligand substituents, and electrode support on the activity and selectivity toward ECR are presented with an emphasis on those studies that controlled for aggregation and minimized mass-transport limitations. Extended three-dimensional (3D) structures such as polymers, metal-organic frameworks (MOFs), and covalent-organic frameworks (COFs) are discussed as highly tunable architectures that begin to mimic the catalytic pockets of enzyme active sites. To achieve the full potential of these catalysts, design principles must emerge based on a combination of deconvoluting measurements to extract intrinsic catalyst properties and more reliable theoretical calculations to predict reaction pathways.

KEYWORDS

CO_2 reduction, electrocatalysis, porphyrins, phthalocyanines, molecular complexes, heterogeneous catalysis

1 Introduction

As atmospheric carbon-dioxide levels continue to rise and pose a greater hazard to the environment, an increasing need exists to reduce CO_2 emissions [1]. Capturing and converting CO_2 into useful fuels and chemicals represents a potentially economical way of mitigating emissions [2]. Electrochemical CO_2 reduction (ECR) is a promising route because it can be performed at mild operating conditions through the application of an appropriate voltage, can use water as a safe and abundant proton source, and can be carbon-neutral if the electricity is derived from renewable sources [3]. These attractive features have led to a large research interest in ECR over the past several decades. As a result, a wide variety of catalysts for ECR have been developed, including metals [4–6], metal-nitrogen-carbons (MNC) [7, 8], and molecular catalysts [9, 10].

This review focuses on discussing the selectivity, activity, mechanisms, and stability of heterogeneous molecular catalysts and their three-dimensional (3D), extended-structure analogs for ECR. The scope of heterogeneous molecular catalysts includes molecular catalysts physically adsorbed or grafted onto electrodes, polymerized catalysts, metal-organic frameworks (MOFs), and covalent-organic frameworks (COFs). Most of the catalysts discussed are transition-metal porphyrin or phthalocyanine derivatives (Fig. 1), since these are the predominant types studied for heterogeneous ECR in the literature. This review seeks to build upon previous reviews for heterogeneous molecular catalysts for ECR [11–15] by providing a more detailed discussion about the intrinsic activity and mechanisms for these catalysts, with an emphasis on appropriate experimental design. Comparisons to other classes of ECR catalysts are only briefly made, so interested readers are directed elsewhere to find reviews on metallic [16–19], MNC [12, 20], and homogeneous molecular catalysts [21, 22] for ECR.

Molecular catalysts are attractive for fundamental studies due to their well-defined active sites and ability to be precisely tuned, which facilitate developing clear structure–activity relationships for rational catalyst design. The metal center and ligands are often the primary means to tune the electronic structure and catalytic activity, but the heterogeneous support can also exert a significant influence. Besides subjects for fundamental studies, molecular catalysts do have some practical characteristics. Some molecular catalysts such as cobalt phthalocyanine (CoPc) and cobalt tetraphenylporphyrin (CoTPP) (Fig. 1) have high activities and selectivities for ECR, comparable to some of the best reported metallic and MNC catalysts [12, 23]. Many molecular catalysts use earth-abundant elements and maximize the utilization of metal atoms, so elemental abundance is less likely to hinder implementation on a large scale.

Molecular catalysts can be studied homogeneously in solution or heterogeneously by adsorption or grafting to an electrode. Heterogeneous catalysts are usually preferred in practical applications for several reasons. One is that diffusion of the catalyst to the electrode is eliminated, reducing mass-transport limitations. Another is that the catalyst does not have to be separated from the products afterward, reducing separation costs and increasing the lifetime of the catalyst. Since many of the molecular catalysts tested for ECR are not water soluble, they can be deposited on an electrode with a low risk of leaching into an aqueous electrolyte. Studying these molecular catalysts heterogeneously is important to evaluate the influence that the immobilization has on their activity, selectivity, and stability, which can differ noticeably from those properties when tested homogeneously. For instance, in comparison to homogeneously tested molecular catalysts, studies have found that immobilization of molecular catalysts can improve their stability, change their

Address correspondence to karthish@mit.edu

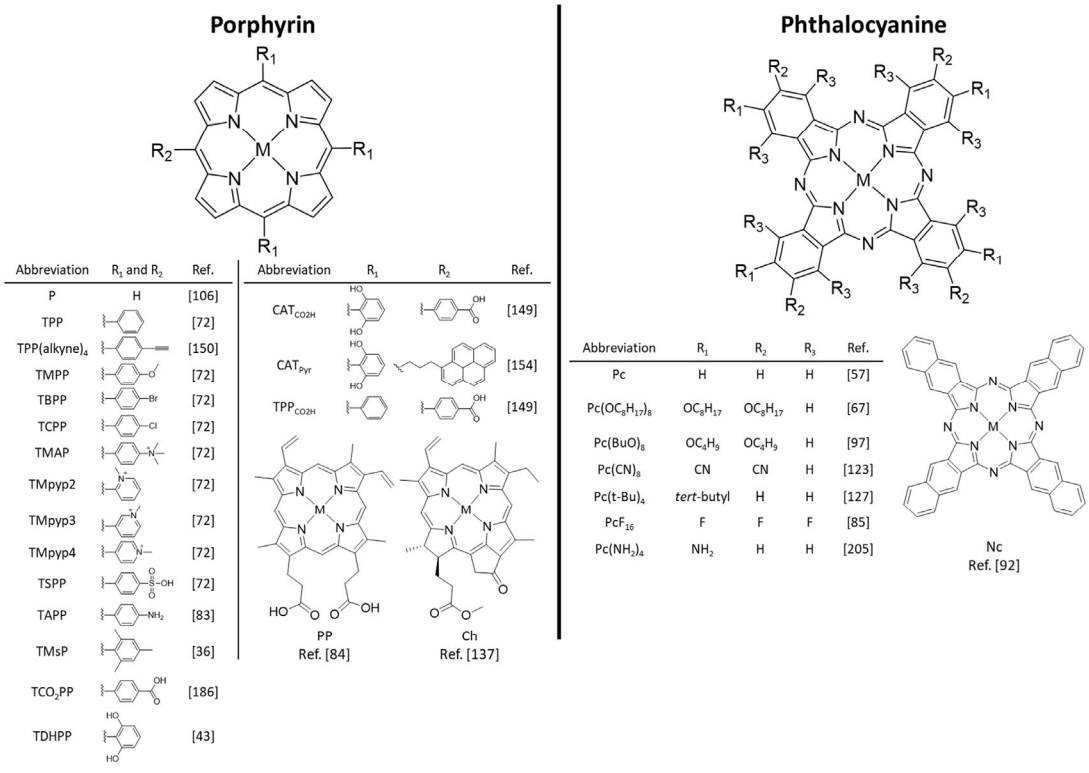

Figure 1 General chemical structures of porphyrins and phthalocyanines as well as abbreviations for the porphyrin and phthalocyanine derivatives discussed in the main text.

reaction mechanisms, and alter their relative catalytic activities to one another [24, 25]. The practical advantages of immobilization and possible differences from homogeneous catalytic performance motivate studying molecular catalysts in a heterogeneous form.

The first part of the discussion centers around the effect of the metal center on product distributions from phthalocyanines and porphyrins. The focus shifts toward measuring the intrinsic activity of catalysts without aggregation to facilitate comparisons and develop catalyst design guidelines. The mechanisms of CoPc and CoTPP are then discussed based on electrokinetic, spectroscopic, and density functional theory (DFT) studies. The effect of ligands and supports on activity and selectivity are mentioned in relation to the discussion on aggregation and intrinsic activity. Catalyst stabilities are addressed followed by an overview of 3D architectures such as polymers, MOFs, and COFs that can enable a denser presentation of electrochemically active catalytic centers and greater active site tunability. An outlook for the field, including research directions and unanswered questions, is proposed.

2 Metal center

2.1 Experimental trends

As with metallic [16, 26], MNC [27], and homogeneous molecular electrocatalysts [28], the identity of the metal center in heterogeneous molecular catalysts plays a significant role in the activity and selectivity of ECR. Many of the earlier studies on metal phthalocyanines (MPcs) for ECR noted that CoPc was the most active (i.e. largest current) for ECR, followed by NiPc [29–31]. Fe and Cu metal centers were found to be somewhat active, while other metal centers such as Mn, Cr, and Sn showed little to no activity. However, these studies found conflicting product distributions from CoPc, with one finding oxalic acid and glycolic acid via a colorimetric assay [29] and the other finding formate and methanol via gas chromatography [30]. In addition, carbon monoxide (CO) has been the primary product seen from CoPc in the majority of other studies.

One of the most detailed studies on the impact of the metal center on ECR with MPcs was performed using gas-diffusion electrodes (GDEs) in 0.5 M $KHCO_3$ [32, 33]. In terms of Faradaic efficiencies (FEs), Co, Ni, Pd, and Cd primarily made CO, while Fe and Zn also made significant amounts of CO (Fig. 2(a)). Sn and Pb were selective toward formate, with In, Zn, and Al having some activity toward formate as well. Cu and Ti were the only metals to make significant amounts of methane. However, many of the tested catalysts were more active toward the hydrogen evolution reaction (HER) than ECR, indicating that only a few metal centers are selective toward ECR. Those metal centers that were ECR-selective did show impressive FEs, with NiPc achieving an FE_{CO} of 100% and CoPc achieving an FE_{CO} of 98%.

Even if a catalyst is selective toward one product, its activity or production rate may be high or low, so evaluation of catalytic activities is also important. In the case of MPcs, CoPc and FePc showed high CO partial current densities (j_{CO}) at lower applied potentials, whereas NiPc required 450 mV more overpotential to drive similar CO current densities (Fig. 2(b)). In fact, given that all of these MPc catalysts were tested at similar total current densities, the activities of CoPc and FePc are distinctly higher due to their lower applied potentials. The combination of high activity and selectivity toward CO has made CoPc one of the most promising heterogeneous ECR catalysts, and as a result, CoPc has been the subject of many studies. These results also reveal that NiPc and FePc could be promising catalysts if the activity of NiPc could be increased or if the selectivity of FePc could be enhanced.

The effect of the metal center on ECR has also been studied in the context of porphyrins. One of the initial studies in this area examined various metal-centered tetraphenyl porphyrins (MTPPs) for ECR on GDEs at 100 mA/cm^2 total current density in 0.5 M $KHCO_3$ [34]. Similar to the phthalocyanines, CoTPP and FeTPP were found to be the most active for ECR. For CoTPP, the FE_{CO} reached 75% at −0.96 V vs. Ag/AgCl, and increased to over 97% under 20 atm of CO_2; the FE_{CO} for FeTPP also increased from 42% to 81% at 20 atm. ZnTPP and CuTPP showed some CO selectivity

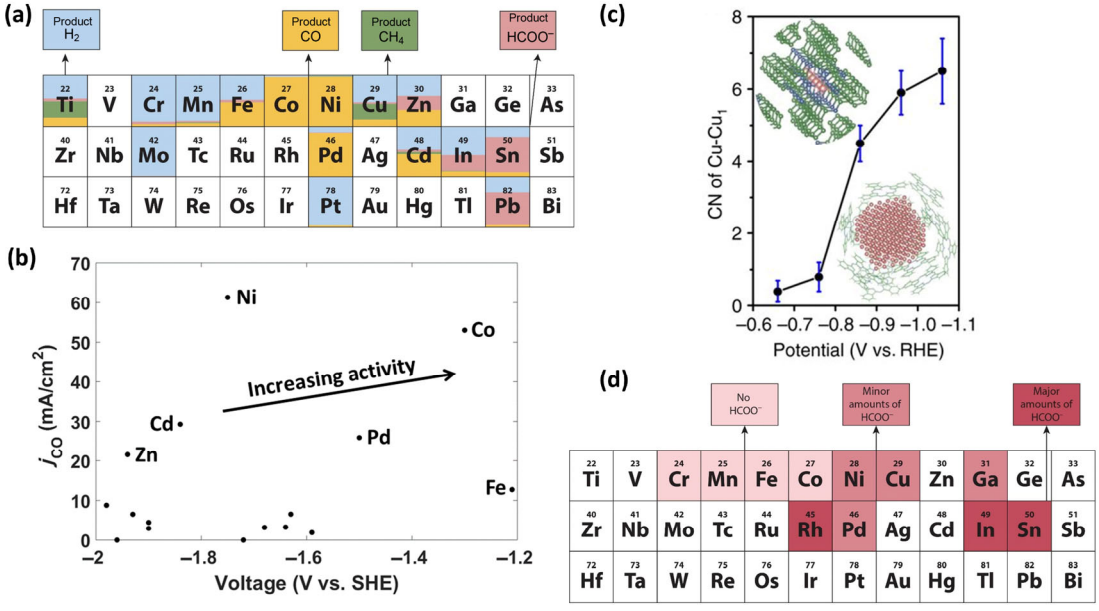

Figure 2 (a) Product distributions from ECR on MPcs loaded on GDEs [32, 33]. (b) CO partial current densities as a function of potential for MPcs loaded on GDEs. Unlabeled points correspond to less CO-active MPcs [32, 33]. (c) First-shell Cu–Cu coordination numbers (CNs) of CuPc at different potentials. The upper left inset shows the CuPc crystal structure, and the lower right inset illustrates a possible configuration of the Cu nanoclusters generated under the electrocatalytic conditions. Color key: green, C; blue, N; pink, Cu. Error bars represent the uncertainty of CN determination from EXAFS analysis. Reprinted with permission from Ref. [42], © Springer Nature 2018. (d) Relative amounts of formate produced during ECR on MPPs [35].

at 1 atm that was also enhanced at 20 atm. NiTPP was not nearly as selective as NiPc, reaching only 12% FE_{CO} at 20 atm. MnTPP, MgTPP, and H_2TPP all showed very little ECR activity at 1 and 20 atm. Additionally, formate and some hydrocarbons were detected as minor products, with CuTPP reaching a 22% FE for formate at 20 atm.

Various metal centers were studied for the production of formate using metalloprotoporphyrins (MPPs) [35]. In, Sn, and Rh were found to be the best metal centers for producing formate, with InPP reaching a 70% formate FE at −1.5 V vs. RHE in pH 6.8 phosphate buffer (Fig. 2(d)). The ability for Sn and In metal centers to produce formate was also seen for phthalocyanines [32, 33], indicating that these metal centers may inherently favor formate production. Ni, Ga, Pd, and Cu made small amounts of formate, while Cr, Mn, Co, and Fe produced little formate. These metal centers were also found to produce little to no formic acid when bound in a phthalocyanine macrocycle. CO was not measured in this study due to difficulties distinguishing it from CO_2 in the mass spectra.

Based on the above discussion, the selectivity of different metal centers appears to be qualitatively consistent across different macrocyclic rings. Nonetheless, zinc(II) 5,10,15,20-tetramesitylporphyrin (ZnTMsP) was found to break this trend by achieving a 95% FE_{CO} at −1.7 V vs. SHE in a mixed water/organic electrolyte [36]. Using *in situ* X-ray absorption spectroscopy (XAS), the Zn metal center was found to remain in the +2 oxidation state under the applied potential, suggesting that the porphyrin ring was the redox mediator. Control experiments using chemical reductants confirmed that the porphyrin ring was indeed reduced instead of the Zn metal center. The CO selectivity was much higher for this Zn porphyrin than ZnTPP, which only reached a 28% FE_{CO} in an aqueous electrolyte. These results suggest that the macrocyclic ring and/or electrolyte can have equally large effects on the activity and selectivity as the metal center and provide a starting point for designing a wider range of molecular catalytic systems for ECR.

A few other studies have examined the catalytic activity of different metal centers in phthalocyanines and related macrocyclic rings; however, these studies subjected the deposited catalysts to high pressures and temperatures, which may have degraded the molecular structure. One study examined Co, Mn, Cu, and Zn phthalocyanines on GDEs in a pH 2 sulfate buffer and found that CoPc was the most selective toward CO, while the others made small amounts of formic acid [37]. The high CO selectivity of CoPc agrees with other reports, while the formic acid production was attributed to the underlying electrode and not the MPcs. The preparation of the GDEs involved a heat treatment at 300 °C under nitrogen followed by compression at 100 MPa. MPcs are actually very thermally stable [38], with CoPc thermally decomposing at temperatures ranging from 407 to 627 °C [39, 40], so the MPcs may have retained their molecular integrity during these heat and pressure treatments. While the molecular structure of the MPcs remaining intact under these conditions is plausible, post-treatment characterization of the catalysts was not reported, so whether the molecular structures did remain intact remains unclear. Another study looked at lutetium- and lithium-phthalocyanine derivatives on GDEs in 0.5 M $KHCO_3$ [41]. The preparation of these GDEs involved a heat treatment at 350 °C and compression under 4.5 tons. FE_{CO}s up to 75% were observed, but no catalyst post-characterization was performed, leading to a similar uncertainty about the nature of the active catalyst. These results do suggest that the surrounding macrocyclic ring, particularly neighboring nitrogen atoms, can play an important role in the catalysis for redox-inactive metal centers. In these cases, the formation of MNC-type catalysts cannot be excluded, which are also known to be good ECR catalysts.

An important side reaction that can occur during electrocatalysis is the reduction and demetallation of the metal center. This phenomenon has been observed during ECR on CuPc catalysts supported on a carbon-nanotube (CNT), glassy-carbon electrode in 0.5 M $KHCO_3$ [42]. The CuPc/CNT catalyst was able to achieve a 66% methane FE at 13 mA/cm^2 at −1.48 V vs. SHE. *In-situ* X-ray absorption near edge structure (XANES) was used to quantify the change in oxidation state of the copper, where at potentials below −1.28 V vs. SHE, Cu(0) peaks started to become apparent. At the operating potential of −1.48 V vs. SHE, most of the copper was in the zero-valent state, yet minor amounts of Cu(II) remained. Additionally, this reduction process was reversible, as the copper returned to the +2 oxidation state at more positive potentials after the applied potential was removed. *In-situ* extended X-ray absorption

fine structure (EXAFS) characterization revealed that the Cu–Cu coordination number increased upon reduction, indicating the formation of ~ 2 nm copper nanoparticles under operating conditions (Fig. 2(c)). The reversibility of this process caused *ex-situ* characterizations to find an unaltered molecular structure of CuPc, whereas under operating conditions, the active catalyst was a metallic nanoparticle. HKUST-1 and [Cu(cyclam)]Cl_2 were also tested and found to exhibit the reduction of the copper to metallic dendrites, but the reduction process was irreversible. A previously tested copper-porphyrin catalyst was also found to exhibit the reversible Cu nanocluster formation, although the earlier report ascribed catalytic activity to Cu(I) [43]. Another earlier report found that crystalline CuPc could reduce CO_2 to ethylene with a 25% FE at −1.40 V vs. SHE [44], but given the reductive potential, formation of metallic copper nanoclusters likely occurred. Even if the metal center is stable at ambient conditions, reductive polarization can cause the metal center to reduce and aggregate in a metallic state.

Metal-center exchange is another phenomenon that can occur under reductive polarization. For FePc co-deposited with metal (Fe, Co, Ni) oxide nanoclusters, Co and Ni exchanged with the iron metal center, producing CoPc/FeO_x and NiPc/FeO_x catalysts, as confirmed by post-experiment *ex-situ* XANES [45]. The exact reason for why the metal centers exchanged is not known, but the authors hypothesized that the slightly larger atomic radii of Co and Ni may be more stable than Fe in the phthalocyanine ring in the zero-valent state. The exchange could also be favored by the more negative redox potential of Fe compared to Co and Ni, which could favor Fe being in the oxide cluster. Nonetheless, the data reveal that metal centers can exchange under ECR operating conditions.

These results suggest that many earlier studies on metal centers for ECR may be convoluted by the formation of metallic nanoparticles under reductive polarization. While more studies are needed to fully elucidate the reasons and mechanisms of demetallation and metal exchange, a couple of hypotheses to explain these phenomena are (i) the small geometric distortion of the phthalocyanine ring upon introduction of different metal centers [46] and (ii) the propensity of a metal center to demetallate being directly related to its redox potential such that those metal atoms that have more positive redox potentials may be more susceptible to forming metallic nanoclusters under reductive conditions [47]. While only Cu has been specifically implicated in forming nanoparticles under ECR reaction conditions, other metal centers which have product distributions similar to those in their pure metallic forms may also need to be investigated *in situ* such as Sn, In, and Pb (formate-producing) [48–50] as well as Pd (CO-producing) [51, 52].

2.2 Theoretical insights

Several attempts have been made to understand the underlying reasons for the trends observed with varying metal centers. The d-electronic structure of the metal center has been invoked, as these electrons likely play an important role in binding reactants, products, and intermediates. However, determining the electronic structure of many gas-phase MPcs has been difficult due to the sensitivity to the model used to interpret experimental results [53]. In addition, DFT can have difficulties describing the degenerate and open-shell electronic structures many MPcs possess [53]. Using a range-separated hybrid DFT functional, one study showed that good agreement with experiment can be obtained for CoPc, although the electronic structure was sensitive to the amount of exact (Hartree-Fock) exchange and at what ranges it was incorporated [54]. A robust theoretical examination of the electronic structures of first row transition metal phthalocyanines (Mn, Fe, Co, Ni, Cu, Zn) was performed using complete active space self-consistent field (CASSCF) calculations [53]. CASSCF calculations are more robust than DFT for dealing with degenerate or open-shell states because these calculations optimize over all valence electronic states [55]. By detailed comparison with available experimental data, the authors were able to resolve disputes related to the electronic structures of CoPc and especially FePc and MnPc (Fig. 3). In particular, the ground state of FePc is nearly degenerate and is probably highly influenced by its environment. These studies highlight that prudence must be taken when choosing an appropriate theoretical methodology to produce accurate and reliable results for metal phthalocyanines.

The occupation of the metal center's d_{z^2} orbital has been invoked to explain selectivity toward CO [33]. Based on a qualitative linear-combination-of-atomic-orbitals approach, the authors deduced that Fe, Co, and Ni would have doubly occupied d_{z^2} orbitals after reduction. These electrons would repulse the lone pair of electrons on CO, leading to the desorption and detection of CO as the major product. This explanation appears to be in qualitative agreement with the CASSCF electronic structures for FePc and CoPc, although NiPc already has two d_{z^2} electrons before any reduction.

In spite of the potential pitfalls associated with using DFT to calculate electronic structures of MPcs, several studies have used this technique to calculate the thermodynamics of reaction intermediates for ECR to help explain the catalytic behavior of different metal centers. Using the Perdew–Burke–Ernzerhof (PBE) functional with explicit water and hydronium ions to incorporate electric-field effects, one study found that among Mn, Fe, Co, Ni, and Cu metal centers, CoPc possessed the most favorable *CO binding energy [56]. The authors verified that the strongest binding energies were with the Co center and not surrounding N or C atoms. This computational prediction agrees qualitatively with experimental data where CoPc was found to have the highest j_{CO} and FE_{CO}. For NiPc, the FEs_{CO} were not nearly as high as those in Refs. [32, 33], although the higher overpotential required to produce CO is in agreement with the previous studies and DFT calculations. The FE_{CO} for FePc agrees with the one from Refs. [32, 33], and interestingly, it dropped off quickly as the applied potential became more reductive. However, some inconsistencies exist between the DFT calculations and experimental results. MnPc was predicted to be more active than FePc for CO production, yet experimentally, it produced much less CO. As will be discussed in more detail later, the rate-determining step (RDS) predicted for CoPc from this study was *CO desorption, which does not agree with most experimental mechanistic evidence [57]. Furthermore, hydronium was used rather than potassium as an interfacial cation, although in the experimental electrolyte (0.5 M $KHCO_3$, pH 7.2), the concentration of hydronium was at least six orders of magnitude lower than potassium. As can be explained by the Sabatier principle, CoPc was found to be the most

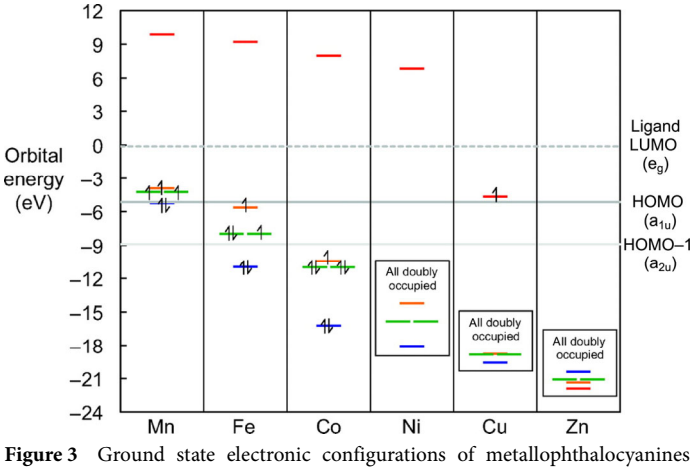

Figure 3 Ground state electronic configurations of metallophthalocyanines (MPc; M = Mn–Zn) at CASSCF/cc-pVDZ level in an active space comprising a complete set of metal-centered orbitals: d_{xy} (blue), d_{xz}/d_{yz} (green), d_{z^2} (orange), and $d_{x^2-y^2}$ (red) (reprinted with permission from Ref. [53], © Canadian Science Publishing 2016).

ideal catalyst of the group because it binds *COOH and *CO neither too strongly nor too weakly.

The selectivity of MPc polymeric monolayers was also investigated with DFT using the PBE functional with DFT-D2 dispersion correction and including implicit solvent [58]. The thermodynamic calculations found that all investigated MPcs could suppress HER and potentially form formic acid (Cr, Mn, Zn), formaldehyde (Co), and methane (Sc, Ti, V, Fe). The methane-producing catalysts were found to require the largest overpotentials, while polymeric MnPc was found to have the lowest overpotential. While experimental ECR data for polymeric monolayer MPcs are not available, comparison with molecular MPc catalysts reveals large discrepancies with experimental and other theoretical data. For example, CoPc is selective toward CO, and MnPc is mainly H_2 selective, requiring large overpotentials. Moreover, CO was not found to be the major product from any of the catalysts studied. While polymerizing MPcs into a monolayer could dramatically affect activity and selectivity, these results may warrant suspicion in the context of other available experimental and computational data.

Regarding porphyrins, a DFT study using the PBE functional with implicit solvation elucidated the most likely reaction intermediates for various metal centers to help explain the selectivity toward CO or formate [59]. *COOH intermediates were anticipated to lead to CO formation, while metal hydride, phlorin, and *OCHO intermediates were anticipated to lead to formate. For metals in Groups 10–14, the binding of *COOH, *H, and *OCHO intermediates to the metal center was found to be unfavorable, while the formation of a phlorin, $[M(PH)]^n$, was determined to be the preferred intermediate (Fig. 4). The attack of CO_2 on the reduced form of this intermediate, $[M(PH)]^{n-1}$, would lead to the production of formate. These results qualitatively agree with experimental data on metal protoporphyrins in that In and Sn are able to produce formate, while Ni, Pd, Cu, and Ga produce smaller amounts of formate [35]. For Group 8 and 9 metals (Co, Fe, Rh), the binding of *COOH and *H to the metal center was found to be favorable in addition to *H binding to the porphyrin ring; *OCHO binding to the metal was still unfavorable. The ability to bind *COOH helped explain why Co and Fe are able to produce CO; however, RhPP was found to be primarily formate-active [35]. Fe was also predicted to have competitive formate-producing pathways, yet no formate was observed experimentally when using FePP. The authors noted the aforementioned difficulty of using DFT to describe the complexes with multiple spin states; the greatest difficulties would be expected for the Co, Fe, and Rh metal centers, which could explain why the computational results could not fully rationalize experimental results. For these complexes, differences on the order of 0.4 eV were noticed when the functional was changed. In the case of Rh, another possible explanation could be the presence of an axial ligand that blocks the Rh metal site, enabling only the formate-producing phlorin pathway to proceed. The HER pathway via a chlorin intermediate was not calculated but was postulated to explain some of the low experimental activities toward formate. Oddly, the phlorin-preferred route for Zn porphyrin contrasts with experimental evidence of CO production from a modified Zn porphyrin as mentioned earlier [36]. This study was able to provide some insight into the most probable intermediates on metal porphyrins for ECR through a careful and nuanced discussion that accounted for the expected errors on the results. The discussion on DFT results for mechanistic understanding of ECR on Co-based molecular catalysts is continued in Section 4.

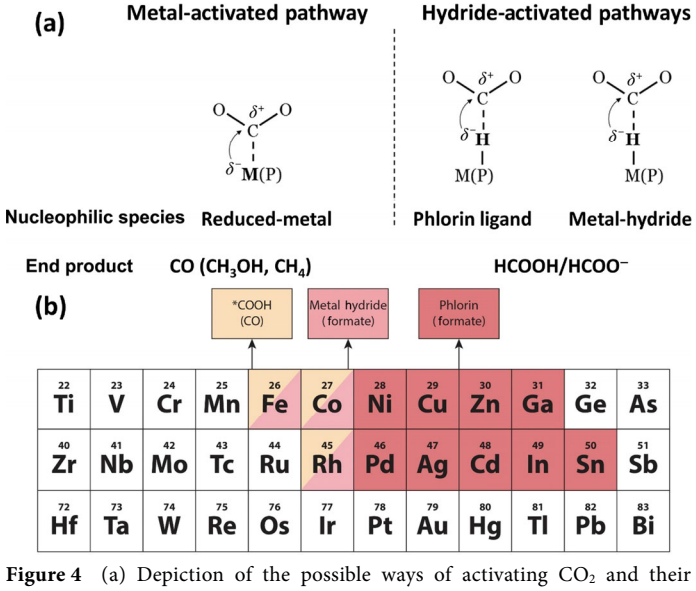

Figure 4 (a) Depiction of the possible ways of activating CO_2 and their consequences on the selectivity of ECR (reprinted with permission from Ref. [59], © American Chemical Society 2018). (b) Predicted favored ECR reaction intermediates on metalloporphyrins.

Based on this discussion, ECR studies using different metal centers have identified several candidates for CO and formate production. Among them, cobalt and iron are active and selective toward CO; consequently, cobalt- and iron-based molecular catalysts have been the subject of a majority of studies for CO production. For formate generation, indium appears to be an active metal center.

3 Extrinsic and intrinsic activity

To further optimize and understand activity and selectivity, ligand and support modifications have been made to these molecular catalysts. To accurately study the effect of ligands and supports as well as provide a reliable benchmark for catalytic activity, the intrinsic activity of the complex needs to be measured [60]. This section focuses on discussing the measurement of intrinsic vs. extrinsic activities, with a focus on how catalyst aggregation can lead to underestimation of intrinsic activities. The discussion will provide a foundation for discussing reaction mechanisms and the effects of ligands and supports.

The intrinsic activity of a catalyst is usually quantified by a turnover frequency (TOF), which is defined as the amount of product produced per active site per second with units of inverse time. The TOF for a given product is usually calculated as the molar production rate of the desired product (mol/(time·area)) divided by the catalyst loading (mol/area). This calculation leads to a lower bound for the TOF because it assumes that all catalyst molecules are active, which may not be true if aggregation is present. The number of electrochemically active sites can also be determined by integrating catalyst redox peaks from cyclic voltammetry [61]. However, uncertainty in the integration can exist if a baseline is not easily drawn; moreover, catalysts that are electrically accessible may not be accessible to reactants. As detailed in the next paragraph, calculating the lower TOF bound using the amount of deposited catalyst is preferred. A measure of the extrinsic activity is the current density toward a given product. This measure is a combination of the intrinsic activity of the catalyst, how many active sites are accessible, and any mass-transport limitations. To rationally design catalysts, these underlying factors contributing to the current density must be measured independently. Here, the discussion focuses on the intrinsic activity and aggregation.

One of the challenges of measuring intrinsic activities of heterogeneous molecular catalysts is catalyst aggregation that blocks or severely hinders mass transport to active sites. For planar, conjugated molecules such as phthalocyanines and porphyrins, favorable π–π stacking interactions exist that can readily lead to aggregation during catalyst deposition [62, 63]. Under aggregation-free conditions, the current density should be directly proportional to the amount of catalyst loaded; this observation has been used in the

oxygen reduction literature to determine when kinetic measurements can be accurately made [64]. Another equivalent metric to assess whether aggregation is convoluting TOF measurements is to test the catalyst at progressively lower loadings until the TOF remains constant (Fig. 5(d)). In these measurements, the total amount of catalyst loaded should be used to calculate TOF, providing a lower bound. As aggregation is minimized, the TOF calculated in this manner approaches the true TOF. The impact of catalyst loading on measured TOF is significant; for CoPc, decreasing the loading from 10^{-7} to 10^{-11} mol/cm^2 resulted in a roughly 1,000-fold increase in apparent TOF_{CO} [57]. The intrinsic TOF_{CO} for CoPc is around 100 s^{-1} at −1.13 V vs. SHE, which is significantly larger than TOF_{CO} values reported for the same and similar catalysts from other studies (Fig. 5(a)). A study on CoTPP supported on CNTs also found that decreasing the catalyst loading resulted in higher TOF_{CO} values [25].

As expected, reducing the catalyst loading leads to lower total current densities (Fig. 5(b)), although at high loadings the current density becomes saturated, as all available surface area is probably covered by catalyst. This decrease may seem suboptimal from a performance perspective; however, if the catalyst cost is high compared to electrolyzer-area cost, then the most economical solution may be to reduce the catalyst loading at the expense of a larger electrolyzer. Based on the data from Ref. [57], decreasing the catalyst loading 99% (from ~ 10^{-7} to 10^{-9} mol/cm^2) only resulted in a 29% decrease in CO current density.

Because HER can compete with ECR in aqueous electrolytes, measuring the intrinsic selectivity of a catalyst is also important. At high loadings, the FE_{CO} for CoPc reached 96% at −1.13 V vs. SHE, whereas at the lowest loading, the FE_{CO} dropped to ~ 80% (Fig. 5(c)) [57]. A probable reason for the drop in FE_{CO} at low loadings was the increase in background HER current from the carbon paper electrode as a fraction of the total current. Therefore, the most reflective measurement of intrinsic selectivity may be at high loadings where background current is minimized. One potential confounding factor here could be differences between interactions with the support and interactions with other CoPc molecules in the crystal aggregate, which could cause the intrinsic catalytic properties to vary.

A key aspect of reducing aggregation is to deposit molecular catalysts from solvents in which they are soluble. Many unsubstituted phthalocyanines have limited or no solubility in common solvents [65]. For example, N,N-dimethylformamide (DMF) and tetrahydrofuran can dissolve CoPc very well, but acetone and dichloromethane cannot. The solubility is also impacted by the metal center; for example, CuPc is not soluble in DMF, while CoPc is. The effect on TOF is significant; for instance, using isopropyl alcohol to disperse CoPc instead of DMF resulted in a reduction in TOF_{CO} by a factor of 30 at a loading of 10^{-9} mol/cm^2 at −1.13 V vs. SHE [57]. Using a completely dissolved catalyst solution minimizes aggregation before the deposition, although aggregation may not be completely eliminated since dimers can still exist in solution [66]. Nevertheless, aggregation can still occur after deposition as the solvent evaporates. Using the deposition procedure from Ref. [57], a loading of 3.09×10^{-9} mol/cm^2 CoPc would result from using a saturated CoPc/DMF solution. However, dilution by two more orders of magnitude was needed to see stabilized $TOFs_{CO}$ unaffected by aggregation.

Increasing the solubility of molecular catalysts through appropriate ligands is another strategy that can reduce aggregation. Substituting bulky alkoxy groups onto CoPc led to a higher TOF_{CO} than that for unsubstituted CoPc [67]. The higher measured intrinsic activity was ascribed to the bulky alkoxy groups increasing the solubility of the complex and inhibiting the formation of aggregates. Both the solvent and functionalization of the molecular catalyst contribute to the degree of aggregation upon deposition from solution.

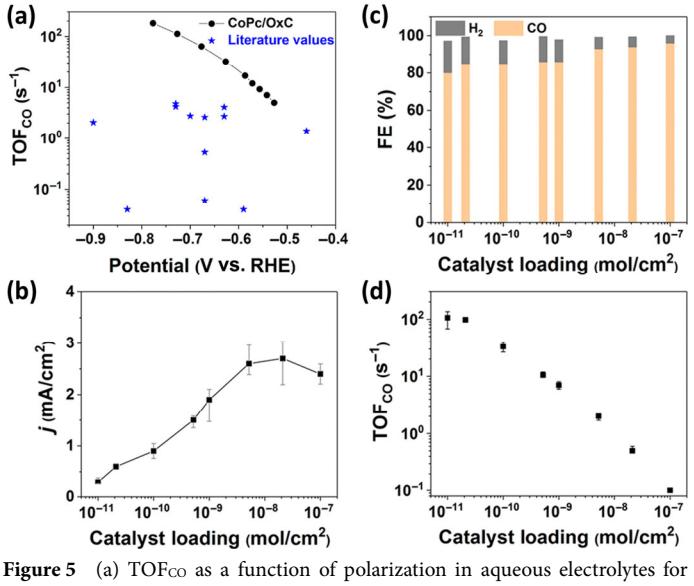

Figure 5 (a) TOF_{CO} as a function of polarization in aqueous electrolytes for reported immobilized molecular catalysts (Table S3 in Ref. [57]) and CoPc/OxC at a low loading of 1×10^{-11} mol/cm^2. (b) Overall current densities, (c) FEs for CO and H_2 production, and (d) TOF_{CO} as a function of CoPc loading. All experiments performed at −1.13 V vs. SHE in 0.1 M $NaHCO_3$. Reprinted with permission from Ref. [57], © American Chemical Society 2018.

4 Mechanism of CO_2 reduction

Understanding the mechanism of ECR on CoPc and related catalysts requires the accurate measurement of the intrinsic activity, as the purpose of mechanistic analysis is to probe what is occurring at the active site. Electrokinetic measurements, *in-situ* spectroscopic data, and DFT calculations have all been used to gain insights into how CO_2 is reduced to CO on CoPc and related catalysts.

4.1 Electrokinetic measurements

Electrokinetic measurements interrogate the RDS of an electrochemical reaction by varying controlled variables such as potential, CO_2 partial pressure, electrolyte composition, and isotopic composition and measuring the kinetic response to these modifications. The electrokinetic results can be combined into a rate law that describes the reaction rate. Typically, the Butler-Volmer equation is used as a starting point for constructing this rate law, although additional features such as coverage effects [68] and higher order electrochemical kinetics (e.g. Marcus-Hush-Chidsey) [69, 70] may be added. In its expanded form, which enables a clearer picture of the governing parameters, the Butler-Volmer equation for an irreversible reduction reaction is [71]

$$i = -nFk_0\left(\prod_{i=1}^{N} C_i^{\nu_i}\right) e^{-\frac{(1-\alpha)F}{RT}E} \quad (1)$$

where i is the cathodic current density (reductive currents by convention have a negative sign), n is the number of electrons transferred in the reaction, F is Faraday's constant (96,485 C/mol), k_0 is a potential-independent kinetic prefactor, C_i is the concentration of species i, ν_i is the reaction order of species i, N is the total number of species in the rate law, α is the transfer coefficient, R is the ideal gas constant (8.314 J/(mol·K)), T is the absolute temperature, and E is the applied potential. Note that E is the applied potential versus a given reference electrode; if the reference electrode changes, so does E, but k_0 also changes to compensate, since the reaction rate should not be different if the reference electrode changes. The reverse reaction can be safely ignored if $\eta > 118$ mV at 25 °C, where η is the overpotential $E - E_{eq}$ [71]. This condition is almost always met for ECR studies.

The potential dependence for an electrochemical reaction is often

reported as a Tafel slope which is related to the transfer coefficient for a reduction reaction by

$$m_{\text{Tafel}} = \left[\frac{\partial(-\text{E})}{\partial \log(-i)}\right]_{C_i, T} = \frac{2.303RT}{(1-\alpha)F} \quad (2)$$

The Tafel slope, often reported in units of mV per decade of current (mV/dec), relates how sensitive the current is to the applied potential. It can also be used to infer information about the RDS and the steps before it, assuming all other steps are in quasi-equilibrium. Under this formulation, the Tafel slope can also be written as [71]

$$m_{\text{Tafel}} = \frac{2.303RT}{F[n+(1-\beta)q]} = \frac{59\ \text{mV/dec}}{n+(1-\beta)q} (T = 25\ ^\circ\text{C}) \quad (3)$$

Here, n is the number of electron transfers before the RDS, β is the symmetry factor (usually assumed to be 0.5), and q is the number of electrons transferred during the RDS. This result implies that the Tafel slope can provide two important pieces of mechanistic information: (i) whether the RDS involves an electron transfer or not and (ii) how many electron transfers occur before the RDS. Of course, to interpret the Tafel slope in such a way, the Tafel plot should be linear, the interfacial concentrations of species should be roughly constant (i.e. no mass transport limitations), and the coverages of adsorbed species should be low, as high coverages can distort Tafel slopes [68]. When mass transport starts to become limiting at high current densities, the Tafel plot becomes curved and its slope increases, so Tafel analyses need to be conducted at low current densities.

Only a handful of studies have reported Tafel slopes for heterogeneous cobalt-based macrocycles (Table 1). Some variance exists in the Tafel slopes reported, with several being around 120 mV/dec and others being well above this value. A Tafel slope of ~ 120 mV/dec implies that the first electron transfer is rate limiting (n = 0, q = 1 in Eq. (3)). Tafel slopes well above 120 mV/dec typically imply that mass transport is becoming a limiting factor. A plot of catalyst loading vs. Tafel slope for CoPc revealed that lower loadings were necessary to observe kinetically interpretable Tafel slopes, suggesting that transport of CO_2 through CoPc aggregates was limiting the reaction rate [57]. However, a similar loading study was performed on CoTPP and found that the Tafel slope was essentially independent of loading [72]. The independence of Tafel slope on loading can be confirmed using data from Ref. [73], which found a similar Tafel slope of 112 mV/dec for CoPc at a loading five orders of magnitude higher than that in Ref. [57]. A plausible explanation here is that the highest current densities are observed at the highest catalyst loadings, so high catalyst loadings are more likely to have CO_2 mass transport limitations through the electrolyte to the catalyst surface or within the catalyst aggregates.

Order-dependence studies are also important to gain information about which species are involved in the RDS as well as to probe if a large fraction of catalysts are occupied by intermediates or poisoned. In CO_2-containing electrolytes, especially with bicarbonate anions, a confounding factor is the dependence of pH on the pressure of CO_2 and bicarbonate concentration

$$CO_2(\text{aq}) + H_2O \rightleftharpoons H^+(\text{aq}) + HCO_3^-(\text{aq}) \quad (4)$$

As one changes the CO_2 pressure or bicarbonate concentration, the pH of the bulk electrolyte will change according to equilibrium described in Eq. (4). Although the equilibrium potentials for ECR reactions depend on the pH, order-dependencies should be measured at the same potential relative to a fixed reference electrode; this constancy is needed to keep the electrochemical potential of the electrons in the electrode constant [74, 75]. If both protons and CO_2, for instance, are in the RDS, then the order-dependence data may appear convoluted because the partial pressure of CO_2 changes the pH according to Eq. (4). However, given the low concentration of protons in many bulk electrolytes used for CO_2 reduction (pH > 6, $[H^+] < 10^{-6}$ M), the diffusion limited current density for protons will be orders of magnitude less than that for CO_2 ($[CO_2]_{\text{aq}} \sim 33$ mM at 25 °C, 1 bar CO_2 [76]). From this reasoning, H^+ is unlikely to be the primary proton donor for ECR in near-neutral electrolytes, so it is also unlikely to be in the electrochemical rate law. Even if the rate were first-order in $[H^+]$, measuring at a constant potential on the RHE scale will not always perfectly account for the $[H^+]$ dependence due to the presence of α in the Butler-Volmer equation (Section S1 in the Electronic Supplementary Material (ESM)). In practice, the equilibrium potential (and therefore appropriate value of RHE) is truly dependent on the pH at the electrochemical interface, which will be more basic than the bulk electrolyte due to the production of OH^- at the interface [77, 78] and is difficult to measure [79]. Based on these arguments, measuring order-dependencies at constant absolute potential is recommended when using near-neutral electrolytes for ECR.

When varying the composition of the electrolyte, an important parameter to keep in mind is the ionic strength of the solution. The ionic strength is proportional to the strength of the electric field in a solution. The ionic strength impacts solution properties by changing the activities of ions [80]. For gases such as CO_2, the salting out effect causes their solubility to decrease when the ionic strength increases [81]. To keep the solubility of CO_2 constant and ion activity coefficients the same during bicarbonate order-dependence tests, the ionic strength of the solution can be kept constant by adding a salt of the same cation with an innocent anion such as perchlorate [74]. However, since the chemical potential of CO_2 is determined by its pressure in the gas phase and not the identity of the electrolyte in typical experiments, keeping the ionic strength constant is not completely necessary, and normalizing data by the CO_2 solubility is not recommended. Secondary effects due to the changing activity coefficients of ions may be present in these experiments, however.

Whether water acts as a proton donor in the RDS cannot be probed by varying its concentration in aqueous electrolytes since it is the solvent. Kinetic isotope effect (KIE) experiments can be used to determine if any proton donor is involved in the RDS [82]. The underlying principle is that deuterons are transferred more slowly than protons due to their heavier mass. If the reaction rate is slowed in the presence of D_2O, then the RDS involves a proton transfer. At this time, KIE experiments are lacking for heterogeneous, ECR molecular catalysts.

Most CO_2 order dependencies on heterogeneous cobalt-based molecular catalysts have yielded an order of one, which intuitively agrees with the requirement of one CO_2 molecule to make CO or formate (Table 1). An order of 0.6 was obtained for CoPc in 1 M $NaHCO_3$ in contrast to an order of 1.0 in 0.1 M $NaHCO_3$ [57]. A few studies found no pH dependence on the CO current density [72, 83, 84], although in another study the selectivity was reported to be higher at higher pH [85], possibly indicating a suppression of the competing HER. However, this study used nitrate anions to maintain ionic strength, which themselves could have been electrochemically reduced [86]. A concentration-dependent bicarbonate order was found on CoPc at a constant potential versus RHE, where the reaction transitioned from a near zeroth-order dependence at lower $[HCO_3^-]$ to a superlinear dependence at higher $[HCO_3^-]$ [57]. This order-dependence shift should in fact have been done at constant potential vs. SHE (or another absolute reference), as was done for CoTPP and CoPP [72, 84], and is the subject of ongoing work in our lab.

The general conclusions from electrokinetic measurements are that for CoPc, CoTPP, and their derivatives, the RDS involves the first electron transfer, one molecule of CO_2, and likely does not depend on pH or bicarbonate. More work needs to be done to elucidate whether proton donation from water occurs during the

Table 1 Summary of electrokinetic measurements made on immobilized molecular catalysts for ECR. Abbreviation for electrodes and chemicals can be found after Table S1 in the ESM

Catalyst	Electrode	Catalyst loading (mol/cm^2)	Electrolyte	Tafel slope (mV/dec)	Order dependencies	Ref.
CoPc	OxCP, Nafion	1×10^{-11}	0.1 M $NaHCO_3$, 1 M $NaHCO_3$	120	CO_2 1 (0.1 M $NaHCO_3$) 0.6 (1 M $NaHCO_3$) HCO_3^- [b] 0.17 ($[HCO_3^-] < 0.3$ M) 1.40 ($[HCO_3^-] > 0.3$ M)	[57]
CoPc	GC	1.75×10^{-8}	0.5 M Na_2SO_4 + 0.1 M $NaHCO_3$	110	CO_2: 1	[30]
CoPc	CFP, Nafion	1.75×10^{-6}	0.5 M $NaHCO_3$	112		[73]
$CoPcF_{16}$	Carbon cloth	1.3×10^{-8}	0.5 M $NaHCO_3$	278	Higher FE_{CO} at higher pH Nitrate to maintain ionic strength	[85]
CoPc				275		
CoPc	ZIS-180, CP, Nafion	5.4×10^{-8}	0.5 M $KHCO_3$	169		[141]
	ZIS-200, CP, Nafion			141		
CoPc	tsGQwire, CP		0.5 M [Bmim]TF_2N ACN	105		[140]
CoPc	CCG, CFP	1.4×10^{-9} [a]	0.1 M $KHCO_3$	170		[67]
$CoPc(OC_8H_{17})_8$		9.0×10^{-10} [a]		172		
CoTPP	CNT, GC	1.7×10^{-7}	0.5 M $KHCO_3$	255		[25]
CoTAPP	Carbon fabric	2.70 to 3.05×10^{-7}	0.5 M $KHCO_3$	270	No pH dependence	[83]
CoTPP	OxCP, Nafion	8×10^{-10}	0.5 M $NaHCO_3$	119	CO_2: 0.99 HCO_3^-: −0.04	[72]
CoTMAP				124	CO_2: 1.10 HCO_3^-: −0.03	
CoTMPP				116	CO_2: 0.90 HCO_3^-: 0.01	
CoTCPP				114	CO_2: 1.27 HCO_3^-: 0.01	
CoTBPP				114	CO_2: 1.04 HCO_3^-: 0.01	
CoTMpyp2				106	CO_2: 1.11 HCO_3^-: 0.08	
CoTMpyp3				126	CO_2: 0.99 HCO_3^-: −0.15	
CoTMpyp4				103	CO_2: 0.80 HCO_3^-: 0.04	
CoTPP	Diazonium reduction graft, CFP	6.9×10^{-10}	0.5 M $KHCO_3$	477		[178]
CoTPP	CFP	8×10^{-8}	0.5 M $KHCO_3$	222		
CoPP	Ox-CNT graft, CFP, Nafion	1.1×10^{-8}	0.5 M $NaHCO_3$	127	CO_2: 1.08 HCO_3^-: 0.03	[84]
FeTMAP	rLCGO, GC	1.3×10^{-9} [a]	0.1 M KCl pH 4.2	96		[138]
GCC-Re(phen)Co_3Cl	Pyrazine graft, GC	2.1×10^{-9}	0.1 M NBu_4PF_6 ACN	150		[24]

[a]Calculated by integrating redox peaks from a CV.
[b]Measured at constant potential vs. RHE.

RDS from KIE experiments. Additionally, some of the Tafel-slope and bicarbonate-order measurements should be redone in light of better experimental design.

4.2 Voltammetry studies

Many of the early mechanistic studies on CoPc and CoTPP relied on cyclic voltammetry (CV) to gain insights into the nature of the active species for CO_2 reduction. An important factor related to the redox transitions of a molecular complex is the degree of electronic coupling with the electrode [87]. In solution as a homogeneous catalyst, no direct electronic coupling exists between the catalyst and electrode. In this environment, the catalyst can undergo electron transfers with or without coupled ion transfer, and the redox state of the metal center can change correspondingly. However, for a molecular catalyst whose electronic levels are strongly coupled with the electrode's, only ion-coupled redox events are allowed to take place with the molecular catalyst. Additionally, the metal center's redox state remains constant.

These phenomena have been observed for molecular catalysts that were pyrazine-linked to glassy carbon, where the conjugated pyrazine linkage provided strong electronic coupling with the electrode (Fig. 6(a)) [87]. For example, a ruthenium catalyst, $[Ru^{II}(dmbpy)_2(phen)]^{2+}$, that undergoes a one-electron transfer in solution did not undergo the same transition when linked to the electrode (Fig. 6(b)). Similarly, $[Rh^{III}Cp^*(phen)Cl]^+$ undergoes a concerted two-electron reduction coupled with chloride dissociation in solution, whereas when coupled to a glassy carbon electrode, it only underwent a one-electron reduction with chloride dissociation.

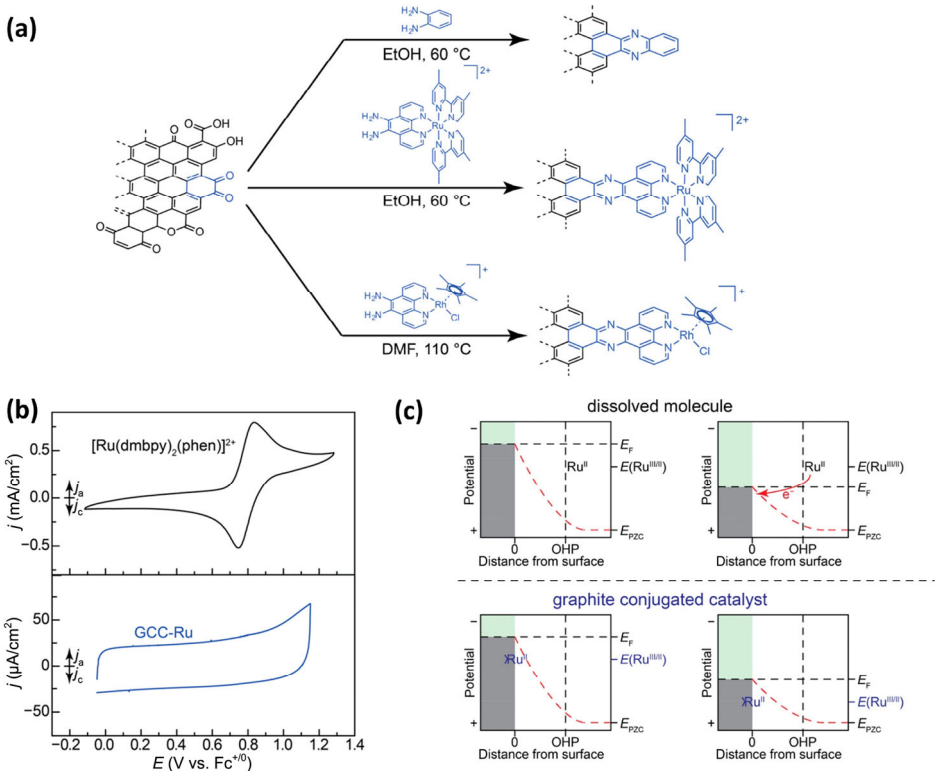

Figure 6 (a) Synthetic schematic for graphite-conjugated catalysts (GCCs) via reaction of an o-phenylenediamine group on the catalyst with an o-quinone group on glassy carbon to form a pyrazine linkage. (b) CVs of homogeneous $[Ru^{II}(dmbpy)_2(phen)]^{2+}$ (5 mM, 100 mV/s) (top) and GCC-Ru (10 mV/s) (bottom) recorded in 0.1 M NBu_4PF_6, ACN electrolyte showing the suppression of the $Ru^{III/II}$ couple upon electronic coupling to the electrode. (c) Putative interfacial free energy diagrams for unmodified electrodes with dissolved Ru^{II} molecules (top) and electrodes modified with conjugated Ru^{II} surface sites (bottom). The diagram denotes the Fermi level of the electrode, E_F, and the redox potential of the molecule, $E(Ru^{III/II})$, upon varying the applied potential (left to right). The electrostatic potential across the electrochemical double layer is indicated by the red dotted line. Varying E_F does not impact $E(Ru^{III/II})$ for the dissolved molecule, leading to classical outer-sphere ET (top) at the interface. For GCCs (bottom), varying E_F simultaneously shifts the energy levels of donor/acceptor states in the conjugated molecule by a similar magnitude, and the driving force for electron transfer remains unchanged. Reprinted with permission from Ref. [87], © American Chemical Society 2017.

In-situ XANES confirmed that the oxidation state of Rh remained the same during the redox event while conjugated to the electrode. For redox transitions that do occur for both the homogeneous and pyrazine-linked catalysts, the redox transition for the linked catalyst is likely to be shifted positively (negatively) due to greater stabilization of excess negative (positive) charge by the delocalized electronic structure of the electrode. In the case of phenazine, the two-electron, two-proton reduction occurs ~ 200 mV more positive when pyrazine-linked than dissolved in solution, illustrating that inference of redox processes on electrode-coupled molecular catalysts from homogeneous redox potentials may not be accurate.

A conceptual model was developed to help explain the difference between redox events for homogeneous and electrode-conjugated molecular catalysts (Fig. 6(c)) [87]. When a potential is applied to an electrode, charge builds up on it, raising its Fermi level and creating a strong electric field in the vicinity of the surface as a result. The driving force for electron transfer is this electric field, which creates an energy difference between an electron at the electrode surface and an electron in a molecule at the outer Helmholtz plane (OHP). For a homogeneous molecular catalyst, changing the electrode potential changes the driving force for electron transfer. However, if the molecular catalyst is electronically coupled to the electrode, the metallic nature of the electrode's electronic structure ensures all bulk and surface atoms have the same Fermi energy and that the separation between occupied and unoccupied levels of surface atoms remains unchanged [88]. Therefore, changing the electrode potential does not create a driving force for electron transfer between the electrode and metal center. Electron-only redox events are no longer possible in this scenario.

However, a potential driving force does still exist between the conjugated molecular catalyst and the electrolyte. Electron transfer can still occur with ions and molecules at the OHP, which helps explain why only ion-coupled electron transfers were seen for electrode-coupled molecular catalysts [87]. In the case of chloride binding, an electron is removed from the chloride as it binds. This electron is not localized on the metal center but rather delocalized over the entire electrode. Here, the entire electrode is acting as the metal center's redox non-innocent ligand. This electron delocalization inhibits the metal's redox center from changing, which is in agreement with the experimental XANES data for the Rh complex.

The electronic coupling to an electrode has been shown to mechanistically change ECR for the same molecular catalyst. $Re(phen)(CO)_3Cl$ was found to have a Tafel slope of 150 mV/dec when conjugated to a glassy carbon surface via pyrazine linkage but a Tafel slope of 60 mV/dec when dissolved in solution [24]. The Tafel slopes suggested a change from a rate-limiting chemical step preceded by an electron transfer as a homogeneous catalyst to a rate-limiting electron-transfer when coupled to the electrode. Based on the previous discussion, this electron transfer should be coupled to the binding of a species from the electrolyte, likely CO_2. This result underscores that the mechanism of a homogeneous molecular catalyst may not be the same once it is immobilized onto an electrode.

The above discussion helps to contextualize many of the early mechanistic studies on heterogeneous molecular catalysts for ECR in terms of observed redox transitions from cyclic voltammetry. Nonetheless, an important question that remains unanswered is the degree of electronic coupling with the electrode for physisorbed and some chemically grafted molecular catalysts. For the common

case of physisorbed molecular complexes, whether the π–π interactions with the electrode are strong enough to prevent the metal center from changing oxidation state is currently unclear. Even with this uncertainty in mind, we would like to discuss some of the voltammetry studies that used redox events to infer information about the state of the molecular catalyst during ECR.

For CoPc, many of the early CV studies implicated a doubly reduced anionic hydride species, $[CoPcH]^-$, as inferred from a Nernstian shift of one of the redox peaks with respect to pH [89–92]. The location of the hydride was initially thought to be on the metal center [89, 93], but a later study argued that the protonation would occur on a peripheral nitrogen on the Pc ring, since the metal hydride would lead to the production of formate, which is not the primary product from CoPc [90]. Another series of studies using pyridine-coordinated CoPc argued for a singly reduced species based on the reduction potential of CoPc in pyridine but did not conduct CV experiments to verify this claim [94, 95].

A similar CV study was conducted for CoTPP axially coordinated to pyridine (CoTPP(py)) to elucidate the nature of the active species [96]. Under a N_2 atmosphere, CoTPP(py) was reduced to a hydride, which could be oxidized during the positive potential sweep. However, in the presence of CO_2, the oxidation peak disappeared, suggesting CO_2 reacted with the CoTPP(py)-hydride species. All of these CV results were performed on heterogenized catalysts and suggested the presence of both electron-only and electron-ion transfers. Based on these data, a possible conclusion regarding electronic coupling to the electrode is that physisorption and pyridine coordination do not achieve the level of coupling that a direct conjugated chemical bond provides (e.g. pyrazine linkages).

A challenge associated with using CV is that the redox peaks may not be reflective of the true catalytic centers. In the same study on CoTPP, roughly 100 times more catalyst was initially deposited than required for a monolayer [96]. Upon washing, the adsorbed layers were removed, leaving a monolayer of CoTPP axially coordinated to pyridines covalently grafted to the electrode. Removing the stacked molecules led to higher CO current densities and FEs. A CV comparing rinsed vs. unrinsed electrodes showed a significant decrease in the anodic peak characteristic of hydride oxidation (Fig. 7(a)). This result reveals that aggregation can create or greatly enhance redox features in CVs, confounding mechanistic insights into the true active sites for a reaction.

4.3 Spectroscopy

Spectroscopic techniques including *in-situ* UV–vis, IR, and XAS have been used to probe the oxidation state of immobilized molecular catalysts as well as to look for reaction intermediates during ECR. These techniques have the potential to provide more insight into the oxidation state of the metal center under operating conditions. *In-situ* potential-step chronoamperospectroscopy (PSCAS) has been used to identify the nature of redox events on CoPc and related derivatives using UV–vis absorbance. Due to the opaqueness of the basal-plane pyrolytic graphite (BPG) electrode, the experiments had to be done homogeneously in pyridine. For CoPc under N_2, the first reduction was found to occur on the metal center while the second occurred on the Pc ring [91]. Under a CO_2 atmosphere, the ligand reduction was absent, indicating a steady state presence of the singly reduced species, Co(I)Pc. Similar homogeneous *in-situ* UV–vis studies were conducted for $CoPc(BuO)_8$ [97] and $CuPc(CN)_8$ [61]; the effect of different substituents is discussed in Section 5. The drawback of these studies is that the redox transitions of the homogeneous catalyst may not correspond to the ones occurring once it is immobilized.

The problems associated with an opaque electrode can be overcome by using transparent fluorine-doped tin oxide (FTO). *In-situ* UV–vis experiments on MOFs and COFs consisting of cobalt porphyrin units found that under ECR potentials, the Co(II) center is reduced to Co(I) [83, 98]. This reduction process did not occur quickly but spanned several hundred millivolts, indicating sluggish charge transfer throughout the frameworks. The electronic coupling of the cobalt centers to the electrode may have been weaker in these materials because (i) they were physically deposited onto the carbon materials and (ii) their electrical conductivities are much smaller than the carbon paper (~ 10^{-6} S/cm for COF-366-Co [83], ~ 10 S/cm for Toray TGP-H carbon paper [99]). Similar *in-situ* UV–vis experiments on an $Al_2(OH)_2$TCCP-Co MOF [98] and an electropolymerized cobalt porphyrin [100] also show features corresponding to the decline of Co(II) species and the increase of Co(I) species at ECR potentials. Many of the cobalt centers in these materials may not be representative of cobalt centers in molecular catalysts adsorbed directly on an electrode, so the observation of Co(I) under ECR potentials may not generalize.

An *in-situ* UV–vis study on molecular F_{16}-CoPc deposited on FTO did reveal a change in cobalt oxidation state upon applying a potential of −0.92 V vs. SHE [85]. However, the high loading of catalyst (1.3×10^{-8} mol/cm^2) likely resulted in aggregation, so whether the UV–vis was probing true active sites or catalytically inactive F_{16}-CoPc remains unclear. This result does suggest some transferability of the UV–vis studies on extended molecular structures to single molecules.

In-situ XAS is another tool that can directly probe the oxidation state of metal centers under reductive polarization. For porphyrin COFs, XAS found a change in oxidation state from Co(II) to Co(I) upon reductive polarization, consistent with the *in-situ* UV–vis results from the same study [83]. However, another *in-situ* XAS study on CoPc adsorbed on carbon fiber paper (CFP) found no oxidation state change under ECR potentials (Fig. 8(a)) [56]. The CoPc loading in this study was high at 3.15×10^{-6} mol/cm^2 so that most of the CoPc molecules were likely not catalytically active. The XAS measurements may have probed the catalytically inactive metal centers rather than the active ones. The discrepancy between these measurements could also be related to an effect of the different ligands on the oxidation state of the cobalt center. In any case, a consensus on the oxidation

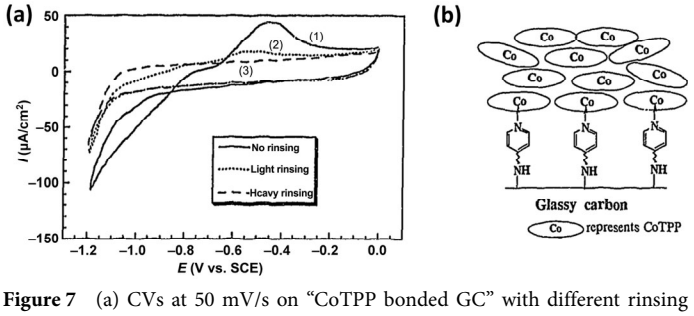

Figure 7 (a) CVs at 50 mV/s on "CoTPP bonded GC" with different rinsing treatments by DCM. The bridging compound is 4-aminoethylpyridine: (1) without rinsing, (2) light rinsing, and (3) heaving rinsing. (b) Schematic diagram of "CoTPP bonded GC" with stacked CoTPP. Reprinted with permission from Ref. [96], © Elsevier B.V. 1997.

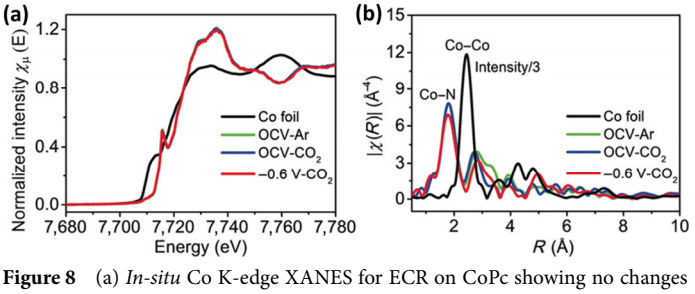

Figure 8 (a) *In-situ* Co K-edge XANES for ECR on CoPc showing no changes under reductive polarization. (b) Fourier-transformed EXAFS spectra in the R-space of CoPc during ECR. Reprinted with permission from Ref. [56], © Wiley-VCH 2018.

state of physisorbed and axially-coordinated cobalt molecular catalysts under ECR conditions is lacking. Ideally, *in-situ* measurements should be conducted on aggregation-free samples, such as those of the pyrazine-linked Rh catalyst from Ref. [87]. A challenge here is that at low enough loadings where aggregation is absent, the amount of active sites may not be enough to generate enough signal for accurate measurements.

To probe reaction intermediates, an *in-situ* Fourier-transform infrared spectroscopy (FTIR) study was conducted for CoPc adsorbed on edge-plane pyrolytic graphite (EPG) [93]. In combination with CV, the authors observed that the first reduction of CoPc was not associated with a proton due to unchanged phosphate bands, while the second reduction did involve a proton transfer due to increased HPO_4^{2-} as $H_2PO_4^-$ deprotonated. The authors proposed that CO_2 reacted with the metal hydride to give an insertion product but then later ascribed a product band at 1,294 cm^{-1} to a Co-CO_2^- intermediate, which has no reduced proton. CO was not detected, probably because it desorbed rapidly from the surface. Carbonate was ruled out as a reactant since its concentration reached a constant plateau once all of the CO_2 near the surface was consumed. While a consistent reaction intermediate could not be proposed, this study did provide useful mechanistic details about ECR on adsorbed CoPc.

In-situ spectroscopies have led to important mechanistic insights for Mn-based molecular catalysts for ECR. A loading-dependent product distribution was noticed for immobilized Mn_{pyr} catalysts (Fig. 9), where the TOF and total production of formate increased as the loading was decreased [101]. Conversely, the TOF_{CO} remained relatively constant across all loadings tested. *In-situ* UV–vis and attenuated total reflectance (ATR) IR were used to identify catalytically active species that correlated with the observed product distributions. At high loadings, zero-valent Mn-Mn species were observed which favored the formation of CO [101, 102]. At low loadings, more manganese hydride (Mn-H) species were present which could lead to the generation for formate. The application of *in-situ* spectroscopies in these studies reveals they can provide important mechanistic insights by identifying intermediate species.

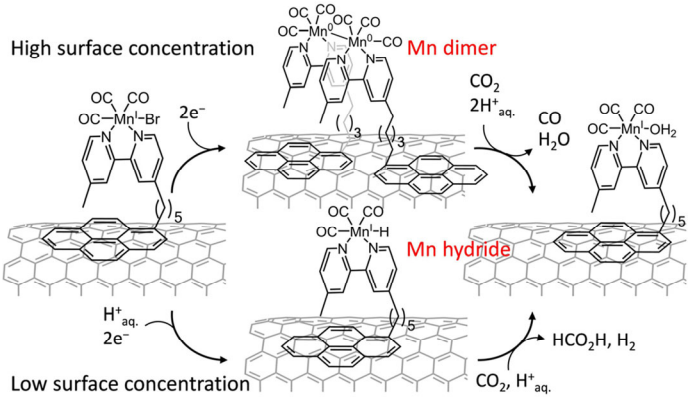

Figure 9 Schematic representation of [MnBr(bpy$_{pyr}$)(CO)$_3$] (Mn$_{pyr}$) immobilized on a CNT sidewall, concentration-dependent dimerization or Mn–H formation, and intermediate-dependent reduction of CO_2 to CO or HCOOH (reprinted with permission from Ref. [101], © American Chemical Society 2017).

4.4 DFT

DFT calculations have also provided insights into the detailed mechanism of ECR on heterogenized molecular catalysts. One of the key aspects of the mechanism on these catalysts is the competition between HER and ECR. A computational study has highlighted a key difference in the HER mechanism on single-site metal-N_4 catalysts compared to metals [103]. On metals, HER can proceed through a favorable Volmer-Tafel pathway, with hydrogen atoms binding to hollow sites (Fig. 10). On single-site metal-N_4 catalysts, hydrogen atoms must bind in an on-top mode, which is a more unfavorable configuration compared to a hollow-site on a metal surface. Additionally, a Volmer-Tafel mechanism on the porphyrin-like active sites was predicted to be unfavorable due to a high energy penalty of binding a second hydrogen atom near the metal center (Fig. 10(b)); HER was concluded to proceed via a Volmer-Heyrovsky pathway instead, which is considered more difficult than the Volmer-Tafel mechanism. If CO_2 can bind more strongly than hydrogen to the metal center, CO_2 can displace adsorbed hydrogen and further prevent HER from occurring. On metals, hydrogen and CO_2 bind to different types of sites, so CO_2 cannot physically occupy all hydrogen binding sites (although adsorbed CO can weaken the hydrogen binding energy [104]). These factors demonstrate the promise molecular catalysts hold for selective ECR and help explain why some molecular catalysts such as CoPc can have very high FE_{CO}. The DFT calculations in Ref. [103] used a Bayesian error estimation functional with van der Waals corrections (BEEF-vdW) to provide error estimates on the calculated binding energies [105]. Many of the binding energy standard deviations are larger than 100 meV, providing further support that DFT calculations on molecular catalysts must be done with care.

Several computational studies have examined the reaction intermediates and proposed mechanisms for CO_2 reduction on a model compound, cobalt porphine (CoP). These studies have modeled the catalyst in solution with an implicit solvation model, although explicit solvation was included for certain calculations. While this type of model does not capture possible effects of being immobilized on an electrode, it can still provide insights into the intermediates through which the reaction likely passes as well as probable rate-determining steps. Validation with experimental data is essential for assessing the reliability of the mechanistic predictions from these calculations.

One set of studies used both DFT calculations and *ab-initio* molecular dynamics (AIMD) simulations to probe the stability of reaction intermediates and propose a mechanism for CO_2 reduction on CoP. The free energies of chemical steps were computed, and redox potentials of the catalyst and intermediates were calculated to gauge the barriers to electron transfer. The proposed mechanism

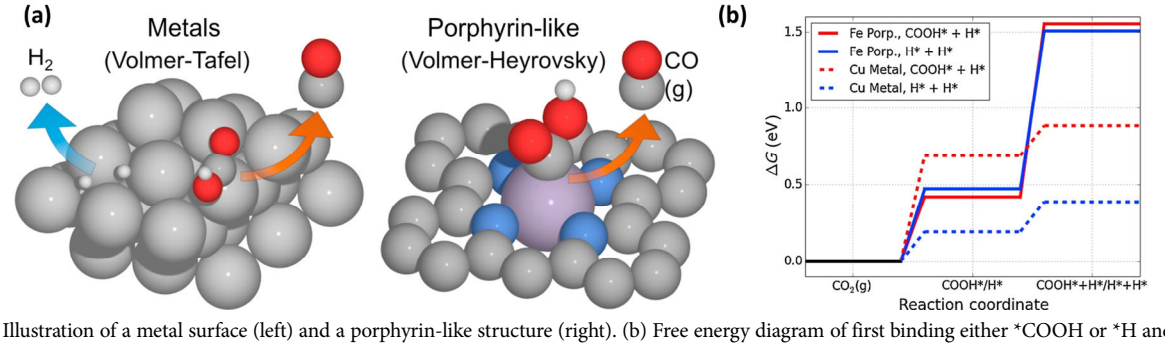

Figure 10 (a) Illustration of a metal surface (left) and a porphyrin-like structure (right). (b) Free energy diagram of first binding either *COOH or *H and the binding a second *H at a nearby site for the relevant Fe porphyrin-like structure and the Cu metal. Reprinted with permission from Ref. [103], © Elsevier B.V. 2017.

involved the reduction of CoP to $[CoP]^-$ followed by CO_2 attacking this nucleophile to form a $[CoP\text{-}COO]^-$ adduct (Fig. 11(a)). This adduct was predicted to be reduced again to form $[CoP\text{-}COO]^{2-}$. AIMD calculations estimated the pKa of this intermediate to be ~ 9, so in a neutral electrolyte, protonation to form $[CoP\text{-}COOH]^-$ would be favorable. The dissociation of OH^- was thermodynamically downhill, and the last step involved CO desorption. Since all of the chemical steps were thermodynamically favorable, the authors surmised that the RDS involved an electron transfer. The difficulties of DFT for describing open-shell electronic configurations for transition metal complexes such as CoP were noted, with B3LYP and PBE providing noticeably different binding energies for open-shell intermediates. In addition, the redox potentials used to determine where electron transfers would be likely to occur did not agree well with experiments. The importance of explicit solvation for anionic intermediates was shown by a significant shortening of the Co-C bond length in the $[CoP\text{-}COO]^-$ intermediate upon inclusion of explicit water molecules.

A study using the computational hydrogen electrode (CHE) proposed a mechanism for ECR on CoP to help rationalize experimental data for a cobalt protoporphyrin (Fig. 11(b)) [106]. CO_2 was found to only bind to the singly reduced $[CoP]^-$ complex with explicit solvation included, which agrees with the anionic intermediate found in Refs. [107, 108]. Mulliken charge analysis showed a partial electron donation from the cobalt center to the adsorbed CO_2, which was in a bent configuration with a similar angle to the CO_2 radical anion. The HOMO-2 of CoP, having a majority Co-3d character, was found to interact most strongly with the adsorbed CO_2. The HOMO-2 was also found to represent the d_{z^2} orbital of the cobalt center for CoPc using CASSCF calculations [53]. After the formation of $[CoP\text{-}COO]^-$, a proton transfer to make $[CoP\text{-}COOH]$ was predicted to occur; the concerted proton-electron transfer (CPET) to make this intermediate directly from CoP was argued to have too high of an activation barrier at room temperature. A CPET to make [CoP-CO] and dissociate water was the next step, after which CO could overcome a reasonable barrier (0.26 eV) to desorb. The importance of carefully considering explicit solvation and multiple spin states was also emphasized in this study.

The pH of the electrolyte can influence whether a CPET or sequential proton-electron transfer (SPET) occurs. The pKas of carboxylate intermediates were calculated to understand when the transition between CPET and SPET may occur for ECR on cobalt porphine [109]. Under conditions when the reorganization energies for the electron transfer (ET) and CPET steps are similar, the pH of the electrolyte relative to the pKa of the carboxylate group determines whether CPET or SPET occurs (Fig. 11(c)). When the pH < pKa, protonation of the carboxylate group is favorable, so the CPET pathway occurs. Conversely, when the pH > pKa, protonation is not favored, so a SPET pathway occurs. For CoP, the pKa of [CoP-COOH] was estimated to be ~ 3.5, and the pKa for $[CoP\text{-}COOH]^-$ was estimated to be 8.6; the latter value is in agreement with the value of ~ 9 found from AIMD simulations [108]. These results highlight that the $[CoP\text{-}COOH]^-$ intermediate may be favored under certain conditions, which was also noted in Refs. [107, 108] but not in Ref. [106]. The predicted mechanism change at pH ~ 3.5 was supported by experimental ECR data on a cobalt protoporphyrin, where the CO selectivity was much higher at pH 3 than pH 1, suggesting that CO_2 activation could occur in the presence of water [110]. Under basic conditions (pH > 8.6), a doubly reduced $[CoP\text{-}COO]^{2-}$ would be anticipated to form. This study revealed that the ECR mechanisms on porphyrin-based molecular catalysts are likely to be dependent on the pH of the electrolyte.

The SPET pathways discussed above always assumed an electron transfer before a proton transfer. One computational study instead suggested that the first step in the ECR mechanism on CoP is the protonation of a pyrrolic nitrogen on the ring, followed by two electron transfers (Fig. 11(d)) [111]. Interestingly, the second reduction from [CoPH] to $[CoPH]^-$ was predicted to be 300 mV more favorable

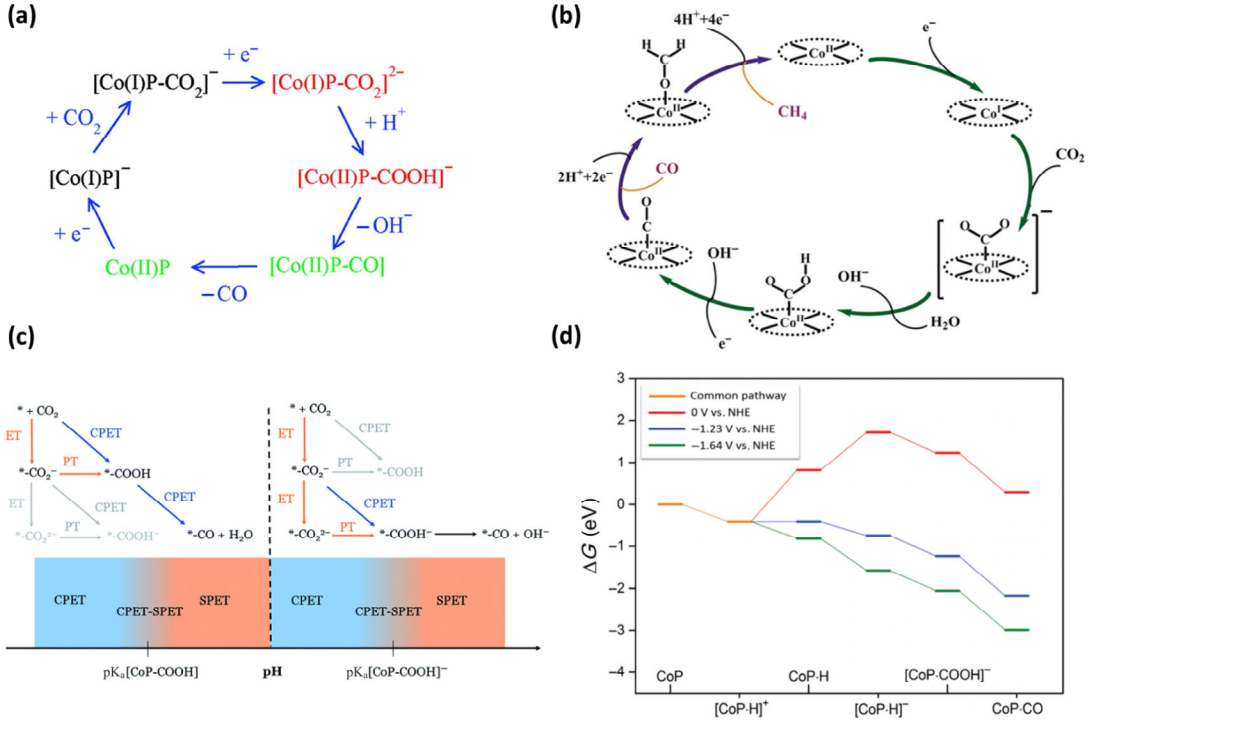

Figure 11 (a) Proposed ECR mechanism on CoP with electron addition deduced from hybrid DFT plus dielectric continuum redox potential calculations via an anionic carboxylate intermediate. Red denotes key intermediates; green species should undergo fast reactions (reprinted with permission from Ref. [108], © American Chemical Society 2010). (b) Predicted DFT mechanism for ECR on CoP via a neutral carboxylate intermediate (reprinted with permission from Ref. [106], © American Chemical Society 2016). (c) Schematic depiction of the dominant mechanism (SPET or CPET) of the formation of the carboxylate intermediate on CoP depending on the pH (reprinted with permission from Ref. [109], © Royal Society of Chemistry 2017). (d) Free energy diagram for ECR on CoP going through a protonated intermediate first before electron transfer (reprinted with permission from Ref. [111], © Royal Society of Chemistry 2017).

than the first reduction from $[CoPH]^+$ to [CoPH], which is opposite of what is predicted for CoP in Ref. [59]. CO_2 then attacks $[CoPH]^-$ to make $[CoP\text{-}COOH]^-$, followed by a proton transfer to release water and form [CoP-CO]. The free energy for CO desorption was found to be 0.25 eV, in good agreement with Ref. [106]. The formation of $[CoP\text{-}COOH]^-$ from CO_2 attacking $[CoPH]^-$ seems difficult given the amount of nuclear motion that would need to happen; the hydrogen atom would need to bind with an oxygen in concert with carbon binding with the metal. The formation of a C–H bond in this situation appears to have a simpler kinetic path, but the direct production of formate ($HCOO^-_{aq}$) from CO_2 attacking a $[CoPH]^-$ intermediate was not explicitly considered [111]. This step was found to have a free energy difference of –1.03 eV in a different study [59], suggesting that formate should be a major product, which is not observed experimentally under acidic conditions [110]. Moreover, the proposed RDS does not involve CO_2, which disagrees with experimental data showing increased ECR selectivities under 10 atm of CO_2 [110]. Some of the disagreement among computational studies could be related to the use of B3LYP in Ref. [111] and PBE in Refs. [59, 106, 109], where significant energy differences between the two functionals have been noted for CoP [107, 108]. B3LYP is also known to have difficulties predicting Co–C bond strengths in tetrapyrroles [112]. Notably, this mechanism was proposed only to work in acidic environments (CoP pKa ~ 6.9), further supporting the notion that electrolyte pH influences the mechanism. Despite some inconsistencies with experimental data and other computational studies, the importance of considering alternative pathways such as protonation followed by electron transfer was highlighted.

Further reduction of CO_2 to products beyond CO and formate has received some theoretical and experimental attention. Cobalt protoporphyrin IX was found to make more methane than CO at pH 1 at –1.38 V vs. SHE, albeit with an FE < 1% [110]. Methane production was less selective at pH 3 even though CO production become much more selective, indicating the importance of proton transfers in the mechanism of CH_4 formation. CO, formaldehyde, and later methanol were all found to be reduced to CH_4, suggesting, but not proving, that they are reaction intermediates. An early study with CoPc and $CoPc(COOH)_4$ found that CO could be reduced to formaldehyde and small amounts of methanol in sulfuric acid [113]. In both studies, formic acid could not be reduced further, signaling that it is an end product. Computational studies have also examined pathways to reduce CO_2 beyond CO. In agreement with experiments, one study found that formaldehyde and methanol are plausible intermediates in the formation of methane, with a predicted potential-limiting step being the CPET of $[CoP\text{-}OCH_3]$ to make [CoP-O] and CH_4 [106]. Another study found that methanol would be favorable to make, although under a reductive enough potential, it could be reduced to methane [111]. The authors emphasized that protonation of the pyrrolic nitrogen atoms would not happen with the presence of carbon intermediates at the metal center, so the protons would need to come from the solution, resulting in a pH dependence for methane formation.

All of the above studies assumed the molecular catalyst is in a homogeneous medium rather than supported on an electrode. An initial look into the effect of a carbon support was performed computationally for ECR on a ruthenium porphine on graphene [114]. Using periodic DFT with PBE and implicit solvation, the authors calculated free energy pathways for ECR, showing that reduction of tightly bound *CO is the potential limiting step toward methane. With the presence of a graphene support, the limiting potential for [RuP-CO] conversion to [RuP-CHO] was found to decrease substantially by 0.77 V. While the graphene did not donate or accept electrons from RuP, it did cause a major redistribution of electrons within RuP, where the Ru center became more positively charged, and the pyrrolic nitrogen atoms become slightly more negatively charged (Fig. 12). Such large differences in intermediate

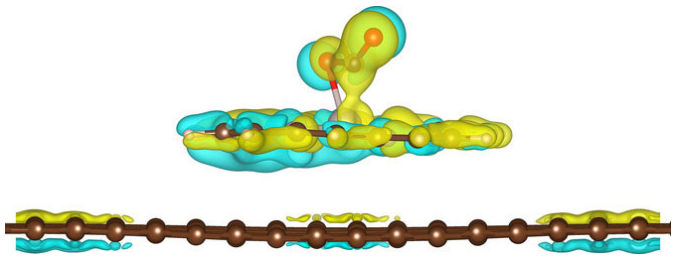

Figure 12 Visualization of the charge density difference for RuP on graphene. Yellow areas represent charge accumulation, and blue areas represent charge depletion (reprinted with permission from Ref. [114], © Wiley-VCH 2018).

energies and charge distributions upon supporting RuP on graphene indicate that neglecting support effects may not be justified when studying reaction mechanisms for supported molecular catalysts for ECR.

4.5 Cation effects

Although the alkali cation of an electrolyte is not formally included in the overall reactions for CO_2 reduction, alkali cations have been demonstrated to impact the rate and selectivity of ECR on metallic catalysts [115–123], with larger alkali cations, such as Cs^+, facilitating ECR better than smaller ones, such as Li^+. Theoretical calculations have suggested that these cations are able to stabilize intermediates on the surface via ion-dipole interactions [124, 125]. For homogeneous molecular ECR, the addition of magnesium ions was found to enhance CO production on iron porphyrins [126].

A few studies have dealt with the effect of cations related to heterogeneous ECR. An experimental study using CoPP found that larger cations favored HER over ECR, contrary to the majority of studies on metallic catalysts [127]. The authors explained the observations by hypothesizing that the smaller cations have larger hydration radii which can impede proton diffusion. Additionally, smaller cations were thought to have stronger ion–dipole interactions with ECR intermediates to help stabilize them. Quantification of the CO production rate would help to further understand the impact of cations on these catalysts.

A DFT study on cobalt porphine helped elucidate why including cations in theoretical modeling of ECR on molecular catalysts is important [128]. Their methodology used a continuum solvation model except for an explicit hydration shell around a sodium ion, $[Na(H_2O)_5]^+$. The computational model was verified by comparison to experimental data for CoTPP and CoPc; good agreement between geometries was obtained, and redox potentials were in error of –0.18 V on average. The study focused on an intermediate step proposed in Ref. [106] of converting $[CoP\text{-}CO_2]^-$ to $[CoP\text{-}COOH]^-$, though this intermediate was not proposed as a part of the mechanism from Ref. [106]. An additional source of disagreement is at the pH examined in this study (pH = 3), the results from Ref. [109] predict that a [CoP-COOH] intermediate would form. The authors rejected the protonation mechanism [111] by calculating that H^+ would preferentially bind to the metal center rather than a nitrogen atom on $[CoP]^-$, leading them to look for a different mechanism. By looking at thermodynamic barriers, the CPET step with proton donation from solvated water was found to be the most reasonable, occurring at –0.74 V vs. RHE. The solvation reduced the energy by 0.6 V, independent of the type of catalyst. Notably, this study suggests the solvation of OH^- is what leads to lower thermodynamic barriers, although they do emphasize that specific interactions between the cation and adsorbates could also occur. The predicted limiting potential of –0.74 V vs. RHE agreed somewhat well with the experimental value of –0.6 V from Ref. [110], which included an error correction of +0.18 V from the error in experimental redox potentials. These results reveal the significant effect that including a cation in the computational model has and underscore that further

computational studies of the ECR mechanism will be needed to develop consensus.

5 Ligand effects

A primary attractive feature of molecular catalysts is the ability to precisely chemically modify the catalyst, in principle allowing for a fine control over binding energies of intermediates and optimization of reaction rates and selectivities. The effects of substituents on molecular electrocatalysts have been studied for homogeneous ECR [129–131] and other reactions [132–136]. In the context of heterogeneous ECR with molecular catalysts, surprisingly only a few studies have systematically examined the effect of peripheral substituents on catalytic activity. Catalyst aggregation can confound accurate comparisons of intrinsic activity as a result of substituents affecting catalyst solubility and aggregation propensity, as discussed earlier. Due to the wide variability between testing conditions, only those reports which directly compared different substituents will be discussed.

A couple of early studies looked at CoPc modified with an electron-donating (butoxy) and an electron-withdrawing (cyano) substituent. Compared to CoPc, $CoPc(BuO)_8$ had a higher TOF_{CO} (306 s^{-1} vs. 15 s^{-1}) and CO/H_2 ratio (4.34 vs. 0.69) at −1.1 V vs. SHE in pH phosphate buffer [97]. $CoPc(CN)_8$ was tested at a less reductive voltage (−0.95 V vs. SHE) but also had a higher CO/H_2 ratio (5.5) than CoPc with a TOF_{CO} of 4.2 s^{-1} [61]. The enhanced activity of $CoPc(BuO)_8$ was attributed to a higher electron density around the metal center, facilitating CO_2 binding and electron transfer, while the higher activity and selectivity of $CoPc(CN)_8$ was attributed to a higher fraction of electroactive metal centers. The mechanism of $CoPc(CN)_8$ was suggested to be different than CoPc or $CoPc(BuO)_8$, whereby the RDS was no longer the second reduction of the catalyst (Fig. 13(c)). Another study comparing CoPc with $CoPc(CN)_8$ supported on CNTs at a high loading (1.8×10^{-8} mol/cm^2) found increased activity and selectivity for the cyano derivative (Figs. 13(a) and 13(b)) [137]. The better performance of $CoPc(CN)_8$ was attributed to a more facile reduction from Co(II) to Co(I). Another study also found electron-withdrawing groups to improve the CO current density and FE for F_{16}-CoPc compared to CoPc [85]. The observations that the addition of both electron-donating and electron-withdrawing substituents to CoPc resulted in higher activity and selectivity toward ECR appears conflicting. The presence of aggregation, noted as a potential source for the enhanced performance in Ref. [61], may be confounding these results, inhibiting a clear understanding of substituent effects.

Other studies have also tested the effects of different ligands. CuPc was modified by adding chlorine functionalities, resulting in higher CO but lower CH_4 current densities and FEs than CuPc [33]. An optimal number of chlorine atoms appeared to exist since the CO and CH_4 FEs initially increased then decreased upon adding more chlorine atoms. However, as previously discussed, CuPc is known to demetallate at ECR potentials, so these results should be interpreted cautiously. Another study looked at CoPc and CoNc immobilized by axial pyridine coordination and found that CoPc had higher CO current densities and FEs than CoNc [92], possibly indicating that increased conjugation in the macrocyclic ligand worsened performance. Aggregation may also be playing a role here since CoNc would be anticipated to have stronger π–π interactions than CoPc.

A more comprehensive study on substituent effects was performed for heterogeneous cobalt-porphyrin derivatives at low loadings to minimize aggregation [72]. To quantify the electron-withdrawing character of different functional groups, DFT calculations were performed to find the Mulliken charge, χ_H, on a test hydrogen atom attached to the functional group (Fig. 14(a)). To validate χ_H as a reliable descriptor, comparisons to established Hammett constants (σ) [138] and experimental $Co^{I/II}$ redox potentials were made (Figs. 14(b) and 14(c)). The advantages of using χ_H are that it is readily calculated, avoiding the complexities associated with simulating the entire metal complex; it can be used when Hammett parameters are not available; and it does not require the synthesis of a complex to measure its redox potential. For substituents with no tabulated Hammett constants, their values were estimated from the linear correlation with χ_H. Within the neutral and cationic derivatives, the $\log(TOF_{CO})$ values of these cobalt-porphyrin derivatives correlated well with the Hammett σ values, with TOF_{CO} increasing as the substituent became more electron-donating (lower σ) (Fig. 14(d)). This feature implied that the RDS involves a loss of charge from the cobalt center, in agreement with electrokinetic measurements which suggested the RDS involves an electron transfer to CO_2. The somewhat low value of the reaction constant, ρ, could be rationalized by considering the inductive effect of the substituent is delocalized over a large macrocyclic ring. The most striking result from this study was the distinct trendlines for neutral and cationic substituents. Separate from through-bond inductive effects, cationic substituents had an additional promotional effect on the reaction, likely via electric fields interacting with the transition state of the RDS. Similar cationic promotional mechanisms have been observed in non-aqueous, homogeneous CO_2 reduction on iron porphyrins [129] and have been postulated to explain the effects of alkali cations on ECR on metallic surfaces [115, 124]. The rigorous evaluation of substituent effects in this study revealed that the combination of both through-bond inductive and electrostatic effects need to be considered when designing an optimal heterogeneous molecular catalyst for ECR.

Ligands can also impact how molecular catalysts are deposited on electrodes. A comparison between a less bulky CoTMPP and a bulkier t-Bu-CuPc found that CoTMPP's FE_{CO} was not strongly impacted by the pore size of the carbon support, whereas the FE_{CO} of t-Bu-CuPc was improved when using microporous activated carbon compared to nanoporous activated carbon fibers [139]. The

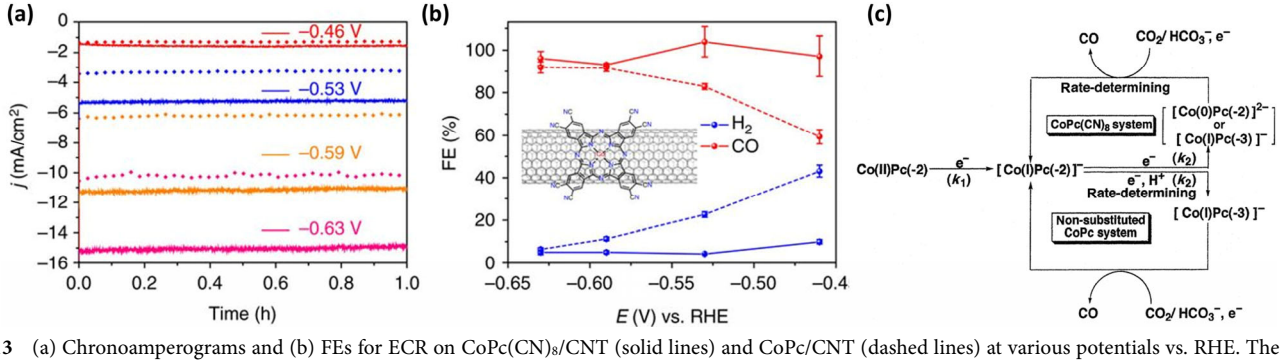

Figure 13 (a) Chronoamperograms and (b) FEs for ECR on $CoPc(CN)_8$/CNT (solid lines) and CoPc/CNT (dashed lines) at various potentials vs. RHE. The inset in (b) shows the molecular structure of $CoPc(CN)_8$, which is anchored on a CNT. Reprinted with permission from Ref. [137], © Springer Nature 2017. (c) Proposed ECR mechanism change for $CoPc(CN)_8$ compared to unsubstituted CoPc (reprinted with permission from Ref. [61], © World Scientific 1997).

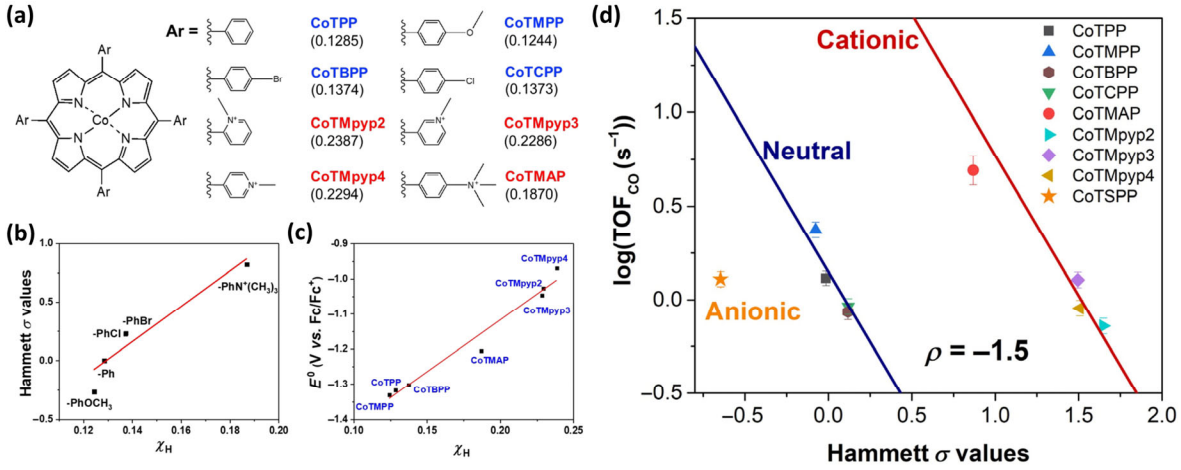

Figure 14 (a) The chemical structures of functionalized cobalt porphyrins and the corresponding Mulliken charge population on a probe hydrogen atom (χ_H) for the aromatic substituents (Ar) shown in parentheses. (b) Correlation between calculated χ_H and the corresponding para position Hammett substituent constant. (c) Correlation between calculated χ_H and experimentally measured Co(I/II) redox potentials. (d) TOF_{CO} of cobalt-porphyrin derivatives with various functionalities versus calculated Hammett σ values (–1.02 V vs. SHE, 8×10^{-10} mol/cm^2). Reprinted with permission from Ref. [72], © Royal Society of Chemistry 2019.

bulkiness of the tert-butyl groups may have made it difficult for the catalyst to disperse on the nanoporous support or hindered transport of reactants in the pores. Another study found that substituting octaalkoxy groups onto CoPc reduced aggregation, leading to higher $TOFs_{CO}$ than unsubstituted CoPc [67]. Since the redox potentials of the two catalysts were similar, the effects could be ascribed to aggregation differences rather than an electron donating effect of the octaalkoxy groups. These results underscore the multifaceted effect ligands can have, going beyond impacting the binding energies of intermediates.

One study found that different ligands coordinating to silver could greatly enhance the ECR activity toward CO compared to a commercial Ag/C catalyst [140]. Phthalocyanine, pyrazole (Pz), and 3,5-diamino-1,2,4-triazole (DAT) ligands enhanced the j_{CO} and FE_{CO} compared to Ag/C. Not all ligands proved to be more effective; a tris[(2-pyridyl)methyl]amine ligand had similar j_{CO} values to the Ag/C. While the j_{CO} values of the Pc-, Pz-, and DAT-ligated silver catalysts were similar to that of 70 nm Ag nanoparticles, the mass activity (mA/(mg·Ag)) was many-fold higher for the ligated silver catalysts. This result could motivate using metal complexes as precursors to create highly-dispersed metallic catalysts. Additionally, the addition of DAT to the commercial Ag/C catalyst greatly enhanced the j_{CO}, which suggests a synergistic effect between the ligand and the metallic catalyst; a control experiment verified DAT alone could not produce CO. Given the tendency of CuPc to demetallate under ECR conditions, the demetallation of these Ag complexes seems likely since Ag is easier to reduce than Cu, but more work is needed to confirm the nature of theses catalysts during ECR.

6 Electrode support effects

A key difference between homogeneous and heterogeneous electrocatalysis with molecular complexes is the direct adsorption of the catalyst onto the electrode. Naturally, the type of support can play a significant role in the catalysis by influencing electron transport rates or changing the electronic structure of the catalyst to impact binding energies of intermediates; this latter phenomenon was observed during a computational study on RuP supported on graphene [114]. As previously discussed, the redox properties of the catalyst can be drastically altered if the electronic coupling to the electrode is large [87]. Metallic supports have been experimentally shown to partially donate charge to MPc metal centers [141–144] and modify reactivity toward O_2 [145], providing further evidence that support-molecular-catalyst interactions cannot be ignored. For ECR, immobilizing catalysts has been shown to alter the reaction mechanism [24], improve stability, and change the relative performances of catalysts [25], in some cases causing a significant reduction in ECR activity [146]. All of these observations suggest that performance when dissolved in solution does not necessary correlate with performance when immobilized on an electrode. To increase consistency, only those studies that directly compared the performance of different supports will be discussed.

The influence of the type of carbon-based electrode support and its pretreatment were assessed for formate production from InPP [147]. Pyrolytic graphite (PG), glassy carbon (GC), and boron-doped diamond (BDD) were examined, and PG was found to yield the highest formate current densities and FEs, followed by BDD. The degree of aggregation was noticed to be less on the PG electrode, since it had a higher electrochemically active surface area (ECSA) and was not saturated with InPP at higher loadings, unlike GC and BDD. Pretreatment procedures were performed on the PG to gain further insight into the influence of surface functionality. An O_2 plasma treatment improved both the current density and FE for CO, while electrochemical anodization improved stability. Conversely, H_2 plasma and electrochemical reduction generally lowered formate current densities and FEs. The increased presence of oxygen functional groups on the O_2-plasma was attributed to the improved performance of InPP, although the anodized PG did not show an improvement with increased oxygen functionalities. The anodized PG was found to exhibit a more amorphous structure similar to GC but with a higher surface area due to delamination of graphite sheets. The results of this study highlight the importance of electrode selection and surface preparation, yet whether the observed phenomena were due to aggregation effects or changes in the intrinsic activity of InPP remains unclear.

Adsorbing molecular catalysts onto nano-structured materials has received attention as an effective way to improve ECR activity and selectivity. CoTPP was found to have a much higher j_{CO} (2.9 vs. 0.028 mA/cm^2) and FE_{CO} (91% vs. 28%) when dispersed in DMF with CNTs on GC at –1.10 V vs. SHE [25]. The improved activity was ascribed to the high surface area and electrical conductivity the nanotubes could provide, causing the mechanism to change from the mechanism under homogeneous conditions. Interestingly, CoTPP mixed with commercial carbon black (CB) had a higher FE_{CO} (97%) but lower j_{CO} (1.8 mA/cm^2) and durability. The authors did notice a saturation effect regarding catalyst loading, which reveals reduced aggregation with the high-surface-area CNTs may have played a prominent role in the observed improvement.

Similar conclusions about the beneficial properties of CNTs for ECR on immobilized molecular catalysts have been reached by other studies. FeTPP was found to yield higher formate current densities when FeTPP was deposited onto CNT-loaded CFP than when it was deposited without CNTs [148]. CoPP physically mixed with OH-functionalized CNTs showed improved FE_{sCO} and current densities at lower catalyst loadings [84]. CoPc supported on CNTs was found to outperform CoPc supported on reduced graphene oxide (rGO) or CB, with at least three times the j_{CO} and 10% higher FE_{CO} [137]. The improvement was attributed to better π–π interactions with the CNTs, which have a higher degree of sp^2 carbons than rGO or CB, as well as their high electrical conductivity. The use of ethanol, in which CoPc is poorly soluble, as a dispersing agent and the observation of current saturation with loading prominently point toward catalyst aggregation also playing a large role in the better performance with high-surface-area CNTs. CNTs were also found to enhance CO production compared to rGO for an immobilized cobalt chlorin (CoCh) complex, using similar arguments about strong π–π interactions [149]. Electron paramagnetic resonance (EPR) spectra suggested that the presence of two closely spaced CoCh complexes was needed for efficient ECR, which the authors believed CNTs facilitated better than rGO.

For charged molecular catalysts, electrostatic interactions with the electrode may play a more important role than π–π interactions. iron tetra-(4-N,N,N-trimethylanilinium) porphyrin (FeTMAP) was tested on liquid crystalline graphene oxide (LCGO) reduced to different extents (Fig. 15) [150]. The native LCGO contained many negatively charged functional groups, which could interact favorably with the positively charged FeTMAP. On the other hand, π–π interactions would be stronger on a fully reduced LCGO, as fewer oxygen functionalities would be present. Measurements found that FeTMAP on highly reduced LCGO had lower j_{CO} and FE_{CO} than partially reduced LCGO. The difference was ascribed to the reduced electrostatic interactions on the highly reduced LCGO, so the amount of active catalyst may have been lower; however, the amount of catalyst was not quantified. An experiment using FeTMAP on unreduced LCGO found a similar CO selectivity and a slightly lower j_{CO} than FeTMAP on reduced LCGO, suggesting *in-situ* reduction of the LCGO produced a similar surface morphology as *ex-situ* reduced LCGO.

One study found that the surface area of different carbonaceous supports correlated negatively with the performance of CoPc [151]. CoPc mixed with vapor-grown carbon fibers (VGCF) exhibited higher j_{CO} and FE_{CO} values than graphite, Vulcan XC-72, and activated carbon. CoPc on VGCF showed increased TOF_{CO} values at lower loadings, hinting that catalyst aggregation was occurring on the VGCF, so the inverse correlation between activity and surface area appears surprising. Notably, the preparation procedure involved a hot-press method, which may have changed the structure of the carbon support as well as CoPc, making comparison of properties measured before and after this treatment difficult.

Other types of supports have been use to adhere molecular catalysts for ECR. Tetra-stranded G-quadruplex nanorods (tsGQwires), which are composed of quinine molecules, were used as a support for CoPc [152]. CoPc supported on tsGQwires had slightly higher j_{CO} values and higher FE_{sCO} than CoPc without them in an ionic-liquid, non-aqueous electrolyte. Single-stranded DNA had no effect on performance, while duplex DNA only marginally improved performance. Similar current density and FE enhancements were seen for FePc toward CO and $[Ru^{II}(bpa)\text{-}(NH_3)_2](PF_6)_2$ toward formic acid. A combination of specific binding of the catalyst to the tsGQwires as well as good electrical conductivity was attributed to the enhanced catalytic performance. Aggregation effects may have played a role since the tsGQwires had a larger ECSA which could have reduced aggregation.

Another study supported CoPc on a zinc-indium sulfide (ZIS) semiconducting support [153]. Compared to just CoPc on carbon paper, CoPc-ZIS had much higher j_{CO} and FE_{CO} values. The improved performance was attributed to the coordination of unsaturated sulfur atoms with the cobalt metal center; these unsaturated sulfur atoms were the result of zinc defects. X-ray photoelectron spectroscopy (XPS) showed both a shift in the CoPc cobalt 2p peak to lower binding energy, while the ZIS sulfur 2p peak was shifted to higher binding energies, an indication of partial charge transfer to the cobalt metal center (Fig. 16). EPR data helped to show a positive correlation between the number of zinc defects and ECR performance. The CoPc loading was chosen based on when j_{CO} and FE_{CO} would not increase anymore with loading. Such a condition suggests catalyst aggregation could be convoluting the results, especially considering the control experiment of CoPc without ZIS, since the dispersion solvent was acetone in which CoPc is not soluble [65].

These prior works demonstrate the need for conclusive tests to confirm the origin of the improved performance of various supports. In fact, many of these studies have noticed a loading dependence on the TOF_{CO} or a saturation in current density, both indications that the intrinsic activity of the catalyst was not being measured [57]. Decoupling the effect of having increased surface area versus a specific electronic interaction with the catalyst is essential for providing rational design guidelines for making high-performance electrodes. This understanding may also have economic implications; for example, if the improved performance when using CNTs is mostly related to their surface area, then cheaper, conductive carbon materials could replace them that also have high surface areas.

6.1 Polymer encapsulation

Polymer encapsulation of molecular catalysts can provide an opportunity for tuning the electronic structure of the active site via

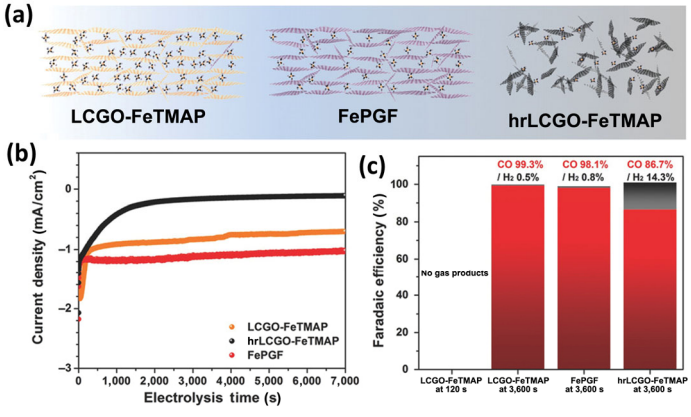

Figure 15 (a) Representations of the ideal structures for the LCGO-FeTMAP, FePGF, and hrLCGO-FeTMAP composites. (b) Current densities and (c) FEs for the three composites at −0.94 V vs. SHE in 0.1 M $KHCO_3$. Reprinted with permission from Ref. [150], © Wiley-VCH 2018.

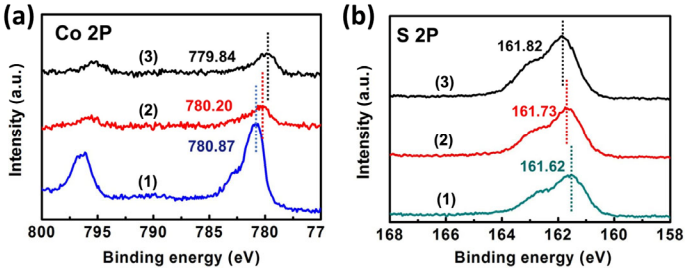

Figure 16 (a) XPS spectra of cobalt for (1) CoPc, (2) 6.2-CoPc/ZIS-180, and (3) 6.2-CoPc/ZIS-200 showing the Co 2p binding energy shift to lower values. (b) XPS spectra of sulfur for (1) pure ZIS, (2) 6.2-CoPc/ZIS-180, and (3) 6.2-CoPc/ZIS-200 showed the S 2p binding energy shift to higher values. Reprinted with permission from Ref. [153], © Royal Society of Chemistry 2018.

polymer interactions, modifying the second-sphere interactions around the active site, and controlling reactant concentrations. Regarding ECR, poly(4-vinylpyridine) (P4VP) has been studied as an encapsulant for CoPc. Early work showed that P4VP-modified basal-plane pyrolytic graphite (BPG) with CoPc was more selective and active for CO compared to electrodes without P4VP [90]. Several possible reasons were hypothesized that could have led to the improved performance: higher CO_2 solubility in the hydrophobic membrane with basic pyridine sites, axial coordination of pyridine residues to the cobalt metal center to enhance CO_2 binding, and abundant local proton sources from pyridine residues. Lower pH electrolytes were found to increase CO production only for the CoPc-P4VP electrodes. Interestingly, greater HER was also observed on CoPc-P4VP electrodes compared to those without P4VP. While P4VP may be ionically conductive to protons, it does not have an electrically conductive backbone due to lack of conjugation. The authors noted that charge hopping between CoPc molecules within the polymer would be unlikely to happen, so only those CoPc molecules near the electrode would be active. However, a later report did suggest that in a P4VP-polystyrene membrane, all molecular catalysts did have an electronic connection with the electrode as indicated by PSCAS [154]. In this study, electronic conduction was proposed to be the major factor for determining the rate of HER, illustrating the need for improving the electrical conductivity in these polymer-encapsulated systems.

A later study by the same authors found an optimal pH for CO production (4.4) and for CO/H_2 selectivity (~ 5) for the CoPc-P4VP system [91]. The study also tested poly(2-vinylpyridine) (P2VP), in which pyridine coordination to CoPc would be sterically forbidden, and found P2VP to be worse for CO production than P4VP; this result illustrated that higher CO_2 concentrations were not the only factor leading to the improved performance of P4VP. The best activity and selectivity for CO production were found at the highest CoPc loadings, although a saturation effect was observed. A mechanism was suggested whereby a concerted protonation–deprotonation step would occur after CO_2 binding to the cobalt center, facilitated by neighboring pyridine residues (Fig. 17(b)). However, some of the evidence for this mechanism was found from homogeneous studies, so the direct transferability to heterogeneous conditions may not be valid. P4VP does not universally improve ECR for molecular catalysts; $CoPc(BuO)_8$ [97] and $CoPc(CN)_8$ [61] were found to have lower activities and selectivities toward CO when mixed with P4VP.

To help further deconvolute the various possible effects of the P4VP membrane on ECR, a systematic investigation was conducted to vary certain aspects of the catalytic environment around CoPc [155]. The study found that neither pyridine coordination without the membrane nor the presence of the hydrophobic polymer with pyridine groups (P2VP) could account for the improved performance of CoPc within the P4VP membrane. Testing CoPc in a P2VP membrane with added pyridine resulted in a similar TOF_{CO} and FE_{CO} to those of CoPc-P4VP, which provided evidence that the combined effects of axial coordination and second-sphere interactions are responsible for the performance of P4VP (Fig. 17(d)). The axial

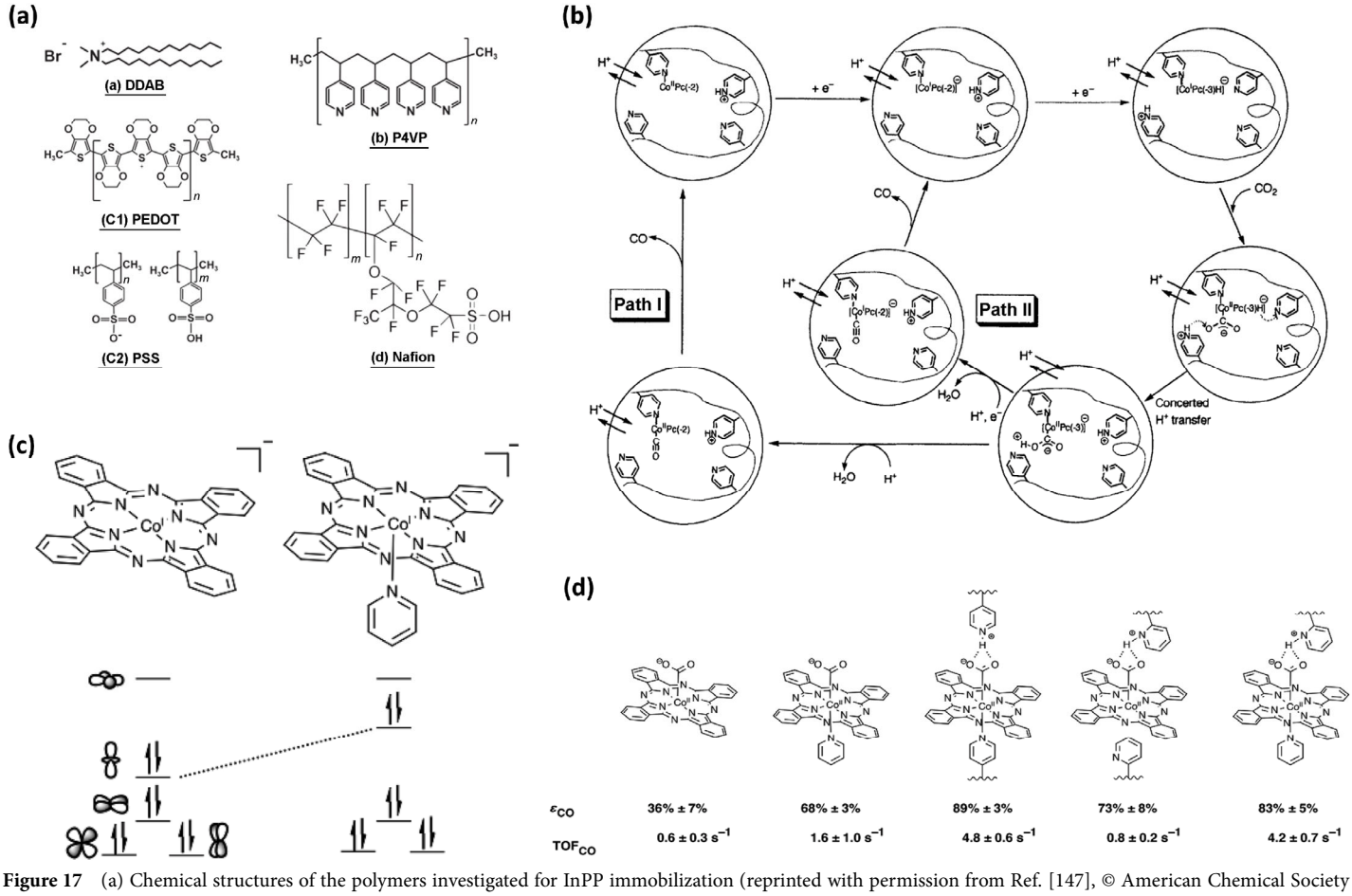

Figure 17 (a) Chemical structures of the polymers investigated for InPP immobilization (reprinted with permission from Ref. [147], © American Chemical Society 2018). (b) Proposed mechanisms for ECR catalyzed by CoPc-P4VP. An equilibrium with respect to H^+ exists between the polymer and bulk electrolyte. Reprinted with permission from Ref. [91], © Elsevier B.V. 1996. (c) Relative energies of the cobalt d orbitals in the 1 e^- reduced forms of CoPc and CoPc(py). Shown is the energy increase of the cobalt d_{z^2} orbital that results from the coordination of the axial pyridine. (d) Proposed active CO_2 complexes and secondary coordination sphere interactions for each catalyst film studied. Also shown are the Faradaic efficiencies (ε_{CO}) and TOF_{CO} values for each catalyst at −1.0 V vs. SHE in 0.1 M NaH_2PO_4 (pH = 4.7). Reprinted with permission from Ref. [155], © Royal Society of Chemistry 2016.

coordination from pyridine was hypothesized to increase the energy of the cobalt d_{z^2} orbital, which could favor CO_2 binding over hydrogen binding (Fig. 17(c)). The suppression of water transport was observed when the H_2 FE decreased significantly when P2VP was used. These results provide a greater understanding of the phenomena affecting ECR within P4VP; however, more work is needed to understand the possible mass-transport effects occurring in the membrane and to spectroscopically observe changes to the active site upon encapsulation with P4VP. Additionally, some of the CoPc molecules could be inactive because of the electronically insulating property of P4VP.

A wider selection of polymers were tested to observe their effects on formate production from InPP (Fig. 17(a)) [147]. P4VP, poly(3,4-ethylenedioxythiophene):polystyrenesulfonate (PEDOT:PSS) and didodecyldimethylammonium bromide (DDAB) were found to generally improve the activity and selectivity toward formate. P4VP had the highest formate FE but the lowest formate current density among these three polymers. Nafion was actually found to decrease the FE and current density toward formate, in agreement with other studies showing adverse effects of Nafion on electrocatalytic performance of immobilized molecular catalysts [156, 157]. Because all polymers provided a more hydrophobic environment, differences in performance could not be ascribed entirely to inhibited water transport. Nonetheless, the greater formate FE of InPP-P4VP could be at least partially ascribed to its lower HER current relative to the other polymers. The polymers that improved the formate current density also showed reasonable ECR activity themselves toward formate; P4VP by itself had a > 20% FE toward formate. These control tests imply the improved performance of mixing InPP with some polymers could be due to the activity of the polymer and not an intrinsic enhancement of the activity of InPP.

6.2 Covalent grafting

Performing chemical modifications to the electrode or the molecular catalyst itself has been a way to improve catalytic performance and durability for ECR. One of the earliest methods employed was to connect a pyridine group chemically bonded to a GC electrode via an amide linkage (Fig. 18(a)) [95]. The grafting procedure involved oxidation of the GC surface to produce carboxylate moieties, chlorination in $SOCl_2$, and amidization with 4-aminopyridine. The pyridinic nitrogen was anticipated to coordinate with the cobalt center of CoTPP, increasing the electron density at the center [94]. The more electron-donating cobalt center would then be able to better bind CO_2, leading to enhanced catalytic activity. Immobilized CoTPP was able to durably produce CO with a 92% FE at 300 mV overpotential in contrast to homogeneous CoTPP, which only had a 10% FE toward formate. Further experiments to probe how the intrinsic activity of immobilized CoTPP was enhanced by the pyridine coordination would be helpful to gain a deeper understanding of the impact of this type of axial ligation. This type of pyridine linkage was also successfully applied to other molecular catalysts including CoTMPP, CoPc, and CoNc for ECR [92].

A similar approach to modifying carbon electrodes involves oxidizing amine groups to form cations which attack and bond to surface moieties. This approach was used to axially coordinate CoTPP to a GC surface with several different linkers (Figs. 18(b)–18(d)) [96]. The linkers all contained a pyridinic nitrogen atom for axial coordination but had varied numbers of atoms between the surface and the aromatic ring. CoTPP supported on all three linkers generally had similar FEs_{CO}, which could indicate that the length of the linker was not important compared to the pyridine coordination to CoTPP. Notably, the pyridine-coordinated CoTPP was able to produce CO at lower overpotentials with greater FE than CoTPP on bare GC. As mentioned earlier, significant catalyst stacking was observed after initial fabrication, revealing that axially ligating surface sites do not necessarily guarantee aggregation-free conditions; however, the strong axial coordination did enable the unbound CoTPP to be selectively washed off. The same approach was applied to cobalt tetrabenzoporphyrin (CoTBzP), where the supramolecular assembly of the catalyst and linker was more catalytically active in the presence

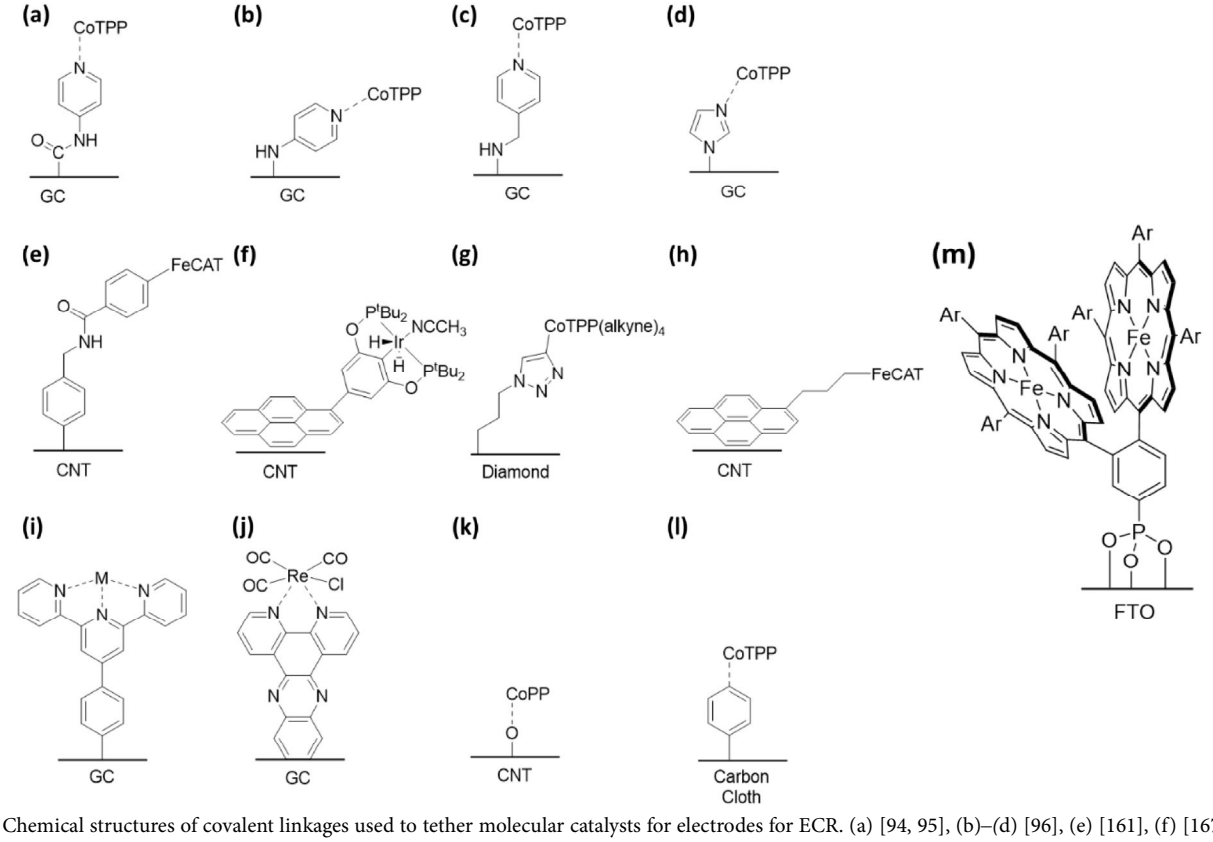

Figure 18 Chemical structures of covalent linkages used to tether molecular catalysts for electrodes for ECR. (a) [94, 95], (b)–(d) [96], (e) [161], (f) [167], (g) [162], (h) [166], (i) [160], (j) [24], (k) [84], (l) [178], (m) [165].

of CO_2 than physically adsorbed catalyst [158, 159], although production quantification was not reported. Performing product quantification would help to further address efficacy of the axial coordination for CoTBzP.

Another synthetic strategy is to covalently attach a linker and then metallate it to form a catalyst. Such a strategy was employed with a terpyridine-terminated linker, with the three nitrogen atoms coordinating to a cobalt ion (Fig. 18(i)) [160]. The cobalt terpyridine (Co-tpy) catalyst was able to reduce CO_2 to CO in DMF, but the activity quickly decayed within 30 min, leading to a small turnover number of 70.

The aforementioned studies all used an axially coordinating nitrogen atom to immobilize catalyst. Using a catalyst with a native axial ligand could lead to an even stronger covalent bond to the metal center. Axial bonding to an oxygen-terminated CNT surface site has been shown to yield improvements in catalyst dispersion and ECR performance. CoPPCl was covalently attached to oxygen functionalities on a CNT surface by refluxing in ethanol with trimethylamine (Fig. 18(k)) [84]. The covalently linked CoPP displayed a higher FE_{CO} and j_{CO} than physically adsorbed CoPP on oxygen-functionalized CNTs. Additionally, the covalent linkage greatly reduced aggregation, as physically adsorbed CoPP showed a lower TOF_{CO} (0.29 s^{-1} vs. 0.84 s^{-1}) at −1.02 V vs. SHE and had aggregates that could be seen under transmission electron microscopy (TEM). The TOF_{CO} of physically adsorbed CoPP at lower loadings approached ~ 1 s^{-1}, which is fairly close in value to the covalently bound TOF_{CO}, suggesting that the oxygen bond serves to reduce aggregation much more so than change the intrinsic activity of the catalyst. The deconvolution of aggregation and intrinsic activity in this study led to a clearer picture on the precise effect of a covalent linkage on the ECR activity of a molecular catalyst.

Other grafting strategies involve linkers covalently bonded to the ligands of the molecular catalyst, which can reduce changes to the metal center's electron density. An iron porphyrin with a carboxylate group (CAT_{CO_2H}, Fig. 18(e)) was appended onto CNTs via an amide linkage to a surface benzyl amine group [161]. The catalyst showed selective ECR activity toward CO, maintaining an FE_{CO} above 80% over 3 h. In this case, the molecular linker was likely not fully conductive due to the sp^3 carbon atom between the phenyl ring and amide group. The electron transfer was probably outer sphere in this system, as a strong electronic coupling to the electrode appears doubtful. In this system, the immobilized catalyst likely behaved similarly to a homogeneous catalyst. A "click" reaction between an azide-functionalized surface and a cobalt tetrephenyl porphyrin with ethynyl groups was successfully performed (Fig. 18(g)) [150]. CO was detected as a product with an estimated TOF_{CO} of 0.8 s^{-1} over a 16 h period. The azide linkage contained a long alkyl chain, so this system was likely not electronically coupled to the electrode and required an outer-sphere electron transfer.

Another type of linkage to the ligands of a molecular catalyst involves forming a pyrazine connection by reacting a phenylenediamine moiety on the catalyst with o-quinone groups, commonly found on glassy carbon surfaces [163]. This immobilization technique was used to anchor a $Re(phen)COCl_3$ catalyst to glassy carbon for ECR (Fig. 18(j)) [24]. As discussed earlier, the strong electronic coupling in this catalyst to the electrode changes the mechanism and redox behavior of the metal center. At −2.0 V vs. Fc/Fc^+, a TOF_{CO} of 2.5 s^{-1} was obtained. At voltages less reductive of −1.9 V vs. Fc/Fc^+, the grafted Re catalyst had a higher TOF_{CO} than its homogeneous counterpart. These results demonstrate that pyrazine linkages to glassy carbon provide a strong covalent bond that can enable heterogenization of molecular catalysts.

Phosphonic acid coupling to a metal oxide surface has enabled successful immobilization of a variety of molecular catalysts. A manganese bipyridine complex was attached to TiO_2 and found to have a lower bound TOF_{CO} of 0.016 s^{-1} with a FE_{CO} of 67% a −1.7 V vs. $Fc^{+/0}$ [102]. Atomic layer deposition (ALD) of TiO_2 was used to encase a Ru-based molecular catalyst [164]. The deposition of a ~ 0.5 nm TiO_2 layer after catalyst adsorption covered the phosphonic acid groups, thereby increasing the stability of the catalyst. A TOF_{CO} of 0.34 s^{-1} was achieved at −1.06 V vs. SHE in 0.5 M $KHCO_3$, although the catalyst deactivated after nearly two hours. A cofacial iron-porphyrin dimer was bound to metal oxide surfaces via a phosphonic-acid linker via heating at 120 °C (Fig. 18(m)) [165]. In DMF/5% H_2O, an impressive TOF_{CO} of 245 s^{-1} with a 93% FE_{CO} was achieved when the catalyst was anchored to FTO. Anchoring on SnO_2 or TiO_2 nanoparticles improved current density, but the TOF_{CO} decreased. The decreases in TOF_{CO} were suggested to come from the poorer electrical conductivity of the metal oxide nanoparticles. These studies highlight that in addition to carbon-based supports, metal oxides can also be used with appropriate functionalization of the molecular catalyst.

Covalent modifications to molecular catalysts do not necessarily need to involve a direct bond with the surface; these modifications can involve substituents that can bind to the electrode via strong non-covalent interactions. In this vein, a couple of studies have used pyrene groups to form strong π–π interactions with CNTs. A pyrene group was appended onto an iron porphyrin catalyst via an alkyl chain and deposited onto CNTs (Fig. 18(h)) [166]. The pyrene-appended catalyst had higher FE_{CO} (97% vs. 90%) and j_{CO} at −1.03 V vs. SHE compared to the catalyst without the pyrene group, illustrating the benefit of having a stronger attachment to the surface. The alkyl groups in the linker prevent a direct electronic pathway between the CNTs and the catalyst, so the electron transfer was likely outer-sphere. A similar grafting strategy was used to immobilize an Ir pincer catalyst on CNTs for ECR to formate (Fig. 18(f)) [167] and a rhenium bipyridine catalyst on carbon black for ECR to CO [168]. In the Ir-pincer study, the pyrene ligand was fully conjugated, so an electronically conducting pathway to the catalyst could have been present. The formate TOF reached 7.4 s^{-1} at −1.3 V vs. SHE on glassy carbon; with a gas-diffusion layer (GDL), the formate TOF more than doubled at the same potential (15.1 s^{-1}). A possible advantage of using strong non-covalent immobilization to the surface rather than covalent immobilization is the ability to remove and replenish deactivated or spent catalyst from the surface more easily.

Various methods have been used successfully to either covalently link molecular catalysts to electrodes or attach functional groups to the catalyst that provide stronger non-covalent interactions with the electrode. Many other possible immobilization routes exist, which should provide many opportunities for future work in this area [169–171]. To gain a deeper understanding of the effects of grafting, more studies need to be performed that isolate the effects of reduced aggregation and changes to intrinsic catalyst activity.

6.3 Metal-porphyrin co-catalytic systems

The support material on which a molecular complex is anchored may in fact be the primary catalyst, with the molecular complex acting as a co-catalyst to promote the desired reaction of interest. Several examples of using porphyrins as co-catalysts to enhance the CO_2 or CO reduction ability of an underlying metal have been experimentally demonstrated. Unmetalated tetra(4-aminophenyl) porphyrin (H_2TAPP) was electropolymerized onto gold substrates, forming a porous polymer network (PPN) [172]. At −0.7 V vs. RHE, the TAPP-PPN-Au electrode had a 95% FE_{CO}, compared to just a 25% FE_{CO} for the bare Au electrode at the same potential. The j_{CO} for the TAPP-PPN-Au electrode was also significantly higher than that for the bare Au over a wide range of potentials (−0.5 to −0.8 V vs. RHE). Control experiments with unpolymerized H_2TAPP and polymerized thiophene porphyrins showed reduced HER but similar CO production as bare Au, suggesting that the polymerization of

amine groups was vital to the improved CO activity. While the FE_{CO} was insensitive to the polymer-layer thickness, j_{CO} reached an optimum at a thickness of 60 nm. Lead underpotential deposition experiments revealed that 83% of the Au surface remained accessible in the presence of the polymer. One observation regarding the FE_{CO} for the bare Au electrode which will require further investigation is that other studies have found the FE_{CO} to be greater than 90% at −0.68 V vs. RHE on planar Au electrodes [173, 174]. Future work to establish a reliable baseline for bare Au will be needed to more accurately understand the effects of overlayers of porphyrin PPNs.

Monomeric porphyrins have also been used to functionalize Au surfaces for ECR. Au nanoparticles (AuNPs) were functionalized with a tetradentate porphyrin with thiol ligands (P1 (n = 1), Fig. 19), with the thiol ligands binding to the Au surface [175]. The P1-AuNPs had higher j_{CO} and FE_{CO} values than oleylamine-ligated AuNPs (OAm-AuNPs) or bare AuNPs. Tafel analysis revealed a 123 mV/dec slope for OAm-AuNPs, while the P1-AuNPs had a 69 mV/dec slope. This difference suggested the P1 ligand changed the nature of the RDS for ECR. The P1-AuNPs also had a higher electrochemically active surface area than the OAm-AuNPs as probed by lead underpotential deposition. Not only did the P1 ligand improve intrinsic activity and surface area but it also dramatically improved the long term stability. The P1-AuNPs showed stable performance over 72 h, whereas the FE_{CO} of OAm-AuNPs decreased from 62% to 10% over 12 h. These results demonstrate that porphyrin ligands can stabilize catalytic intermediates bound to other catalysts as well as those catalysts themselves.

Similar tetradentate porphyrin ligands have also been shown to affect CO reduction on copper (Fig. 19) [176]. The addition of the porphyrin ligands increased the production and selectivity towards oxygenates (ethanol and acetate), while the selectivity towards ethylene remained unaffected. The importance of the cage-like structures created by the porphyrins was investigated via control experiments. By changing the position of the thiol linkers from the ortho to the para position on the phenyl rings, the porphyrin rings would either lie flat on the surface or orient perpendicular to it. The selectivity towards C_2 products diminished when the linkers were in the para position, which implies the cage-like structure is important for the observed catalytic activity. Using a 3-mercapto-N-phenylpropanamide ligand, which resembles a single thiol linker on the porphyrin, the oxygenate selectivity was still less than the full porphyrin ligand, illustrating that the porphyrin ring plays an important role in the reaction. Moreover, lead underpotential deposition confirmed that the porphyrin cages were not restricting access to the underlying copper. Varying the length of the thiol linker impacted the selectivity towards oxygenates; an aliphatic chain length of n = 2 was found to be the optimum for oxygenate selectivity. Changing the metal center of the porphyrin also had an effect, with Fe promoting ethanol selectivity and Ni promoting HER and ethylene production. With an electrodeposited copper surface and Fe metal center, the porphyrin-copper system was able to achieve a 57% FE towards ethanol and an 83% FE towards C_2 products at −0.4 V vs. RHE in 0.1 M KOH. DFT calculations suggested that the increased oxygenate selectivity could originate from a ketene intermediate being stabilized by hydrogen bonding with an amide hydrogen on the thiol linker. The combination of metallic surfaces with porphyrin-based ligands may enable the design of catalytic pockets that tune the activity and selectivity of ECR.

7 Catalyst stability

High activity and selectivity toward ECR are certainly important metrics for a catalyst, but just as important is how constant these properties are over time. A variety of mechanisms could be responsible for immobilized molecular catalyst decay including leaching, aggregation, demetallation, poisoning, metal impurity deposition, and change in molecular structure. Catalyst stability has been frequently investigated, owing to its importance for practical operation. The turnover number (TON) of a catalyst is how many reactions each active site catalyzed during the duration of the experiment. The average TOF can be found by dividing the TON by the experiment duration. The TON, testing duration, and average current density are important metrics on which to assess molecular catalysts. From an economic perspective, TON relates to the revenue of product generated per cost of catalyst. The testing duration relates to how often catalyst must be replaced, which could involve costs associated with stopping and restarting production. Current density is related to the capital cost of equipment, as higher current densities can enable fewer electrolysis units at a given production rate. A few studies have demonstrated operating times of at least 24 h [94, 138, 177–179], and others have demonstrated TON over one million [57, 90, 94] for both phthalocyanines and porphyrins. These results are promising, especially considering that these tests likely did not lead to catalyst exhaustion (i.e. the activity and selectivity at the end of the test were not significantly diminished compared to those at the start). For practical usage, these catalysts probably need to have long-term stabilities on the order of thousands of hours to be industrially viable [180].

Several studies have found that immobilization of cobalt-based molecular catalysts led to superior stability when compared to their homogeneous counterparts. CoTPP physically adsorbed on CNTs [25] and axially coordinated to surface pyridine groups [94] was found to have improved stability; a similar observation was seen for CoPc [89]. Covalently grafting catalysts can provide significant stability enhancements, as seen for CoTPP covalently bound to carbon cloth [178] (Fig. 18(l)) and CoPP axially bound via an oxygen bond to CNTs [84]. Likewise, polymer encapsulation has been reported to lead to stability improvements for CoPc (P4VP) [90], InPP (P4VP, PEDOT:PSS), and a cationic iron porphyrin (Nafion) [177]. Hypotheses surrounding these stability improvements include reduced leaching for water-soluble catalysts, aggregation, and ligand hydrogenation, although more work is needed to confirm what the primary deactivation mechanisms are for immobilized molecular catalysts under ECR operating conditions.

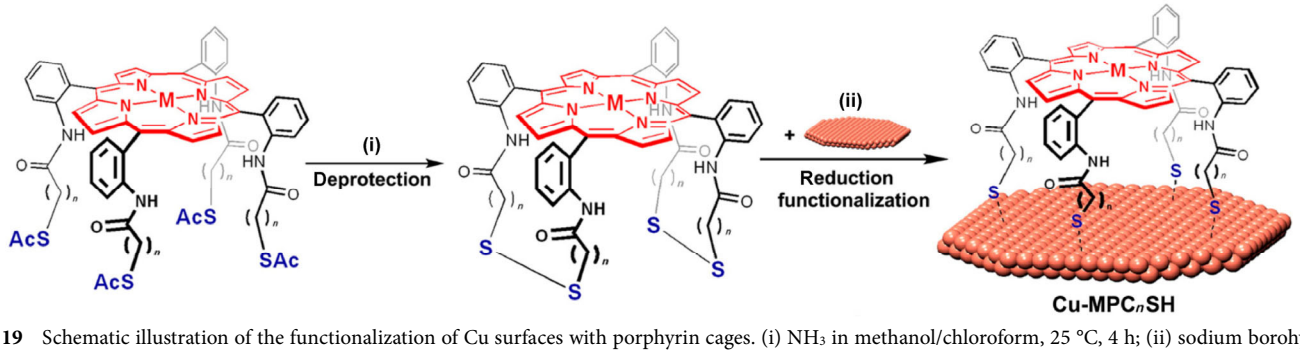

Figure 19 Schematic illustration of the functionalization of Cu surfaces with porphyrin cages. (i) NH_3 in methanol/chloroform, 25 °C, 4 h; (ii) sodium borohydride, DMF, 25 °C, 12 h. The structure of P1 from Ref. [175] is the porphyrin cage for n = 1. Reprinted with permission from Ref. [176], © American Chemical Society 2017.

An important breakthrough in improving the stability of homogeneous ECR catalysts was to use a bacteriochlorin macrocycle instead of a porphyrin one [181]. An issue with porphyrins under reductive conditions in the presence of proton donors is irreversible hydrogenation of the double bonds in the 2H-pyrrole rings (Fig. 20(a)) [182, 183]. This hydrogenation occurs because one set of opposite pairs of these double bonds are not part of the macrocycle's aromatic system; these pairs can be hydrogenated without breaking aromaticity. A bacteriochlorin ring already has these non-aromatic double bonds reduced, so further reduction of the macrocyclic ring is inhibited. The stability of a free-base (i.e. no metal center) bacteriochlorin catalyst was compared to a free-base porphyrin. Using UV–vis spectroscopy, the absorbance spectra of the bacteriochlorin only reduced by 30% over 20 h compared to a 60% decrease for the porphyrin over 3 h, with a complete degradation after 22 h. To gain theoretical insight into the increased stability of the bacteriochlorin, DFT calculations were performed to look at the lowest unoccupied molecular orbital (LUMO) of each macrocycle, since the LUMO should be involved in reduction reactions (Fig. 20(c)). A noticeable LUMO electron density is present at the vulnerable double bonds in the porphyrin, whereas the same bonds in the bacteriochlorin have much less electron density. While obtained for homogeneous molecular catalysts, the insights into deactivation mechanisms and strategies to overcome them appear relevant to immobilized molecular catalysts for ECR.

8 3D and extended structures

An end goal for ECR catalysts is to achieve practically relevant performance. With respect to current density, technoeconomic analyses have suggested > 100 mA/cm^2 is necessary for CO production [184]. Therefore, densely incorporating molecular catalyst active sites into heterogeneous materials is important. Physical adsorption of monomeric catalysts onto high surface area substrates is one option, though this often results in catalyst aggregation at high catalyst loadings, rendering many deposited active sites inaccessible and limiting total achievable current. Another promising option is to chemically link molecular complexes into 3D architectures such as MOFs, COFs, or porous polymers, where the formation of chemically linked, rigid networks can reduce catalyst aggregation. Such 3D architectures could in theory also enable one to engineer the nature of the 3D environment surrounding the active site in a fashion similar to an enzyme active site for better performance. Thus, these 3D architectures represent a promising platform in which to incorporate molecular complexes into high performance catalysts.

Within such 3D catalysts, the overall current density is affected not only by the intrinsic activity at individual catalytic centers but also by additional phenomena including species transport and electronic conductivity within the bulk material. One should ideally deconvolute effects from these various factors when studying and designing these types of catalysts. Below, we review recent works that have incorporated molecular complexes, with an emphasis on cobalt and iron tetrapyrroles, into 3D structures.

8.1 Metal organic frameworks

Metal organic frameworks are crystalline structures whose building blocks are connected via coordination of organic linkers to metal ions. MOFs, due to their porous and well-ordered nature, are a promising class of materials in which to incorporate molecular catalysts. MOFs have been used for electrocatalytic reactions including HER, oxygen evolution (OER), and oxygen reduction (ORR) [185]. Below, we review recent works that have used MOFs composed of tetrapyrrolic building blocks for ECR.

Iron tetrakis(4-carboxyphenyl)porphyrin (FeTCO$_2$PP) catalysts were incorporated into MOF-525 via hexa zirconium(IV) nodes and used for ECR (Fig. 21(a)) [186]. From transient chronoamperometric measurements, by integrating total charge passed for the Fe(III)/Fe(II) reduction, the authors estimated the density of electroactive Fe sites to be 6.2 × 10^{-8} mol/cm^2, which is three orders of magnitude higher than their estimated loading for a single monolayer of FeTCO$_2$PP on a flat electrode. However, even with such high catalyst loadings, the current density at −1.3 V vs. NHE in acetonitrile was 2.3 mA/cm^2, lower than what the authors obtained using a homogenous FeTCO$_2$PP

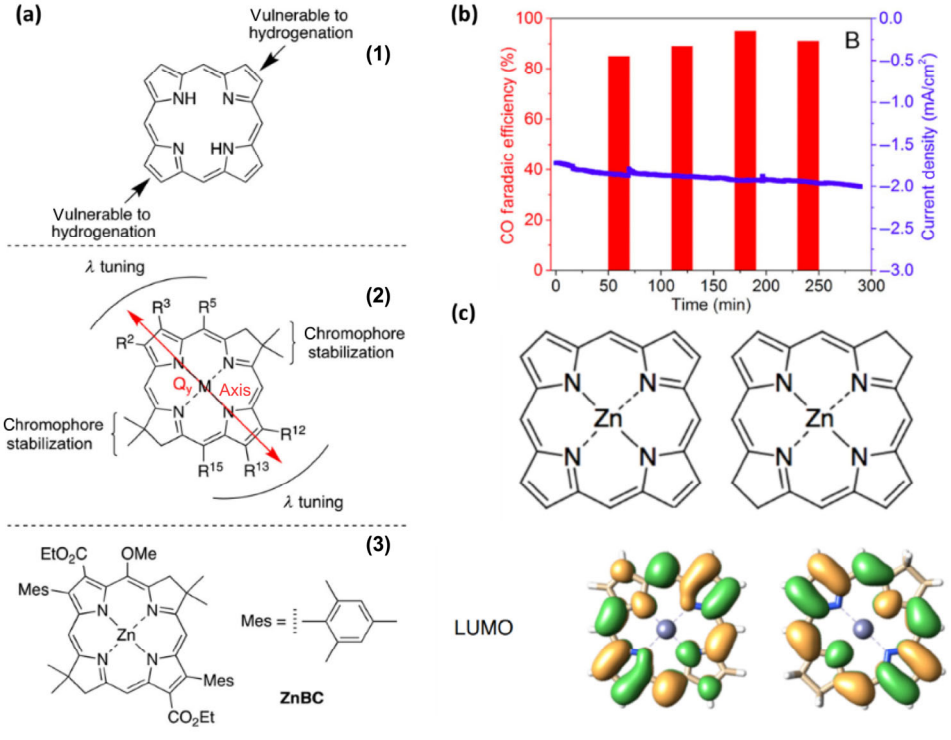

Figure 20 (a) (1) Structure of a porphyrin framework depicting where hydrogenation is likely to occur. (2) Molecular design of a synthetic bacteriochlorin. (3) Chemical structure of the zinc bacteriochlorin (ZnBC). (b) Stability test of the ZnBC at −1.9 V vs. Ag/AgCl in 0.1 M NBu_4PF_6, 5 M H_2O in DMF. (c) DFT-calculated LUMOs for simple zinc porphyrin (left) and bacteriochlorin (right) structures. Reprinted with permission from Ref. [181], © American Chemical Society 2018.

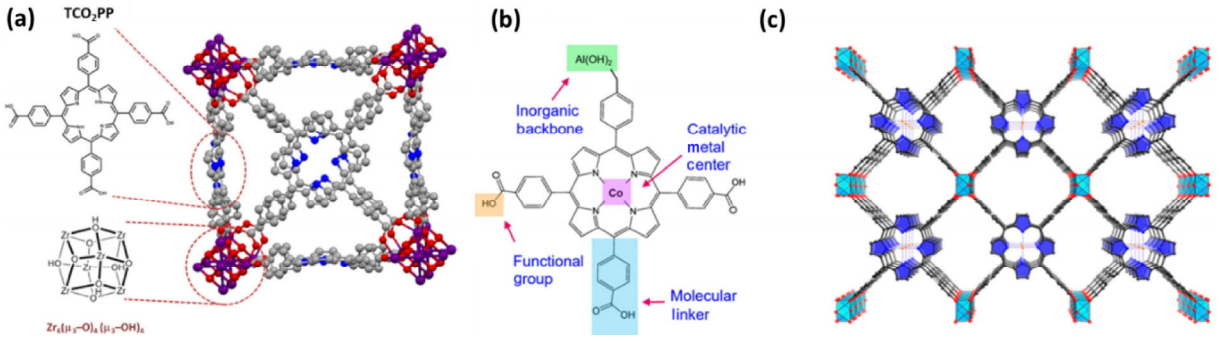

Figure 21 Porphyrin-based MOF catalysts reported in literature. (a) Diagram of MOF-525, incorporating $FeTCO_2PP$ macrocycles connected via hexa zirconium(IV) nodes (reprinted with permission from Ref. [186], © American Chemical Society 2015). (b) Chemical structure of the organic building units, $CoTCO_2PP$. (c) Diagram of $CoTCO_2PP$-based MOF connected via aluminum linkages. Reprinted with permission from Ref. [98], © American Chemical Society 2015.

catalyst (12 mA/cm^2), which translated to a heterogeneous TOF_{CO} that was 16 times lower than that for the homogeneous complex. The authors postulated that the lower TOF_{CO} was due to limited charge transport within the MOF. From chronoamperometry experiments, they estimated the charge carrier diffusion coefficient to be 5×10^{-13} cm^2/s, indicating a characteristic charge transfer timescale longer than the reaction timescale indicated by the TOF_{CO} of homogenous $FeTCO_2PP$. To conclude, the authors noted that an improved MOF material would be more conductive and more stable (the MOF degraded after 5 h of use).

A cobalt tetrakis(4-carboxyphenyl)porphyrin ($CoTCO_2PP$)-based MOF was synthesized via aluminum ion linkages (Figs. 21(b) and 21(c)) [98]. At the optimum MOF thickness of 30–70 nm, the total loading of cobalt was around 1.1×10^{-7} mol/cm^2. At this loading, the authors achieved current densities around 1 mA/cm^2 and estimated a TOF_{CO} of 0.06 s^{-1} at −0.7 V vs. RHE. The authors reported a Tafel slope of 165 mV/dec, suggesting that the first electron transfer was probably involved in the rate determining step, but the somewhat high Tafel slope could indicate that the measurements were taken under conditions of mass transport limitations. Finally, the authors used *in-situ* UV–vis to demonstrate that most Co species were Co(I) under ECR conditions, which confirmed both that the most likely catalytically active Co species was Co(I) and that most of the Co sites were in fact electrically connected to the electrode.

A $CuTCO_2PP$-based MOF connected via Cu paddle-wheel nodes was also used for ECR [187]. After 15 min of electrolysis, a morphology change from crystalline nanosheets to partially amorphous structures was observed, accompanied by the appearance of new *ex-situ* X-ray diffraction (XRD) peaks that corresponded to formation of various Cu oxides and hydroxides. The authors hypothesized that under operating conditions, the catalyst consisted of $CuTCO_2PP$ units covalently linked to Cu-oxide clusters. However, given previous works that have shown demetallation of Cu porphyrins under ECR conditions [42], $CuTCO_2PP$ may have demetallated during the reaction. Though this catalyst showed a high FE for formate of up to 68.4%, an opportunity remains to better elucidate the catalyst structure during operating conditions and to better understand the nature of the various Cu-based active sites and their cross-interactions.

MOFs with non-tetrapyrrolic subunits have also been reported for ECR [188]. They are discussed in several reviews already, so they are not explicitly discussed here [185, 189]. In these review works, electrical conductivity within the framework is consistently a limiting factor, causing apparent TOFs at the metal centers to be at least an order of magnitude lower than what might be expected from the monomeric macrocycle analogue. Electrical conductivity in MOFs is an active area of research and is thought to occur via electron/hole redox hopping from redox active linkers [190] or installed functional groups [191]. Another important aspect of MOFs is that the structural linkage incorporates a metal ion—The role of this ion, whether it indirectly affects catalysis by modulating MOF electronic structure or if it can itself act as a separate catalytic active site, is an interesting but unanswered question.

8.2 Covalent organic frameworks

COFs are crystalline materials whose structural linkages are formed through covalent bonds rather than coordination of organic linkers to metal ions [192, 193]. Similar to MOFs, COFs have the advantage of providing well-defined, porous 3D structures with a high degree of synthetic tunability. Because COFs are connected via covalent bonds, they also tend to be more thermally stable than MOFs [189]. Tetrapyrroles such as porphyrins and phthalocyanines form two-dimensional (2D) COFs [193], which are planar sheets that stack on top of each other. These systems have high charge carrier mobility due to π conjugation in plane and π–π stacking between planes [83]. To date, various COFs have been tested for electrocatalytic reactions including HER, OER, ORR, and ECR [83]. Below, we review some works that have incorporated tetrapyrrolic building blocks into COFs for ECR applications.

In an initial report of COFs for ECR, COF-366-Co and COF-367-Co were synthesized from cobalt tetraaminophenyl porphyrin (CoTAPP) subunits connected via imine linkages (Fig. 22(a)) [83]. Interestingly, the authors estimated from integration of the Co(II)/(I) CV peak that only 4%–8% of the deposited Co sites were electrochemically active. The authors hypothesized that this low percentage was due to insufficient electrical contact between the COF powder and carbon fabric substrate. Another possible explanation is that the stacking geometry of the COF crystals, in which the metal centers stack on top of one another, rendered many Co sites inaccessible. At −0.67 V vs. RHE (550 mV overpotential), the authors achieved a CO_2 to CO reduction current of 3.2 mA/cm^2, which translated to a TOF_{CO} of 0.53 s^{-1} at electrochemically accessible Co sites.

To better understand the various phenomena affecting performance of the COF materials, the authors also studied the ECR mechanism, COF-pore-size effect, conductivity, and diffusion within the material. In electrokinetic studies on COF materials, the authors reported Tafel slopes between 470 to 550 mV/dec, a first-order CO_2 dependence, and no proton dependence for ECR to CO. Although the reported Tafel slopes are outside of a kinetically interpretable range, these kinetic results are consistent with other reported mechanisms on CoTPP, where the rate-determining step is the initial electron transfer to CO_2 [72]. Upon changing from a shorter linker molecule (COF-366-Co) to a longer linker molecule (COF-367-Co), the authors saw an increase in TOF_{CO} on a per-deposited-cobalt basis (from 0.027 to 0.046 s^{-1}) but saw a decrease in TOF_{CO} on a per-electroactive-cobalt basis (from 0.69 to 0.53 s^{-1}). Finally, the authors characterized charge transport through COF thin-films, using

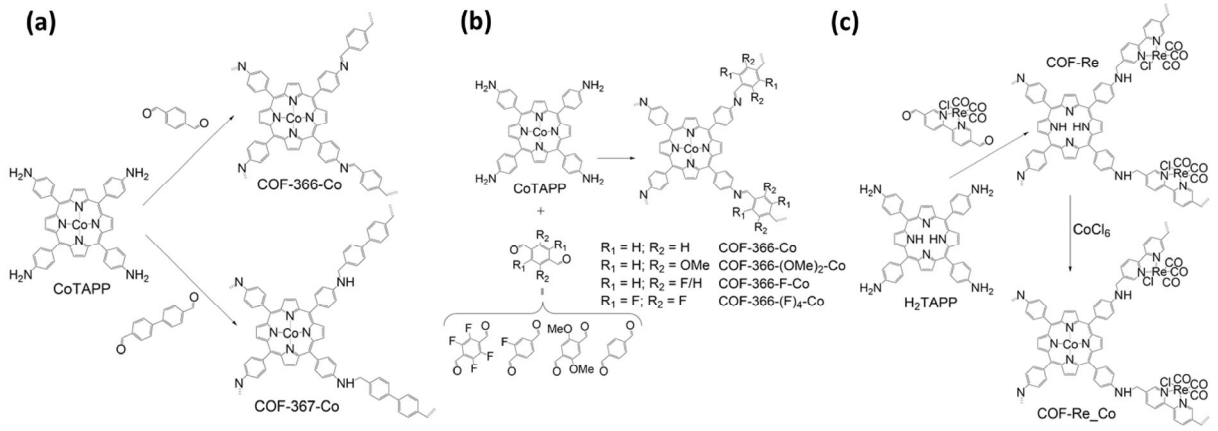

Figure 22 Structures of various porphyrin-based COF catalysts for ECR. (a) Synthetic scheme for COF-366-Co and COF-367-Co, which incorporate different length linker molecules [83]. (b) Scheme for COF-366-Co, COF-366-(OMe)2-Co, COF-366-F-Co, and COF-366-(F)4-Co, a series of COFs with differently functionalized linker molecules [194]. (c) Scheme for COF-Re_Co, which incorporate linker molecules with a catalytically active metal center [195].

spectroelectrochemistry to observe the rate of Co(II)/(I) reduction within a film held under reductive conditions. The apparent charge carrier diffusion coefficient was determined to be 2×10^{-12} cm^2/s. Direct current conductivity measurements yielded a value of 1×10^{-6} S/cm, which is in the conductivity range of a semiconductor.

Following this initial study, COF-366-Co was modified to contain functional groups of varying electron withdrawing propensity (Fig. 22(b)) [194]. The authors used XAS L-edge absorption data to determine differences in electronic character of Co active sites caused by inductive effects from the COF framework. Measurements for ECR to CO were then performed at −0.67 V vs. RHE. The authors found the following results, with the COFs listed from least to most electron-withdrawing (as determined from XAS), and ECR activity in parentheses: COF-366-Co (45 mA/mg) < COF-366-(OMe)$_2$-Co (46 mA/mg) < COF-366-(F)$_4$-Co (38 mA/mg) < COF-366-F-Co (65 mA/mg). Surprisingly, the linker with one electron-withdrawing fluorine group resulted in a COF with metal centers that were more electron-deficient than that of the linker with four fluorine groups. The authors claimed that electron-withdrawing groups improved activity because the first step in ECR on these frameworks is the reduction of Co(II) to Co(I) (which is then followed by adsorption of CO_2), so removing electron density from Co made the initial reduction of Co(II) more facile. This explanation is surprising because earlier work by the same group showed a majority of cobalt centers in COF-366 were in the Co(I) state, which suggested that the Co(II) → Co(I) transition was not rate-limiting [83]. Interestingly, the observation that electron-withdrawing groups improve activity at Co porphyrins is inconsistent with other studies [72]. The authors also suggested that COF-366-(F)$_4$-Co breaks the expected activity-electronegativity trend because it is too hydrophobic; further studies to probe this hypothesis would be useful in future work. This study lays a foundation for beginning to understand electronic effects from the COF linker, but further efforts are needed to deconvolute effects from intrinsic activity vs. availability of reactants at the active site. In particular, COF-366-Co and COF-366-(OMe)$_2$-Co showed very similar activities, and adding electron-withdrawing fluorine groups both increased (COF-366-F-Co) and decreased (COF-366-(F)$_4$-Co) the activity of resulting COFs.

A CoTAPP-based COF connected via rhenium bipyridine (Re-bipy) containing linkages was also tested for ECR (Fig. 22(c)) [195]. COFs based on CoTPP (COF-Re_Co) and FeTPP (COF-Re_Fe) were used to explore the idea of building COFs with electrocatalytically active linker molecules. Notably, the authors only achieved partial metalation of the porphyrin units within the COFs: 53% in COF-Re_Co and 30% in COF-Re_Fe. Separately, the Re-bipy complex and CoTPP were both highly selective (FE_{CO} > 80%) for ECR, but the FE_{CO} of COF-Re_Co was only 18.2% at a j_{CO} of 0.17 mA/cm^2. The FE_{CO} of COF-Re_Fe was < 2% with a j_{CO} of 0.07 mA/cm^2. To explain their results, the authors mentioned that diffusion of reactants within the COF pores was likely limited and also suggested that incorporation of Re-bipy and CoTPP into the same COF could cause competition between metal centers for electrons. The presence of unmetalated TPP, or H_2TPP, which is known to be selective for only hydrogen evolution [196], may have also contributed to the low FE_{CO} values observed. Though this work begins to explore the design principle of introducing multiple metal centers in a single framework, which is relevant to MOFs as well, an opportunity remains to further identify and deconvolute the following: reaction rates at each type of metal center (and unmetallated porphyrin centers); electronic effects of having two metal centers in the same covalent framework; and transport of reactants within the COF.

Although not reviewed here, COFs containing non-tetrapyrrolic active sites have also been reported for ECR [197, 198]. A general challenge for the rational design of COFs for ECR is deconvoluting various physical processes that occur within the 3D structure. How changes to the COF framework modulate the transport of reactants to and the intrinsic activity at specific active sites remains to be better understood. Also, molecular macrocycles such as CoTPP typically form 2D COFs, where the natural stacking of COF sheets could be a barrier to exposing a large number of active sites. Controlling interlayer interactions in 2D COF frameworks to affect porosity and crystallinity has been generally explored [192, 199] and may be important to consider for COF ECR catalysts as well. Additionally, because COFs are synthesized through the formation of reversible bonds, the resulting materials can have limited chemical stability because these bonds are not strong. The imine linkages reported for the above COFs are stable in water, though their general lack of robustness toward environmental conditions may be unideal for practical electrolyzer applications [200]. Strategies for enhancing stability by transforming imine bonds to amine bonds have been reported [198], though they likely disrupt extended conjugation and reduce electrical conductivity within the COF.

8.3 Polymers and other structures

Relatively less ordered structures have also been extensively used to immobilize tetrapyrrolic macrocycles at higher loadings. Though these polymeric materials are less structurally well-defined, they still constitute promising catalyst candidates as tunable and synthetically accessible materials.

Electropolymerization of metal porphyrins and phthalocyanines from their amine-containing analogues has been generally studied and reported [201, 202]. These polymer films are thought to be formed via an oxidative, polyaniline-type mechanism. Several studies have used these films for ECR. Heterogenized CuPc monomers

and polymers tested in methanol electrolyte were found to produce methyl formate and CO [203]. However, with current knowledge about demetallation of CuPc at reductive potentials [42], demetallation of CuPc to form Cu nanoparticles may have also occurred. Electropolymerized CoTAPP films were reported to reduce CO_2 to CO with 64.9% FE in ionic-liquid electrolytes [204]. However, another study reported similar electropolymerized films of cobalt tetraamino phthalocyanine ($CoPc(NH_2)_4$) that produced exclusively formic acid in perchloric acid electrolytes [205]. The latter is an unexpected result because monomeric CoPcs, just like CoTPPs, are known to produce almost exclusively CO [33]. The authors surmised that this unusual selectivity could be due to a geometric or electronic property of the polymer film. The authors also noted that morphology of the electropolymerized films was highly condition-dependent, which is consistent with what is generally known about the electropolymerization of aniline to polyaniline [206]. This variability makes interpretation of results across different studies difficult, since changes to the morphology or oxidation state of the polyaniline-like film due to changes in polymerization or testing conditions can be difficult to characterize but could cause important differences in catalytically relevant material properties.

Polymers of CoPc have been directly grown onto CNTs via *in-situ* growth (Fig. 23(a)) [73]. The electrochemically active concentration of Co, estimated from CV charge integration, was estimated to be about 14.5% of the total deposited Co sites. Notably, this number is larger than the percentage of active sites reported for COF-367-Co (8%) [83]. With this material, the authors were able to achieve current densities of 50 mA/cm^2 at −0.6 V vs. RHE, which translated to a TOF_{CO} of 1.36 s^{-1}. Notably, this number is about an order of magnitude lower than what has been reported for CoPc monomers [57]. From electrokinetic (Tafel slope of 121 mV/dec) and DFT studies, the authors concluded that the mechanism and rate of CO_2 reduction at the phthalocyanine metal centers was unaffected by polymerization onto CNTs. The main advantage of such a system was to improve the exposure of CoPc active sites while maintaining high electrical conductivity throughout the material.

The role of polymer defects in promoting catalyst activity has also been investigated [207]. CoPc-based polymers with defects (D-P-CoPc) and without defects (P-CoPc) (Fig. 23(b)) were compared for ECR, and presence of defects enhanced catalytic activity by about two-fold. Interestingly, the calculated TOF_{CO} at electrochemically active Co sites (as estimated by CV integration) for D-P-CoPc (0.11 s^{-1}) was also higher than that of P-CoPc (0.055 s^{-1}), implying that the Co active sites were intrinsically more active in the defective CoPc polymer. The authors generally ascribed this phenomenon to a modulated electronic structure of the material caused by the defects. This result is surprising given that the defects in this material were essentially nodes of incomplete polymerization, and most studies using tetrapyrrole-derived polymers, including several works reviewed above, typically assume that the intrinsic active site activity is not affected by the degree of polymerization of the macrocycle [73, 186]. Thus, these conflicting results and interpretations highlight the need for careful deconvolution of intrinsic activity and reactant transport effects that affect the measured performance of these 3D materials.

FeTPP was incorporated into porous organic cages (POCs) prior to deposition on a substrate (Fig. 23(c)) as another strategy for avoiding aggregation [208]. When depositing FeTPP POCs with 6.78×10^{-9} mol of Fe onto CNT-coated glassy carbon, the authors found that 54.6% of the deposited Fe centers were electrochemically active for the POC material (from CV integration), compared to 36.9% of the Fe centers for similarly deposited FeTPP monomers. Interestingly, as reviewed above, the authors in Ref. [186] estimated the coverage for a single monolayer of a similar molecule, $FeTCO_2PP$,

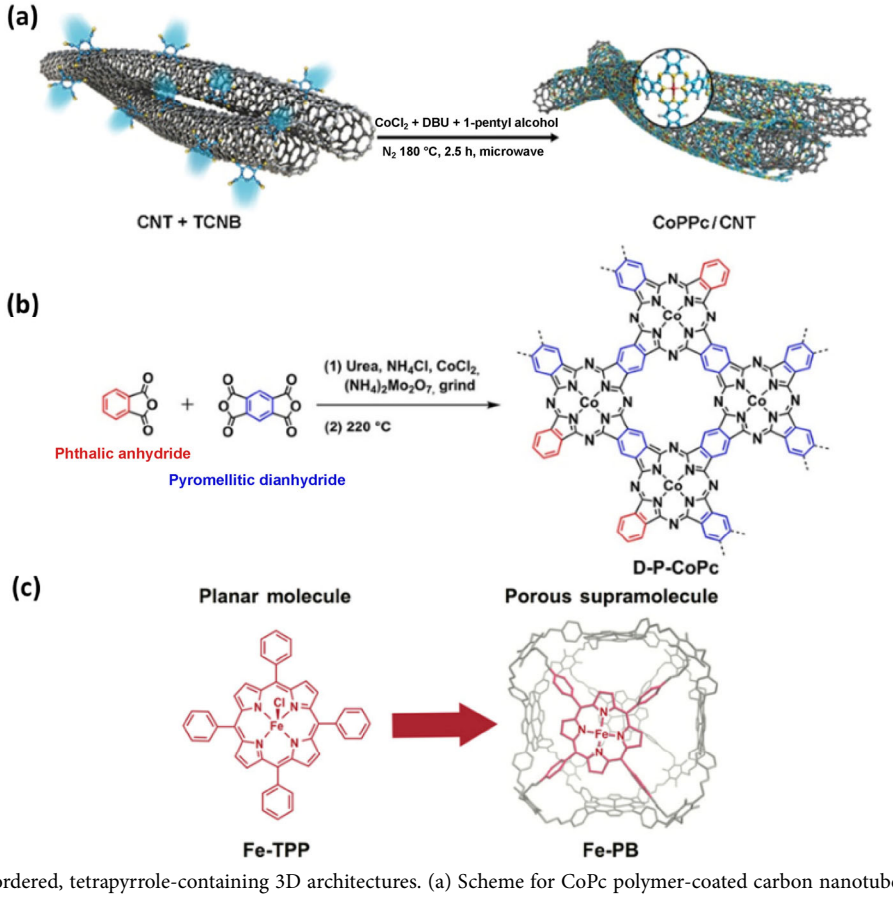

Figure 23 Schematics of less ordered, tetrapyrrole-containing 3D architectures. (a) Scheme for CoPc polymer-coated carbon nanotubes (reprinted with permission from Ref. [73], © Cell Press 2017). (b) Defect-containing CoPc polymers, with defect moieties highlighted in red (reprinted with permission from Ref. [207], © Wiley-VCH 2018. (c) FeTPP-based porous organic cage (reprinted with permission from Ref. [208], © Wiley-VCH 2018).

to be only 7×10^{-11} mol/cm^2. With the FeTPP POCs, the authors were able to achieve a current density of 0.49 mA/cm^2 at −0.63 V vs. RHE. This j_{CO} translated to a TOF_{CO} of 1.74 s^{-1}, which was notably higher than the TOF_{CO} of 0.94 s^{-1} that the authors reported for deposited FeTPP monomers. This result also implied that incorporation of FeTPP into 3D POC structures altered the intrinsic reactivity at the FeTPP active site.

As an alternative strategy for avoiding aggregation when depositing high loadings of molecular complexes, the cationic porphyrin iron tetra-(4-N,N,N-trimethylanilinium) porphyrin chloride (FeTMAPCl) was incorporated into 3D graphene hydrogels via reduction with LCGO (Fig. 24) [209]. Evidence of strong π–π and electrostatic interactions between FeTMAP and LCGO were observed via UV–vis and Raman spectroscopy. The coverage of active sites, estimated from CV integration, was 4.2×10^{-9} mol/cm^2. The catalyst was found to be active for ECR at low overpotentials, achieving a current density of 0.42 mA/cm^2 at −0.39 V vs. RHE, which translated to a TOF_{CO} of 0.5 s^{-1}. This value is higher than what has been reported for monomeric FeTMAP [177].

A number of other works have also polymerized non-tetrapyrrolic molecular catalysts into electrocatalytic materials [210–213]. Additionally, CoPc derivatives have been incorporated into polymers of intrinsic microporosity for thermal catalysis [214]. In the context of polymerized metal tetrapyrroles for ECR as reviewed above, significant progress has been made in designing diverse architectures that allow for improved exposure of catalytic active sites at higher loadings. The amorphous nature of polymers has made understanding the effects of polymer chemical composition and morphology on active site activity, number of accessible active sites, and transport within the material an active challenge.

9 Best practices for data reporting

To continue to facilitate rational catalyst design, the deconvolution of intrinsic activity, catalyst aggregation, and mass transport must be performed. A major problem that appears persistent in the literature is the presence of catalyst aggregation, which impedes an understanding of whether a catalyst modification changes the intrinsic activity of the active site or the number of exposed active sites. Measured TOFs are especially sensitive to the degree of catalyst aggregation and can change by orders of magnitude as a result. Performing kinetic measurements at current densities well below (< 10%) the transport-limited current is important as well; changes in interfacial species concentrations due to insufficient mass transport make electrokinetic data difficult to reliably interpret, as reflected in Tafel slopes above 120 mV/dec, assuming the typical transfer coefficient value of 0.5.

As the number of studies on immobilized molecular catalysts for ECR increases, a growing need will be to develop standardized reporting procedures to enable facile and reliable comparisons among reported catalysts. Such standardized reporting procedures have already been developed for OER and HER [215, 216]. Currently, most heterogeneous molecular catalysts are compared based on data at a single potential, and often these data are not reported at the same potential. An issue here is that under kinetically controlled conditions, the current density is exponentially sensitive to the potential, so accurately comparing the activities of catalysts evaluated at different potentials can be challenging. Measuring and reporting the intrinsic kinetic parameters of a catalyst provides a more robust way to compare catalysts. In the homogeneous ECR literature, such benchmarking protocols have been established in the case of Tafel kinetics, where reporting the Tafel slope and TOF extrapolated to zero overpotential (TOF_0) can characterize the performance of a molecular catalyst [60, 217]. At zero overpotential, the rates of the forward and reverse reactions are equal (no net current), but these rates are nonzero, which is why TOF_0 is a nonzero value. The Tafel slope and TOF_0 are ideal metrics because they should be the same regardless of the type of electrochemical cell used, enabling more consistent comparison across research groups. Given that many reported heterogeneous molecular catalysts have linear Tafel plots, the benchmarking for homogeneous ECR catalysts could inspire methods for heterogeneous ones. As previously mentioned, taking appropriate precautions to ensure aggregation and mass transport are minimized is essential to reporting accurate intrinsic kinetic parameters.

The measurement and documentation of intrinsic catalytic

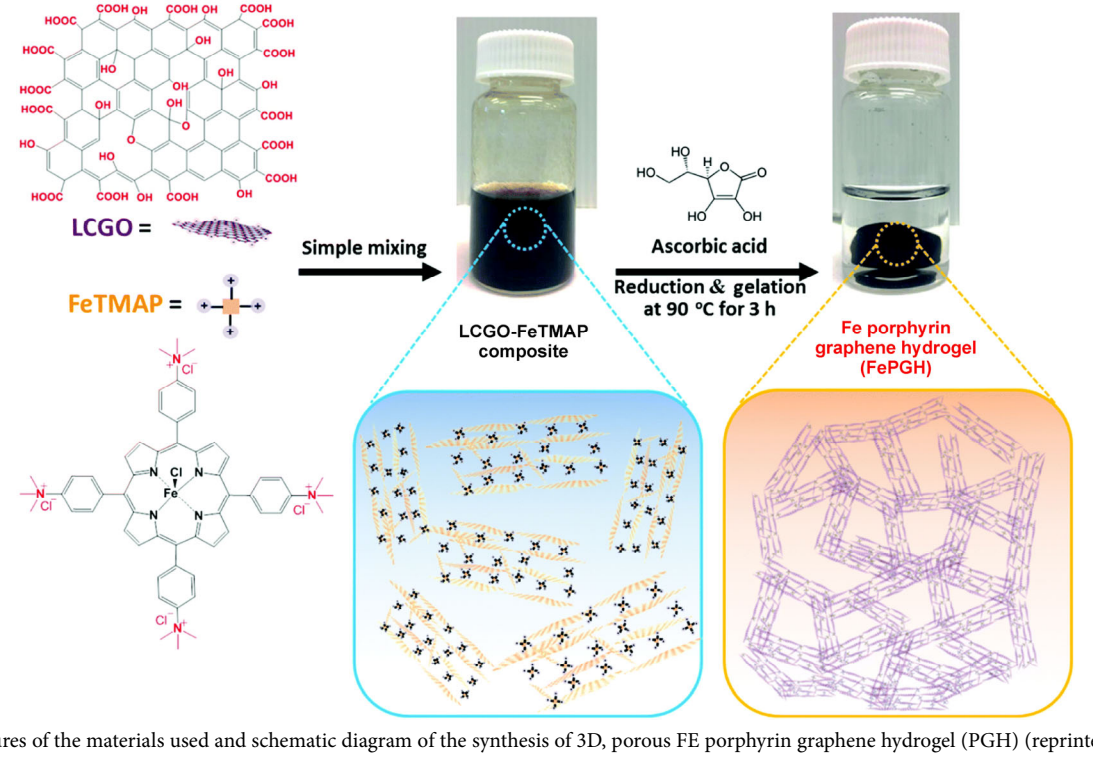

Figure 24 Structures of the materials used and schematic diagram of the synthesis of 3D, porous FE porphyrin graphene hydrogel (PGH) (reprinted with permission from Ref. [209], © Royal Society of Chemistry 2019).

parameters as well as reaction orders enables the construction of empirical rate laws. As discussed earlier, these rate laws can provide mechanistic insights into the nature of the RDS and the steps before it. These rate laws are also practical in that they can facilitate design of larger-scale electrochemical reactors by combining them with mass-transport models in order to predict and optimize cell design [76, 218–220]. Constructing electrochemical rate laws should therefore be a goal of experimental studies seeking to understand the catalytic behavior of ECR catalysts from mechanistic, comparability, and practical perspectives.

An additional metric that has practical importance is the energy efficiency (EE) of the catalyst [100, 138, 209]. Many definitions of the energy efficiency exist, which hampers consistent comparison across studies. Some reports have used a half-cell energy efficiency to isolate the EE of the catalyst under investigation [100]. However, the EE defined in this way is sensitive to the reference electrode used to define the half-cell potentials, so it is not an absolute metric. Typically, the definitions of EE assume that CO is a desired product, yet for syngas applications, both the H_2 and CO produced would be valuable, so a more representative energy efficient calculation would involve the combined FE of CO and H_2. Other reports have used the entire applied cell voltage to calculate energy efficiency [85], but the EE defined in this manner incorporates the anodic catalyst's efficiency as well as the conductivity of the electrolyte, so it is not entirely reflective of the ECR catalyst. Moreover, the EE is dependent on potential and is difficult to compare accurately between reported values at different potentials. It can be biased toward measurements at lower overpotentials and does not have any explicit consideration of how active a catalyst is, only its selectivity. A similar metric that is more absolute is the energy loss, which can be calculated as the overpotential of each product multiplied by its current density. Nonetheless, this metric can be sensitive to the mass transport in the system, as the pH at the interface and therefore the actual overpotential can differ from those values in the bulk electrolyte. Given the difficulties with measuring interfacial pH, the energy loss may be difficult to accurately calculate for the catalyst under investigation. Ultimately, reporting and comparing energy-based metrics for ECR catalysts can suffer from biases created by differences in mass transport, electrolyte conductivity, and choice of anodic catalyst, so such metrics may not be the most suitable for the purpose of catalyst comparison.

An even more difficult quantity to compare across studies is catalyst stability. Usually, catalyst stability is reported as a TON after a given amount of time with an occasional quantification of the degree of decay over that timespan. Because studies often measure for different timespans, long-term stability comparisons become difficult. In addition, many stability tests show little to no decay, so the true usable lifespan of the catalyst remains unknown. For practical implementation, thousands of hours are likely to be required for these catalysts, but testing for that long can be cumbersome. For homogeneous molecular catalysts, a simple first-order decay model has been proposed to quantify the deactivation of the catalyst [60]. While this first-order decay model may not apply to every catalyst, it does provide a starting point to begin quantifying catalyst decay in a manner that is conducive to comparison across studies.

Having an understanding of the RDS from experimental data allows for a more rigorous comparison with theoretical calculations. At their current stage, most computational efforts seek to understand the mechanism of a reaction by qualitative agreement with experiment. Often, good agreement is assumed if the calculated thermodynamic limiting potential is within a few hundred millivolts of an experimental onset potential or if two catalysts are being compared, the less active catalyst has a more unfavorable reaction pathway. These are necessary conditions for the theoretical model to be valid, but they are not sufficient and do not have to agree with all aspects of the experimental data. A qualitatively accurate theoretical model should be able to predict an RDS that is in agreement with electrokinetic data from experiments, but this comparison is frequently not made. Given the difficulties of quantum chemical calculations on many molecular catalysts and the mechanistic disagreement in the literature, we recommend comparison to reliable experimental information regarding the RDS as a key validation step in ensuring a theoretical model is appropriately describing the various reaction pathways on the catalyst.

10 Conclusions and future outlook

The electrocatalytic activity of a molecular complex is typically closely tied to its metal center. For phthalocyanines and porphyrins, many metal centers have been investigated, and cobalt appears to be the most active and selective toward CO for immobilized catalysts. Formate has been produced from various p-block metals including In, Sn, and Pb. The metal center may not be stable under the reductive voltages needed to drive ECR, leading to the formation of metallic nanoclusters or metal-center exchanges. In some cases, the catalysis can be mediated by the ligand for a redox-inactive metal center. While some theoretical insights have emerged regarding electronic structure and binding energies of intermediates to rationalize observed products and their associated rates, DFT methods can have difficulty accurately describing the electronic structures of these molecules. Future work will need to examine *in situ* the oxidation state and coordination number of metals that are susceptible to reduction during ECR to confirm the integrity of the molecular catalyst. If demetallation is occurring, a possibility exists to use organometallic complexes as precursors to highly dispersed metallic nanoclusters, which can increase the atomic utilization of precious metals such as gold.

In order to compare catalysts and optimize their performances, measurements of their intrinsic activities are needed. Catalyst aggregation, favored by intermolecular π–π interactions, can block or impede the transport of reactants to active sites. Calculated TOFs can be orders of magnitude lower in the presence of aggregation if based on the total amount of catalyst loaded; estimating active catalyst from redox peaks can partly alleviate this issue, although observing these redox peaks is not always possible. Under fully dispersed conditions, the TOF should not depend on the amount of catalyst deposited, allowing for a simple, empirical way to know when aggregation has been minimized. The experimental catalyst deposition protocol is important in this regard. For example, catalyst aggregation can be severely increased if the catalyst is deposited from a solvent in which it is poorly soluble. More effort needs to be taken to ensure molecular catalysts are tested under aggregation-free conditions to maximize the accuracy of measured TOFs.

Understanding the mechanism of ECR on heterogenized molecular catalysts is important for rational catalyst design and development of kinetic rate laws. Electrokinetic measurements, which include Tafel slopes and reaction orders, provide a means to develop a rate law while also gaining mechanistic insight. However, these experiments must be done under proper conditions by, for instance, ensuring no mass transport limitations and working on an absolute potential scale. These mechanistic experiments also have practical relevance in that the kinetic rate laws can be incorporated into models that predict overall electrolyzer performance. Voltammetry and *in-situ* spectroscopy provide alternative experimental probes into mechanisms. Regarding oxidation states, the degree of electronic coupling between the catalyst and electrode may dictate whether redox peaks are observed; for physically adsorbed catalysts, more work is needed to elucidate whether the redox state of the metal center actually changes during catalysis, as conflicting reports exist in the literature.

DFT calculations have also been used to gain insight into ECR

mechanisms on cobalt-based tetrapyrroles. These calculations have shown the ECR mechanism is likely dependent on pH. Based on the lack of consensus on mechanism, more effort may be warranted in developing computational strategies that contain the appropriate balance of method and model accuracy [221] to accurately simulate the electrochemical interface. In terms of the model, computing electrochemical activation barriers, including the catalyst support, and incorporating the electric double layer are all relevant physics that future studies on ECR mechanisms may need to incorporate [126, 222–224]. Future efforts may lead to reconciliation of experimentally and theoretically predicted RDSs.

One of the attractive features of using molecular catalysts is the ability to tune them by changing the substituents on the ligand. For CoTPP derivatives, TOF_{CO} values under minimized aggregation were correlated to the electron-donating character of the ligands via DFT Mulliken charges, $Co^{I/II}$ redox potentials, and Hammett σ parameters. By analyzing the substituent effects in this rigorous way, the observation of separate through-bond inductive and electrostatic effects on the TOF_{CO} were observed, providing a more complete picture on how to rationally design active catalysts. However, more such robust studies are needed in this space, especially for CoPc where reports have shown that both electron-withdrawing and electron-donating groups enhanced activity. Certain ligand modifications, such as using a more saturated bacteriochlorin macrocyle instead of a porphyrin, can also be used to tune and improve catalyst stability, though this design strategy needs to be tested for heterogenized molecular catalysts.

A significant amount of attention has been devoted to how molecular catalysts have been immobilized and on the nature of the support. Carbon nanomaterials, especially CNTs, have been frequently cited as improving current densities, FEs, and stabilities for ECR for porphyrins and phthalocyanines. Oft-cited reasons for these improvements include stronger π–π interactions with the molecular catalyst (and for charged molecules, electrostatic interactions), higher surface area, and higher electronic conductivity. Studies aimed at deconvoluting aggregation effects will provide additional insights into the degree to which each of these factors contributes to improved performance. Polymer encapsulation has been shown to improve stability and control the reaction environment around the catalyst, enabling increased selectivity toward ECR. In this context, more work needs to be done to fully deconvolute the effects of species transport, axial coordination, and second sphere hydrogen bond/proton relays to understand how to design improved polymer coatings. Covalent grafting has also proved a valuable method to improve catalyst stability and reduce aggregation, with a need to isolate intrinsic activity enhancements from improved catalyst dispersion in future work. Elucidating the fundamental effects of these modifications will enable rational electrode design.

An alternative strategy to increase the number of active sites while maintaining tunability is to synthesize extended, 3D materials containing atomically precise active sites which resemble their molecular analogs. Generally, many of the reviewed studies were able to immobilize molecular complexes at higher effective loadings while maintaining catalysis characteristics similar to the monomeric analogues. Following these pioneering studies, strategies for decoupling the various complex phenomena that occur within these materials are being developed. On a molecular length scale, the electronic structure of the active site, which may or may not be affected by incorporation into an extended network, affects intrinsic activity. On a microscopic length scale, the morphology and functionalities installed in various materials affect exposure of active sites, reactant availability, and electronic conductivity. It will be particularly important to develop testing procedures and characterization techniques that can decouple the effects of these various factors.

Eventually, the relatively well-defined architectures and abundant design handles of these materials could enable even more complex and interesting catalysis. Borrowing more complex design principles from biology such as "catalytic pocket" type motifs that use functionality many bonds away from the active site to stabilize reactive intermediates or designing catalytic networks, in which multiple types of active sites are incorporated into one material and work in concert with one another, may become eventual possibilities. These prospects are all exciting and emerge once we begin to understand and decouple the various phenomena that affect activity within these materials.

Aside from being interesting from a fundamental perspective, some molecular catalysts have shown potential for practical, large-scale electrolysis. A recent study constructed a microflow cell with a GDE cathode to facilitate CO_2 mass transport [225]. In a basic 1 M KOH electrolyte, a $CoPc(CN)_8$/CNT cathodic catalyst coupled with a CoO_x/CNT anodic catalyst was able to produce CO at 32–36 mA/cm^2 stably over 10 h at a full-cell overpotential of 0.66 V. The GDE architecture and flowing electrolyte reduced mass transport limitations, allowing for higher current densities. However, j_{CO} maxed out around 80 mA/cm^2 before a sharp decrease in j_{CO} was observed, and more work will be needed to increase j_{CO} to match those using Ag catalysts [226–228]. These results are promising and demonstrate that heterogeneous molecular catalysts could be viable catalysts for large-scale CO_2 electrolyzers.

An underexplored area of study for molecular ECR catalysts is tolerance to gas feed impurities. As avoiding CO_2 purification prior to utilizing it in ECR may prove more economically viable [184, 229–231], molecular catalysts which can maintain ECR activity in the presence of common gas feed impurities are desirable. Efforts to understand the impact of O_2 impurities on HER and metallic ECR catalysis have been undertaken and may provide a foundation for similar ECR studies on molecular catalysts [232, 233]. Additionally, studying the effects of NO_x, SO_x, and particulates will also be important. Thus far, work in the vein of molecular catalysis for dilute CO_2 streams has only been conducted using inert gases as the balance [234].

As heterogenized molecular catalysts become increasingly studied for ECR, a systematic, reliable, and reproducible way needs to be established to report results. Ideally, such a framework would involve reporting intrinsic parameters such as Tafel slopes, order dependencies, and TOF_0 to enable accurate activity comparisons. Other metrics such as aggregation extent and stability are also important, but widely accepted intrinsic metrics for these are currently lacking. Whether molecular catalysts are used directly in practical electrolyzers or studied to provide mechanistic insights and design guidelines for other classes of ECR catalysts, having a robust set of decoupled, intrinsic data from fundamental studies will be necessary to efficiently reach these goals and effect the positive change on society such technology promises.

Acknowledgements

We gratefully acknowledge financial support from Cenovus Energy. N. C. was supported by a NSF Graduate Research Fellowship.

Electronic Supplementary Material: Supplementary material (performance and stability data compiled from the literature as well as discussion of measuring order-dependencies at constant potential vs. RHE) is available in the online version of this article at https://doi.org/10.1007/s12274-019-2403-y

References

[1] IPCC. Summary for policymakers. In *Climate Change 2014: Impacts, Adaptation, and Vulnerability. Part A: Global and Sectoral Aspects. Contribution of Working Group II to the Fifth Assessment Report of the Intergovernmental Panel on Climate Change*; Field, C. B.; Barros, V. R.; Dokken, D. J.; Mach, K. J.; Mastrandrea, M. D.; Bilir, T. E.; Chatterjee,

M.; Ebi, K. L.; Estrada, Y. O.; Genova, R. C. et al., Eds.; Cambridge University Press: Cambridge, UK and New York, 2014.
[2] Spurgeon, J. M.; Kumar, B. A comparative technoeconomic analysis of pathways for commercial electrochemical CO_2 reduction to liquid products. *Energy Environ. Sci.* **2018**, *11*, 1536–1551.
[3] Schiffer, Z. J.; Manthiram, K. Electrification and decarbonization of the chemical industry. *Joule* **2017**, *1*, 10–14.
[4] Kuhl, K. P.; Hatsukade, T.; Cave, E. R.; Abram, D. N.; Kibsgaard, J.; Jaramillo, T. F. Electrocatalytic conversion of carbon dioxide to methane and methanol on transition metal surfaces. *J. Am. Chem. Soc.* **2014**, *136*, 14107–14113.
[5] Chen, Y. H.; Li, C. W.; Kanan, M. W. Aqueous CO_2 reduction at very low overpotential on oxide-derived Au nanoparticles. *J. Am. Chem. Soc*. **2012**, *134*, 19969–19972.
[6] Chen, Y. H.; Kanan, M. W. Tin oxide dependence of the CO_2 reduction efficiency on tin electrodes and enhanced activity for tin/tin oxide thin-film catalysts. *J. Am. Chem. Soc*. **2012**, *134*, 1986–1989.
[7] Jiang, K.; Siahrostami, S.; Zheng, T. T.; Hu, Y. F.; Hwang, S.; Stavitski, E.; Peng, Y. D.; Dynes, J.; Gangisetty, M.; Su, D. et al. Isolated Ni single atoms in graphene nanosheets for high-performance CO_2 reduction. *Energy Environ. Sci*. **2018**, *11*, 893–903.
[8] Pan, Y.; Lin, R.; Chen, Y. J.; Liu, S. J.; Zhu, W.; Cao, X.; Chen, W. X.; Wu, K. L.; Cheong, W. C.; Wang, Y. et al. Design of single-atom Co–N_5 catalytic site: A robust electrocatalyst for CO_2 reduction with nearly 100% CO selectivity and remarkable stability. *J. Am. Chem. Soc*. **2018**, *140*, 4218–4221.
[9] Costentin, C.; Passard, G.; Robert, M.; Savéant, J. M. Ultraefficient homogeneous catalyst for the CO_2-to-CO electrochemical conversion. *Proc. Natl. Acad. Sci. USA* **2014**, *111*, 14990–14994.
[10] Costentin, C.; Robert, M.; Savéant, J. M.; Tatin, A. Efficient and selective molecular catalyst for the CO_2-to-CO electrochemical conversion in water. *Proc. Natl. Acad. Sci. USA* **2015**, *112*, 6882–6886.
[11] Manbeck, G. F.; Fujita, E. A review of iron and cobalt porphyrins, phthalocyanines and related complexes for electrochemical and photochemical reduction of carbon dioxide. *J. Porphyr. Phthalocya.* **2015**, *19*, 45–64.
[12] Varela, A. S.; Ju, W.; Strasser, P. Molecular nitrogen–carbon catalysts, solid metal organic framework catalysts, and solid metal/nitrogen-doped carbon (MNC) catalysts for the electrochemical CO_2 reduction. *Adv. Energy Mater*. **2018**, *8*, 1703614.
[13] Costamagna, J. A.; Isaacs, M.; Aguirre, M. J.; Ramírez, G.; Azocar, I. Electroreduction of CO_2 catalyzed by metallomacrocyclics. In *N_4-Macrocyclic Metal Complexes*; Zagal, J. H.; Bedioui, F.; Dodelet, J. P., Eds.; Springer: New York, 2006; pp 191–254.
[14] Inglis, J. L.; MacLean, B. J.; Pryce, M. T.; Vos, J. G. Electrocatalytic pathways towards sustainable fuel production from water and CO_2. *Coord. Chem. Rev.* **2012**, *256*, 2571–2600.
[15] Sun, C. F.; Gobetto, R.; Nervi, C. Recent advances in catalytic CO_2 reduction by organometal complexes anchored on modified electrodes. *New J. Chem.* **2016**, *40*, 5656–5661.
[16] Hori, Y. Electrochemical CO_2 reduction on metal electrodes. In *Modern Aspects of Electrochemistry*; Vayenas, C. G.; White, R. E.; Gamboa-Aldeco, M. E., Eds.; Springer: New York, 2008; pp 89–189.
[17] Li, F. W.; MacFarlane, D. R.; Zhang, J. Recent advances in the nanoengineering of electrocatalysts for CO_2 reduction. *Nanoscale* **2018**, *10*, 6235–6260.
[18] Pander III, J. E.; Ren, D.; Huang, Y.; Loo, N. W. X.; Hong, S. H. L.; Yeo, B. S. Understanding the heterogeneous electrocatalytic reduction of carbon dioxide on oxide-derived catalysts. *ChemElectroChem* **2018**, *5*, 219–237.
[19] Strasser, P.; Gliech, M.; Kuehl, S.; Moeller, T. Electrochemical processes on solid shaped nanoparticles with defined facets. *Chem. Soc. Rev.* **2018**, *47*, 715–735.
[20] Wu, J. J.; Sharifi, T.; Gao, Y.; Zhang, T. Y.; Ajayan, P. M. Emerging carbon-based heterogeneous catalysts for electrochemical reduction of carbon dioxide into value-added chemicals. *Adv. Mater.* **2019**, *31*, 1804257.
[21] Bonin, J.; Maurin, A.; Robert, M. Molecular catalysis of the electrochemical and photochemical reduction of CO_2 with Fe and Co metal based complexes. Recent advances. *Coord. Chem. Rev.* **2017**, *334*, 184–198.
[22] Costentin, C.; Robert, M.; Savéant, J. M. Catalysis of the electrochemical reduction of carbon dioxide. *Chem. Soc. Rev.* **2013**, *42*, 2423–2436.
[23] Zhang, X.; Wu, Z. S.; Zhang, X.; Li, L. W.; Li, Y. Y.; Xu, H. M.; Li, X. X.; Yu, X. L.; Zhang, Z.S.; Liang, Y. Y. et al. Highly selective and active CO_2 reduction electrocatalysts based on cobalt phthalocyanine/carbon nanotube hybrid structures. *Nat. Commun*. **2017**, *8*, 14675.
[24] Oh, S.; Gallagher, J. R.; Miller, J. T.; Surendranath, Y. Graphite-conjugated rhenium catalysts for carbon dioxide reduction. *J. Am. Chem. Soc*. **2016**, *138*, 1820–1823.
[25] Hu, X. M.; Rønne, M. H.; Pedersen, S. U.; Skrydstrup, T.; Daasbjerg, K. Enhanced catalytic activity of cobalt porphyrin in CO_2 electroreduction upon immobilization on carbon materials. *Angew. Chem., Int. Ed.* **2017**, *56*, 6468–6472.
[26] Bagger, A.; Ju, W.; Varela, A. S.; Strasser, P.; Rossmeisl, J. Electrochemical CO_2 reduction: A classification problem. *ChemPhysChem* **2017**, *18*, 3266–3273.
[27] Pan, F. P.; Deng, W.; Justiniano, C.; Li, Y. Identification of champion transition metals centers in metal and nitrogen-codoped carbon catalysts for CO_2 reduction. *Appl. Catal. B Environ.* **2018**, *226*, 463–472.
[28] Chen, L. J.; Guo, Z. G.; Wei, X. G.; Gallenkamp, C.; Bonin, J.; Anxolabéhère-Mallart, E.; Lau, K. C.; Lau, T. C.; Robert, M. Molecular catalysis of the electrochemical and photochemical reduction of CO_2 with earth-abundant metal complexes. Selective production of CO vs HCOOH by switching of the metal center. *J. Am. Chem. Soc.* **2015**, *137*, 10918–10921.
[29] Meshitsuka, S.; Ichikawa, M.; Tamaru, K. Electrocatalysis by metal phthalocyanines in the reduction of carbon dioxide. *J. Chem. Soc. Chem. Commun.* **1974**, 158–159.
[30] Kapusta, S.; Hackerman, N. Carbon dioxide reduction at a metal phthalocyanine catalyzed carbon electrode. *J. Electrochem. Soc.* **1984**, *131*, 1511–1514.
[31] Tanabe, H.; Ohno, K. Electrocatalysis of metal phthalocyanine thin film prepared by the plasma-assisted deposition on a glassy carbon in the reduction of carbon dioxide. *Electrochim. Acta* **1987**, *32*, 1121–1124.
[32] Furuya, N.; Matsui, K. Electroreduction of carbon dioxide on gas-diffusion electrodes modified by metal phthalocyanines. *J. Electroanal. Chem. Interfacial Electrochem.* **1989**, *271*, 181–191.
[33] Furuya, N.; Koide, S. Electroreduction of carbon dioxide by metal phthalocyanines. *Electrochim. Acta* **1991**, *36*, 1309–1313.
[34] Sonoyama, N.; Kirii, M.; Sakata, T. Electrochemical reduction of CO_2 at metal-porphyrin supported gas diffusion electrodes under high pressure CO_2. *Electrochem. Commun.* **1999**, *1*, 213–216.
[35] Birdja, Y. Y.; Shen, J.; Koper, M. T. M. Influence of the metal center of metalloprotoporphyrins on the electrocatalytic CO_2 reduction to formic acid. *Catal. Today* **2017**, *288*, 37–47.
[36] Wu, Y. S.; Jiang, J. B.; Weng, Z.; Wang, M. Y.; Broere, D. L. J.; Zhong, Y. R.; Brudvig, G. W.; Feng, Z. X.; Wang, H. L. Electroreduction of CO_2 catalyzed by a heterogenized Zn-porphyrin complex with a redox-innocent metal center. *ACS Cent. Sci*. **2017**, *3*, 847–852.
[37] Mahmood, M. N.; Masheder, D.; Harty, C. J. Use of gas-diffusion electrodes for high-rate electrochemical reduction of carbon dioxide. II. Reduction at metal phthalocyanine-impregnated electrodes. *J. Appl. Electrochem.* **1987**, *17*, 1223–1227.
[38] Lawton, E. A. The thermal stability of copper phthalocyanine. *J. Phys. Chem.* **1958**, *62*, 384.
[39] Sabik, A.; Gołek, F.; Antczak, G. Thermal desorption and stability of cobalt phthalocyanine on Ag(100). *Appl. Surf. Sci.* **2018**, *435*, 894–902.
[40] Scardamaglia, M.; Struzzi, C.; Lizzit, S.; Dalmiglio, M.; Lacovig, P.; Baraldi, A.; Mariani, C.; Betti, M. G. Energetics and hierarchical interactions of metal-phthalocyanines adsorbed on graphene/Ir(111). *Langmuir* **2013**, *29*, 10440–10447.
[41] Magdesieva, T. V.; Butin, K. P.; Yamamoto, T.; Tryk, D. A.; Fujishima, A. Lutetium monophthalocyanine and diphthalocyanine complexes and lithium naphthalocyanine as catalysts for electrochemical CO_2 reduction. *J. Electrochem. Soc.* **2003**, *150*, E608–E612.
[42] Weng, Z.; Wu, Y. S.; Wang, M. Y.; Jiang, J. B.; Yang, K.; Huo, S. J.; Wang, X. F.; Ma, Q.; Brudvig, G. W.; Batista, V. S. et al. Active sites of copper-complex catalytic materials for electrochemical carbon dioxide reduction. *Nat. Commun.* **2018**, *9*, 415.
[43] Weng, Z.; Jiang, J. B.; Wu, Y. S.; Wu, Z. S.; Guo, X. T.; Materna, K. L.; Liu, W.; Batista, V. S.; Brudvig, G. W.; Wang, H. L. Electrochemical CO_2 reduction to hydrocarbons on a heterogeneous molecular Cu catalyst in aqueous solution. *J. Am. Chem. Soc.* **2016**, *138*, 8076–8079.
[44] Kusama, S.; Saito, T.; Hashiba, H.; Sakai, A.; Yotsuhashi, S. Crystalline copper(II) phthalocyanine catalysts for electrochemical reduction of carbon dioxide in aqueous media. *ACS Catal.* **2017**, *7*, 8382–8385.
[45] Cheng, Y.; Veder, J. P.; Thomsen, L.; Zhao, S. Y.; Saunders, M.; Demichelis, R.; Liu, C.; De Marco, R.; Jiang, S. P. Electrochemically substituted metal phthalocyanines, e-MPc (M = Co, Ni), as highly active and selective

catalysts for CO_2 reduction. *J. Mater. Chem. A* **2018**, *6*, 1370–1375.
[46] Ruan, C. Y.; Mastryukov, V.; Fink, M. Electron diffraction studies of metal phthalocyanines, MPc, where M = Sn, Mg, and Zn (reinvestigation). *J. Chem. Phys.* **1999**, *111*, 3035–3041.
[47] Kaeffer, N.; Chavarot-Kerlidou, M.; Artero, V. Hydrogen evolution catalyzed by cobalt diimine–dioxime complexes. *Acc. Chem. Res.* **2015**, *48*, 1286–1295.
[48] Lee, C. W.; Cho, N. H.; Yang, K. D.; Nam, K. T. Reaction mechanisms of the electrochemical conversion of carbon dioxide to formic acid on tin oxide electrodes. *ChemElectroChem* **2017**, *4*, 2130–2136.
[49] Lee, C. H.; Kanan, M. W. Controlling H^+ vs. CO_2 reduction selectivity on Pb electrodes. *ACS Catal.* **2015**, *5*, 465–469.
[50] Luo, W.; Xie, W.; Li, M.; Züttel, A. 3D hierarchical porous indium catalyst for highly efficient electroreduction of CO_2. *J. Mater. Chem. A* **2019**, *7*, 4505–4515.
[51] Zhu, W. J.; Zhang, L.; Yang, P. P.; Hu, C. L.; Luo, Z. B.; Chang, X. X.; Zhao, Z. J.; Gong, J. L. Low-coordinated edge sites on ultrathin palladium nanosheets boost carbon dioxide electroreduction performance. *Angew. Chem., Int. Ed.* **2018**, *57*, 11544–11548.
[52] Hori, Y.; Wakebe, H.; Tsukamoto, T.; Koga, O. Electrocatalytic process of CO selectivity in electrochemical reduction of CO_2 at metal electrodes in aqueous media. *Electrochim. Acta* **1994**, *39*, 1833–1839.
[53] Wallace, A. J.; Williamson, B. E.; Crittenden, D. L. CASSCF-based explicit ligand field models clarify the ground state electronic structures of transition metal phthalocyanines (MPc; M = Mn, Fe, Co, Ni, Cu, Zn). *Can. J. Chem.* **2016**, *94*, 1163–1168.
[54] Brumboiu, I. E.; Prokopiou, G.; Kronik, L.; Brena, B. Valence electronic structure of cobalt phthalocyanine from an optimally tuned range-separated hybrid functional. *J. Chem. Phys.* **2017**, *147*, 044301.
[55] Jensen, F. *Introduction to Computational Chemistry*; John Wiley & Sons, Ltd: Chichester, 2007.
[56] Zhang, Z.; Xiao, J. P.; Chen, X. J.; Yu, S.; Yu, L.; Si, R.; Wang, Y.; Wang, S.; Meng, X. G.; Wang, Y. et al. Reaction mechanisms of well-defined metal–N_4 sites in electrocatalytic CO_2 reduction. *Angew. Chem., Int. Ed.* **2018**, *57*, 16339–16342.
[57] Zhu, M. H.; Ye, R. Q.; Jin, K.; Lazouski, N.; Manthiram, K. Elucidating the reactivity and mechanism of CO_2 electroreduction at highly dispersed cobalt phthalocyanine. *ACS Energy Lett.* **2018**, *3*, 1381–1386.
[58] Liu, J. H.; Yang, L. M.; Ganz, E. Efficient and selective electroreduction of CO_2 by single-atom catalyst two-dimensional TM-Pc monolayers. *ACS Sustainable Chem. Eng.* **2018**, *6*, 15494–15502.
[59] Göttle, A. J.; Koper, M. T. M. Determinant role of electrogenerated reactive nucleophilic species on selectivity during reduction of CO_2 catalyzed by metalloporphyrins. *J. Am. Chem. Soc.* **2018**, *140*, 4826–4834.
[60] Costentin, C.; Passard, G.; Savéant, J. M. Benchmarking of homogeneous electrocatalysts: Overpotential, turnover frequency, limiting turnover number. *J. Am. Chem. Soc.* **2015**, *137*, 5461–5467.
[61] Abe, T.; Imaya, H.; Yoshida, T.; Tokita, S.; Schlettwein, D.; Wöhrle, D.; Kaneko, M. Electrochemical CO_2 reduction catalysed by cobalt octacyanophthalocyanine and its mechanism. *J. Porphyr. Phthalocya.* **1997**, *1*, 315–321.
[62] Mizuguchi, J. π–π interactions of magnesium phthalocyanine as evaluated by energy partition analysis. *J. Phys. Chem. A* **2001**, *105*, 10719–10722.
[63] Bottari, G.; Ballesteros, B.; Collado, J. F.; Torres, T. Hydrogen-bonding and pi-stacking induced self-assembly of picolinic acid-substituted phthalocyanine derivatives. In *Proceedings of the 227th ECS Meeting*, Chicago, 2015, p 996.
[64] Boulatov, R.; Collman, J. P.; Shiryaeva, I. M.; Sunderland, C. J. Functional analogues of the dioxygen reduction site in cytochrome oxidase: Mechanistic aspects and possible effects of Cu_B. *J. Am. Chem. Soc.* **2002**, *124*, 11923–11935.
[65] Ghani, F.; Kristen, J.; Riegler, H. Solubility properties of unsubstituted metal phthalocyanines in different types of solvents. *J. Chem. Eng. Data* **2012**, *57*, 439–449.
[66] Cheng, Z. H.; Cui, N.; Zhang, H. X.; Zhu, L. J.; Xia, D. H. Synthesis and dimerization behavior of five metallophthalocyanines in different solvents. *Adv. Mater. Sci. Eng.* **2014**, *2014*, 914916.
[67] Choi, J.; Wagner, P.; Gambhir, S.; Jalili, R.; Macfarlane, D. R.; Wallace, G. G.; Officer, D. L. Steric modification of a cobalt phthalocyanine/graphene catalyst to give enhanced and stable electrochemical CO_2 reduction to CO. *ACS Energy Lett.* **2019**, *4*, 666–672.
[68] Shinagawa, T.; Garcia-Esparza, A. T.; Takanabe, K. Insight on Tafel slopes from a microkinetic analysis of aqueous electrocatalysis for energy conversion. *Sci. Rep.* **2015**, *5*, 13801.
[69] Zeng, Y.; Bai, P.; Smith, R. B.; Bazant, M. Z. Simple formula for asymmetric Marcus-Hush kinetics. *J. Electroanal. Chem.* **2015**, *748*, 52–57.
[70] Marcus, R. A. On the theory of electron-transfer reactions. VI. Unified treatment for homogeneous and electrode reactions. *J. Chem. Phys.* **1965**, *43*, 679–701.
[71] Bard, A. J.; Faulkner, L. R. *Electrochemical Methods: Fundamentals and Applications*, 2nd ed.; John Wiley & Sons, Inc.: New York, 2001.
[72] Zhu, M. H.; Yang, D. T.; Ye, R. Q.; Zeng, J.; Corbin, N.; Manthiram, K. Inductive and electrostatic effects on cobalt porphyrins for heterogeneous electrocatalytic carbon dioxide reduction. *Catal. Sci. Technol.* **2019**, *9*, 974–980.
[73] Han, N.; Wang, Y.; Ma, L.; Wen, J. G.; Li, J.; Zheng, H. C.; Nie, K. Q.; Wang, X. X.; Zhao, F. P.; Li, Y. F. et al. Supported cobalt polyphthalocyanine for high-performance electrocatalytic CO_2 reduction. *Chem* **2017**, *3*, 652–664.
[74] Wuttig, A.; Yoon, Y.; Ryu, J.; Surendranath, Y. Bicarbonate is not a general acid in Au-catalyzed CO_2 electroreduction. *J. Am. Chem. Soc.* **2017**, *139*, 17109–17113.
[75] Chlistunoff, J. RRDE and voltammetric study of ORR on pyrolyzed Fe/polyaniline catalyst. On the origins of variable tafel slopes. *J. Phys. Chem. C* **2011**, *115*, 6496–6507.
[76] Singh, M. R.; Clark, E. L.; Bell, A. T. Effects of electrolyte, catalyst, and membrane composition and operating conditions on the performance of solar-driven electrochemical reduction of carbon dioxide. *Phys. Chem. Chem. Phys.* **2015**, *17*, 18924–18936.
[77] Raciti, D.; Mao, M.; Park, J. H.; Wang, C. Mass transfer effects in CO_2 reduction on Cu nanowire electrocatalysts. *Catal. Sci. Technol.* **2018**, *8*, 2364–2369.
[78] Dunwell, M.; Yang, X.; Setzler, B. P.; Anibal, J.; Yan, Y. S.; Xu, B. J. Examination of near-electrode concentration gradients and kinetic impacts on the electrochemical reduction of CO_2 using surface-enhanced infrared spectroscopy. *ACS Catal.* **2018**, *8*, 3999–4008.
[79] Ryu, J.; Wuttig, A.; Surendranath, Y. Quantification of interfacial pH variation at molecular length scales using a concurrent non-faradaic reaction. *Angew. Chem., Int. Ed.* **2018**, *57*, 9300–9304.
[80] Harris, D. C. *Quantitative Chemical Analysis*, 7th ed.; W. H. Freeman and Company: New York, 2007.
[81] Weisenberger, S.; Schumpe, A. Estimation of gas solubilities in salt solutions at temperatures from 273 K to 363 K. *AIChE J.* **1996**, 42, 298–300.
[82] Schowen, R. L. Hydrogen bonds, transition-state stabilization, and enzyme catalysis. In *Isotope Effects in Chemistry and Biology*; Kohen, A.; Limbach, H. H., Eds.; CRC Press, Taylor & Francis Group: Boca Raton, Florida, USA, 2005; pp 765–792.
[83] Lin, S.; Diercks, C. S.; Zhang, Y. B.; Kornienko, N.; Nichols, E. M.; Zhao, Y. B.; Paris, A. R.; Kim, D.; Yang, P. D.; Yaghi, O. M. et al. Covalent organic frameworks comprising cobalt porphyrins for catalytic CO_2 reduction in water. *Science* **2015**, *349*, 1208–1213.
[84] Zhu, M. H.; Chen, J. C.; Huang, L. B.; Ye, R. Q.; Xu, J.; Han, Y. F. Covalently grafting cobalt porphyrin onto carbon nanotubes for efficient CO_2 electroreduction. *Angew. Chem., Int. Ed.* **2019**, *58*, 6595–6599.
[85] Morlanés, N.; Takanabe, K.; Rodionov, V. Simultaneous reduction of CO_2 and splitting of H_2O by a single immobilized cobalt phthalocyanine electrocatalyst. *ACS Catal.* **2016**, *6*, 3092–3095.
[86] Chebotareva, N.; Nyokong, T. Metallophthalocyanine catalysed electroreduction of nitrate and nitrite ions in alkaline media. *J. Appl. Electrochem.* **1997**, *27*, 975–981.
[87] Jackson, M. N.; Oh, S.; Kaminsky, C. J.; Chu, S. B.; Zhang, G. H.; Miller, J. T.; Surendranath, Y. Strong electronic coupling of molecular sites to graphitic electrodes via pyrazine conjugation. *J. Am. Chem. Soc.* **2018**, *140*, 1004–1010.
[88] Schmickler, W.; Santos, E. *Interfacial Electrochemistry*; Springer: Berlin, 2010.
[89] Lieber, C. M.; Lewis, N. S. Catalytic reduction of carbon dioxide at carbon electrodes modified with cobalt phthalocyanine. *J. Am. Chem. Soc.* **1984**, *106*, 5033–5034.
[90] Yoshida, T.; Kamato, K.; Tsukamoto, M.; Iida, T.; Schlettwein, D.; Wöhrle, D.; Kaneko, M. Selective electroacatalysis for CO_2 reduction in the aqueous phase using cobalt phthalocyanine/poly-4-vinylpyridine modified electrodes. *J. Electroanal. Chem.* **1995**, *385*, 209–225.
[91] Abe, T.; Yoshida, T.; Tokita, S.; Taguchi, F.; Imaya, H.; Kaneko, M. Factors

affecting selective electrocatalytic CO_2 reduction with cobalt phthalocyanine incorporated in a polyvinylpyridine membrane coated on a graphite electrode. *J. Electroanal. Chem.* **1996**, *412*, 125–132.

[92] Aga, H.; Aramata, A.; Hisaeda, Y. The electroreduction of carbon dioxide by macrocyclic cobalt complexes chemically modified on a glassy carbon electrode. *J. Electroanal. Chem*. **1997**, *437*, 111–118.

[93] Christensen, P. A.; Hamnett, A.; Muir, A. V. G. An *in-situ* FTIR study of the electroreduction of CO_2 by CoPc-coated edge graphite electrodes. *J. Electroanal. Chem. Interfacial Electrochem.* **1988**, *241*, 361–371.

[94] Atoguchi, T.; Aramata, A.; Kazusaka, A.; Enyo, M. Electrocatalytic activity of Co^{II} TPP-pyridine complex modified carbon electrode for CO_2 reduction. *J. Electroanal. Chem. Interfacial Electrochem.* **1991**, *318*, 309–320.

[95] Atoguchi, T.; Aramata, A.; Kazusaka, A.; Enyo, M. Cobalt(II)–tetraphenylporphyrin–pyridine complex fixed on a glassy carbon electrode and its prominent catalytic activity for reduction of carbon dioxide. *J. Chem. Soc. Chem. Commun.* **1991**, 156–157.

[96] Tanaka, H.; Aramata, A. Aminopyridyl cation radical method for bridging between metal complex and glassy carbon: Cobalt(II) tetraphenylporphyrin bonded on glassy carbon for enhancement of CO_2 electroreduction. *J. Electroanal. Chem.* **1997**, *437*, 29–35.

[97] Abe, T.; Taguchi, F.; Yoshida, T.; Tokita, S.; Schnurpfeil, G.; Wöhrle, D.; Kaneko, M. Electrocatalytic CO_2 reduction by cobalt octabutoxyphthalocyanine coated on graphite electrode. *J. Mol. Catal. A Chem.* **1996**, *112*, 55–61.

[98] Kornienko, N.; Zhao, Y. B.; Kley, C. S.; Zhu, C. H.; Kim, D.; Lin, S.; Chang, C. J.; Yaghi, O. M.; Yang, P. D. Metal–organic frameworks for electrocatalytic reduction of carbon dioxide. *J. Am. Chem. Soc*. **2015**, *137*, 14129–14135.

[99] *Toray Carbon Fiber Paper "TGP-H"* [Online]. https://www.fuelcellsetc.com/store/DS/Toray-Paper-TGP-H-Datasheet.pdf (accessed Feb 11, 2019).

[100] Pander III, J. E.; Fogg, A.; Bocarsly, A. B. Utilization of electropolymerized films of cobalt porphyrin for the reduction of carbon dioxide in aqueous media. *ChemCatChem* **2016**, *8*, 3536–3545.

[101] Reuillard, B.; Ly, K. H.; Rosser, T. E.; Kuehnel, M. F.; Zebger, I.; Reisner, E. Tuning product selectivity for aqueous CO_2 reduction with a Mn(bipyridine)-pyrene catalyst immobilized on a carbon nanotube electrode. *J. Am. Chem. Soc.* **2017**, *139*, 14425–14435.

[102] Rosser, T. E.; Windle, C. D.; Reisner, E. Electrocatalytic and solar-driven CO_2 reduction to CO with a molecular manganese catalyst immobilized on mesoporous TiO_2. *Angew. Chem., Int. Ed.* **2016**, *55*, 7388–7392.

[103] Bagger, A.; Ju, W.; Varela, A. S.; Strasser, P.; Rossmeisl, J. Single site porphyrine-like structures advantages over metals for selective electrochemical CO_2 reduction. *Catal. Today* **2017**, *288*, 74–78.

[104] Zhang, Y. J.; Sethuraman, V.; Michalsky, R.; Peterson, A. A. Competition between CO_2 reduction and H_2 evolution on transition-metal electrocatalysts. *ACS Catal*. **2014**, *4*, 3742–3748.

[105] Wellendorff, J.; Lundgaard, K. T.; Møgelhøj, A.; Petzold, V.; Landis, D. D.; Nørskov, J. K.; Bligaard, T.; Jacobsen, K. W. Density functionals for surface science: Exchange-correlation model development with Bayesian error estimation. *Phys. Rev. B* **2012**, *85*, 235149.

[106] Shen, J.; Kolb, M. J.; Göttle, A. J.; Koper, M. T. M. DFT study on the mechanism of the electrochemical reduction of CO_2 catalyzed by cobalt porphyrins. *J. Phys. Chem. C* **2016**, *120*, 15714–15721.

[107] Nielsen, I. M. B.; Leung, K. Cobalt–porphyrin catalyzed electrochemical reduction of carbon dioxide in water. 1. A density functional study of intermediates. *J. Phys. Chem. A* **2010**, *114*, 10166–10173.

[108] Leung, K.; Nielsen, I. M. B.; Sai, N.; Medforth, C.; Shelnutt, J. A. Cobalt−porphyrin catalyzed electrochemical reduction of carbon dioxide in water. 2. Mechanism from first principles. *J. Phys. Chem. A* **2010**, *114*, 10174–10184.

[109] Göttle, A. J.; Koper, M. T. M. Proton-coupled electron transfer in the electrocatalysis of CO_2 reduction: Prediction of sequential vs. concerted pathways using DFT. *Chem. Sci.* **2017**, *8*, 458–465.

[110] Shen, J.; Kortlever, R.; Kas, R.; Birdja, Y. Y.; Diaz-Morales, O.; Kwon, Y.; Ledezma-Yanez, I.; Schouten, K. J. P.; Mul, G.; Koper, M. T. M. Electrocatalytic reduction of carbon dioxide to carbon monoxide and methane at an immobilized cobalt protoporphyrin. *Nat. Commun.* **2015**, *6*, 8177.

[111] Yao, C. L.; Li, J. C.; Gao, W.; Jiang, Q. Cobalt-porphine catalyzed CO_2 electro-reduction: A novel protonation mechanism. *Phys. Chem. Chem. Phys.* **2017**, *19*, 15067–15072.

[112] Jensen, K. P.; Ryde, U. Theoretical prediction of the Co–C bond strength in cobalamins. *J. Phys. Chem. A* **2003**, *107*, 7539–7545.

[113] Kusuda, K.; Ishihara, R.; Yamaguchi, H.; Izumi, I. Electrochemical investigation of thin films of cobalt phthalocyanine and cobalt-4,4′,4″,4‴-tetracarboxyphthalocyanine and the reduction of carbon monoxide, formic acid and formaldehyde mediated by the Co(I) complexes. *Electrochim. Acta* **1986**, *31*, 657–663.

[114] Szkaradek, K.; Buzar, K.; Pidko, E. A.; Szyja, B. M. Supported Ru metalloporphyrins for electrocatalytic CO_2 conversion. *ChemCatChem* **2018**, *10*, 1814–1820.

[115] Resasco, J.; Chen, L. D.; Clark, E.; Tsai, C.; Hahn, C.; Jaramillo, T. F.; Chan, K.; Bell, A. T. Promoter effects of alkali metal cations on the electrochemical reduction of carbon dioxide. *J. Am. Chem. Soc.* **2017**, *139*, 11277–11287.

[116] Liu, M.; Pang, Y. J.; Zhang, B.; De Luna, P.; Voznyy, O.; Xu, J. X.; Zheng, X. L.; Dinh, C. T.; Fan, F. J; Cao, C. H. et al. Enhanced electrocatalytic CO_2 reduction via field-induced reagent concentration. *Nature* **2016**, *537*, 382–386.

[117] Thorson, M. R.; Siil, K. I.; Kenis, P. J. A. Effect of cations on the electrochemical conversion of CO_2 to CO. *J. Electrochem. Soc.* **2013**, *160*, F69–F74.

[118] Murata, A.; Hori, Y. Product selectivity affected by cationic species in electrochemical reduction of CO_2 and CO at a Cu electrode. *Bull. Chem. Soc. Jpn.* **1991**, *64*, 123–127.

[119] Kyriacou, G. Z.; Anagnostopoulos, A. K. Influence CO_2 partial pressure and the supporting electrolyte cation on the product distribution in CO_2 electroreduction. *J. Appl. Electrochem*. **1993**, *23*, 483–486.

[120] Schizodimou, A.; Kyriacou, G. Acceleration of the reduction of carbon dioxide in the presence of multivalent cations. *Electrochim. Acta* **2012**, *78*, 171–176.

[121] Kaneco, S.; Iiba, K.; Katsumata, H.; Suzuki, T.; Ohta, K. Effect of sodium cation on the electrochemical reduction of CO_2 at a copper electrode in methanol. *J. Solid State Electrochem.* **2007**, *11*, 490–495.

[122] Pérez-Gallent, E.; Marcandalli, G.; Figueiredo, M. C.; Calle-Vallejo, F.; Koper, M. T. M. Structure- and potential-dependent cation effects on CO reduction at copper single-crystal electrodes. *J. Am. Chem. Soc.* **2017**, *139*, 16412–16419.

[123] Ikemiya, N.; Natsui, K.; Nakata, K.; Einaga, Y. Effect of alkali-metal cations on the electrochemical reduction of carbon dioxide to formic acid using boron-doped diamond electrodes. *RSC Adv.* **2017**, *7*, 22510–22514.

[124] Chen, L. D.; Urushihara, M.; Chan, K.; Norskov, J. K. Electric field effects in electrochemical CO_2 reduction. *ACS Catal.* **2016**, *6*, 7133–7139.

[125] Zhao, C. X.; Bu, Y. F.; Gao, W.; Jiang, Q. CO_2 reduction mechanism on the Pb(111) surface: Effect of solvent and cations. *J. Phys. Chem. C* **2017**, *121*, 19767–19773.

[126] Hammouche, M.; Lexa, D.; Momenteau, M.; Saveant, J. M. Chemical catalysis of electrochemical reactions. Homogeneous catalysis of the electrochemical reduction of carbon dioxide by iron("0") porphyrins. Role of the addition of magnesium cations. *J. Am. Chem. Soc.* **1991**, *113*, 8455–8466.

[127] Shen, J.; Lan, D. H.; Yang, T. J. Influence of supporting electrolyte on the electrocatalysis of CO_2 reduction by cobalt protoporphyrin. *Int. J. Electrochem. Sci.* **2018**, *13*, 9847–9857.

[128] Miyamoto, K.; Asahi, R. Cation impact on cobalt-porphyrin catalyzed electrochemical reduction of CO_2 [Online]. 2018. https://arxiv.org/pdf/1806.10285.pdf (accessed Feb 18, 2019).

[129] Azcarate, I.; Costentin, C.; Robert, M.; Savéant, J. M. Through-space charge interaction substituent effects in molecular catalysis leading to the design of the most efficient catalyst of CO_2-to-CO electrochemical conversion. *J. Am. Chem. Soc.* **2016**, *138*, 16639–16644.

[130] DeLuca, E. E.; Xu, Z.; Lam, J.; Wolf, M. O. Improved electrocatalytic CO_2 reduction with palladium bis(NHC) pincer complexes bearing cationic side chains. *Organometallics* **2019**, *38*, 1330–1343.

[131] Zahran, Z. N.; Mohamed, E. A.; Naruta, Y. Bio-inspired cofacial Fe porphyrin dimers for efficient electrocatalytic CO_2 to CO conversion: Overpotential tuning by substituents at the porphyrin rings. *Sci. Rep.* **2016**, *6*, 24533.

[132] Ochoa, G.; Geraldo, D.; Linares, C.; Nyokong, T.; Bedioui, F.; Zagal, J. H. Tuning the formal potential of metallomacrocyclics for maximum catalytic activity for the oxidation of thiols and hydrazine. *ECS Trans*. **2009**, *19*, 97–112.

[133] Bedioui, F.; Griveau, S.; Nyokong, T.; John Appleby, A.; Caro, C. A.; Gulppi, M.; Ochoa, G.; Zagal, J. H. Tuning the redox properties of

metalloporphyrin- and metallophthalocyanine-based molecular electrodes for the highest electrocatalytic activity in the oxidation of thiols. *Phys. Chem. Chem. Phys*. **2007**, *9*, 3383–3396.

[134] Villagra, E.; Bedioui, F.; Nyokong, T.; Canales, J. C.; Sancy, M.; Páez, M. A.; Costamagna, J.; Zagal, J. H. Tuning the redox properties of Co-N4 macrocyclic complexes for the catalytic electrooxidation of glucose. *Electrochim. Acta* **2008**, *53*, 4883–4888.

[135] Geraldo, D.; Linares, C.; Chen, Y. Y.; Ureta-Zañartu, S.; Zagal, J. H. Volcano correlations between formal potential and Hammett parameters of substituted cobalt phthalocyanines and their activity for hydrazine electro-oxidation. *Electrochem. Commun*. **2002**, *4*, 182–187.

[136] Aguirre, M. J.; Isaacs, M.; Armijo, F.; Basáez, L.; Zagal, J. H. Effect of the substituents on the ligand of iron phthalocyanines adsorbed on graphite electrodes on their activity for the electrooxidation of 2-mercaptoethanol. *Electroanalysis* **2002**, *14*, 356–362.

[137] Zhang, X.; Wu, Z. S.; Zhang, X.; Li, L. W.; Li, Y. Y.; Xu, H. M.; Li, X. X.; Yu, X. L.; Zhang, Z. S.; Liang, Y. Y. et al. Highly selective and active CO_2 reduction electrocatalysts based on cobalt phthalocyanine/carbon nanotube hybrid structures. *Nat. Commun.* **2017**, *8*, 14675.

[138] Hansch, C.; Leo, A.; Taft, R. W. A survey of Hammett substituent constants and resonance and field parameters. *Chem. Rev.* **1991**, *91*, 165–195.

[139] Magdesieva, T. V.; Yamamoto, T.; Tryk, D. A.; Fujishima, A. Electrochemical reduction of CO_2 with transition metal phthalocyanine and porphyrin complexes supported on activated carbon fibers. *J. Electrochem. Soc.* **2002**, *149*, D89–D95.

[140] Tornow, C. E.; Thorson, M. R.; Ma, S. C.; Gewirth, A. A.; Kenis, P. J. A. Nitrogen-based catalysts for the electrochemical reduction of CO_2 to CO. *J. Am. Chem. Soc*. **2012**, *134*, 19520–19523.

[141] Petraki, F.; Peisert, H.; Biswas, I.; Aygül, U.; Latteyer, F.; Vollmer, A.; Chassé, T. Interaction between cobalt phthalocyanine and gold studied by X-ray absorption and resonant photoemission spectroscopy. *J. Phys. Chem. Lett.* **2010**, *1*, 3380–3384.

[142] Petraki, F.; Peisert, H.; Biswas, I.; Chassé, T. Electronic structure of Co-phthalocyanine on gold investigated by photoexcited electron spectroscopies: Indication of Co ion–metal interaction. *J. Phys. Chem. C* **2010**, *114*, 17638–17643.

[143] Petraki, F.; Peisert, H.; Aygül, U.; Latteyer, F.; Uihlein, J.; Vollmer, A.; Chassé, T. Electronic structure of FePc and interface properties on Ag(111) and Au(100). *J. Phys. Chem. C* **2012**, *116*, 11110–11116.

[144] Uihlein, J.; Peisert, H.; Glaser, M.; Polek, M.; Adler, H.; Petraki, F.; Ovsyannikov, R.; Bauer, M.; Chassé, T. Communication: Influence of graphene interlayers on the interaction between cobalt phthalocyanine and Ni(111). *J. Chem. Phys.* **2013**, *138*, 081101.

[145] Duncan, D. A.; Deimel, P. S.; Wiengarten, A.; Han, R. Y.; Acres, R. G.; Auwärter, W.; Feulner, P.; Papageorgiou, A. C.; Allegretti, F.; Barth, J. V. Immobilised molecular catalysts and the role of the supporting metal substrate. *Chem. Commun*. **2015**, *51*, 9483–9486.

[146] Walsh, J. J.; Smith, C. L.; Neri, G.; Whitehead, G. F. S.; Robertson, C. M.; Cowan, A. J. Improving the efficiency of electrochemical CO_2 reduction using immobilized manganese complexes. *Faraday Discuss*. **2015**, *183*, 147–160.

[147] Birdja, Y. Y.; Vos, R. E.; Wezendonk, T. A.; Jiang, L.; Kapteijn, F.; Koper, M. T. M. Effects of substrate and polymer encapsulation on CO_2 electroreduction by immobilized indium(III) protoporphyrin. *ACS Catal.* **2018**, *8*, 4420–4428.

[148] Zhao, H. Z.; Chang, Y. Y.; Liu, C. Electrodes modified with iron porphyrin and carbon nanotubes: application to CO_2 reduction and mechanism of synergistic electrocatalysis. *J. Solid State Electrochem*. **2013**, *17*, 1657–1664.

[149] Aoi, S.; Mase, K.; Ohkubo, K.; Fukuzumi, S. Selective electrochemical reduction of CO_2 to CO with a cobalt chlorin complex adsorbed on multi-walled carbon nanotubes in water. *Chem. Commun.* **2015**, *51*, 10226–10228.

[150] Choi, J.; Wagner, P.; Jalili, R.; Kim, J.; MacFarlane, D. R.; Wallace, G. G.; Officer, D. L. A porphyrin/graphene framework: A highly efficient and robust electrocatalyst for carbon dioxide reduction. *Adv. Energy Mater.* **2018**, *8*, 1801280.

[151] Yamanaka, I.; Tabata, K.; Mino, W.; Furusawa, T. Electroreduction of carbon dioxide to carbon monoxide by Co-pthalocyanine electrocatalyst under ambient conditions. *ISIJ Int.* **2015**, *55*, 399–403.

[152] He, L.; Sun, X. F.; Zhang, H.; Shao, F. W. G-quadruplex nanowires to direct the efficiency and selectivity of electrocatalytic CO_2 reduction. Angew. *Chem., Int. Ed.* **2018**, *57*, 12453–12457.

[153] Chen, C. J.; Sun, X. F.; Yang, D. X.; Lu, L.; Wu, H. H.; Zheng, L. R.; An, P. F.; Zhang, J.; Han, B. X. Enhanced CO_2 electroreduction via interaction of dangling S bonds and Co sites in cobalt phthalocyanine/$ZnIn_2S_4$ hybrids. *Chem. Sci.* **2019**, *10*, 1659–1663.

[154] Zhao, F.; Zhang, J.; Abe, T.; Wöhrle, D.; Kaneko, M. Electrocatalytic proton reduction by phthalocyanine cobalt derivatives incorporated in poly(4-vinylpyridine-co-styrene) film. *J. Mol. Catal. A Chem.* **1999**, *145*, 245–256.

[155] Kramer, W. W.; McCrory, C. C. L. Polymer coordination promotes selective CO_2 reduction by cobalt phthalocyanine. *Chem. Sci.* **2016**, *7*, 2506–2515.

[156] Buttry, D. A.; Anson, F. C. New strategies for electrocatalysis at polymer-coated electrodes. Reduction of dioxygen by cobalt porphyrins immobilized in Nafion coatings on graphite electrodes. *J. Am. Chem. Soc.* **1984**, *106*, 59–64.

[157] Jarzębińska, A.; Rowiński, P.; Zawisza, I.; Bilewicz, R.; Siegfried, L.; Kaden, T. Modified electrode surfaces for catalytic reduction of carbon dioxide. *Anal. Chim. Acta* **1999**, *396*, 1–12.

[158] Ramírez, G.; Ferraudi, G.; Chen, Y. Y.; Trollund, E.; Villagra, D. Enhanced photoelectrochemical catalysis of CO_2 reduction mediated by a supramolecular electrode of packed CoII(tetrabenzoporphyrin). *Inorganica Chim. Acta* **2009**, *362*, 5–10.

[159] Ramírez, G.; Lucero, M.; Riquelme, A.; Villagrán, M.; Costamagna, J.; Trollund, E.; Aguirre, M. J. A supramolecular cobalt-porphyrin-modified electrode, toward the electroreduction of CO_2. *J. Coord. Chem.* **2004**, *57*, 249–255.

[160] Elgrishi, N.; Griveau, S.; Chambers, M. B.; Bedioui, F.; Fontecave, M. Versatile functionalization of carbon electrodes with a polypyridine ligand: Metallation and electrocatalytic H^+ and CO_2 reduction. *Chem. Commun.* **2015**, *51*, 2995–2998.

[161] Maurin, A.; Robert, M. Catalytic CO_2-to-CO conversion in water by covalently functionalized carbon nanotubes with a molecular iron catalyst. *Chem. Commun.* **2016**, *52*, 12084–12087.

[162] Yao, S. A.; Ruther, R. E.; Zhang, L. H.; Franking, R. A.; Hamers, R. J.; Berry, J. F. Covalent attachment of catalyst molecules to conductive diamond: CO_2 reduction using "smart" electrodes. *J. Am. Chem. Soc.* **2012**, *134*, 15632–15635.

[163] Thorogood, C. A.; Wildgoose, G. G.; Crossley, A.; Jacobs, R. M. J.; Jones, J. H.; Compton, R. G. Differentiating between ortho- and para-quinone surface groups on graphite, glassy carbon, and carbon nanotubes using organic and inorganic voltammetric and X-ray photoelectron spectroscopy labels. *Chem. Mater.* **2007**, *19*, 4964–4974.

[164] Wang, Y.; Marquard, S. L.; Wang, D. G.; Dares, C.; Meyer, T. J. Single-site, heterogeneous electrocatalytic reduction of CO_2 in water as the solvent. *ACS Energy Lett.* **2017**, *2*, 1395–1399.

[165] Mohamed, E. A.; Zahran, Z. N.; Naruta, Y. Efficient heterogeneous CO_2 to CO conversion with a phosphonic acid fabricated cofacial iron porphyrin dimer. *Chem. Mater.* **2017**, *29*, 7140–7150.

[166] Maurin, A.; Robert, M. Noncovalent immobilization of a molecular iron-based electrocatalyst on carbon electrodes for selective, efficient CO_2-to-CO conversion in water. *J. Am. Chem. Soc.* **2016**, *138*, 2492–2495.

[167] Kang, P.; Zhang, S.; Meyer, T. J.; Brookhart, M. Rapid selective electrocatalytic reduction of carbon dioxide to formate by an iridium pincer catalyst immobilized on carbon nanotube electrodes. *Angew. Chem., Int. Ed.* **2014**, *53*, 8709–8713.

[168] Blakemore, J. D.; Gupta, A.; Warren, J. J.; Brunschwig, B. S.; Gray, H. B. Noncovalent immobilization of electrocatalysts on carbon electrodes for fuel production. *J. Am. Chem. Soc.* **2013**, *135*, 18288–18291.

[169] Fukuzumi, S.; Lee, Y. M.; Nam, W. Immobilization of molecular catalysts for enhanced redox catalysis. *ChemCatChem* **2018**, *10*, 1686–1702.

[170] Bullock, R. M.; Das, A. K.; Appel, A. M. Surface immobilization of molecular electrocatalysts for energy conversion. *Chem.—Eur. J.* **2017**, *23*, 7626–7641.

[171] Louis, M. E.; Fenton, T. G.; Rondeau, J.; Jin, T.; Li, G. H. Solar CO_2 reduction using surface-immobilized molecular catalysts. *Comments Inorg. Chem.* **2016**, *36*, 38–60.

[172] Cai, X.; Liu, H. Y.; Wei, X.; Yin, Z. L.; Chu, J.; Tang, M. L.; Zhuang, L.; Deng, H. X. Molecularly defined interface created by porous polymeric networks on gold surface for concerted and selective CO_2 reduction. *ACS Sustainable Chem. Eng.* **2018**, *6*, 17277–17283.

[173] Cave, E. R.; Montoya, J. H.; Kuhl, K. P.; Abram, D. N.; Hatsukade, T.;

Shi, C.; Hahn, C.; Nørskov, J. K.; Jaramillo, T. F. Electrochemical CO_2 reduction on Au surfaces: Mechanistic aspects regarding the formation of major and minor products. *Phys. Chem. Chem. Phys.* **2017**, *19*, 15856–15863.

[174] Hori, Y.; Murata, A.; Kikuchi, K.; Suzuki, S. Electrochemical reduction of carbon dioxides to carbon monoxide at a gold electrode in aqueous potassium hydrogen carbonate. *J. Chem. Soc. Chem. Commun.* **1987**, 728–729.

[175] Cao, Z.; Zacate, S. B.; Sun, X. D.; Liu, J. J.; Hale, E. M.; Carson, W. P.; Tyndall, S. B.; Xu, J.; Liu, X. W.; Liu, X. C. et al. Tuning gold nanoparticles with chelating ligands for highly efficient electrocatalytic CO_2 reduction. *Angew. Chem., Int. Ed.* **2018**, *57*, 12675–12679.

[176] Gong, M.; Cao, Z.; Liu, W.; Nichols, E. M.; Smith, P. T.; Derrick, J. S.; Liu, Y. S.; Liu, J. J.; Wen, X. D.; Chang, C. J. Supramolecular porphyrin cages assembled at molecular–materials interfaces for electrocatalytic CO reduction. *ACS Cent. Sci.* **2017**, *3*, 1032–1040.

[177] Tatin, A.; Comminges, C.; Kokoh, B.; Costentin, C.; Robert, M.; Savéant, J. M. Efficient electrolyzer for CO_2 splitting in neutral water using earth-abundant materials. *Proc. Natl. Acad. Sci. USA* **2016**, *113*, 5526– 5529.

[178] Marianov, A. N.; Jiang, Y. J. Covalent ligation of Co molecular catalyst to carbon cloth for efficient electroreduction of CO_2 in water. *Appl. Catal. B Environ.* **2019**, *244*, 881–888.

[179] Kapusta, S.; Hackerman, N. The electroreduction of carbon dioxide and formic acid on tin and indium electrodes. *J. Electrochem. Soc.* **1983**, *130*, 607–613.

[180] Dominguez-Ramos, A.; Singh, B.; Zhang, X.; Hertwich, E. G.; Irabien, A. Global warming footprint of the electrochemical reduction of carbon dioxide to formate. *J. Clean. Prod.* **2015**, *104*, 148–155.

[181] Jiang, J. B.; Matula, A. J.; Swierk, J. R.; Romano, N.; Wu, Y. S.; Batista, V. S.; Crabtree, R. H.; Lindsey, J. S.; Wang, H. L.; Brudvig, G. W. Unusual stability of a bacteriochlorin electrocatalyst under reductive conditions. A case study on CO_2 conversion to CO. *ACS Catal.* **2018**, *8*, 10131–10136.

[182] Bruhn, T.; Brückner, C. Origin of the regioselective reduction of chlorins. *J. Org. Chem.* **2015**, *80*, 4861–4868.

[183] Jiang, J. B.; Materna, K. L.; Hedström, S.; Yang, K. R.; Crabtree, R. H.; Batista, V. S.; Brudvig, G. W. Antimony complexes for electrocatalysis: Activity of a main-group element in proton reduction. *Angew. Chem., Int. Ed.* **2017**, *56*, 9111–9115.

[184] Verma, S.; Kim, B.; Jhong, H. R. M.; Ma, S. C.; Kenis, P. J. A. A gross-margin model for defining technoeconomic benchmarks in the electroreduction of CO_2. *ChemSusChem* **2016**, *9*, 1972–1979.

[185] Mahmood, A.; Guo, W. H.; Tabassum, H.; Zou, R. Q. Metal-organic framework-based nanomaterials for electrocatalysis. *Adv. Energy Mater.* **2016**, *6*, 1600423.

[186] Hod, I.; Sampson, M. D.; Deria, P.; Kubiak, C. P.; Farha, O. K.; Hupp, J. T. Fe-porphyrin-based metal-organic framework films as high-surface concentration, heterogeneous catalysts for electrochemical reduction of CO_2. *ACS Catal.* **2015**, *5*, 6302–6309.

[187] Wu, J. X.; Hou, S. Z.; Zhang, X. D.; Xu, M.; Yang, H. F.; Cao, P. S.; Gu, Z. Y. Cathodized copper porphyrin metal–organic framework nanosheets for selective formate and acetate production from CO_2 electroreduction. *Chem. Sci.* **2019**, *10*, 2199–2205.

[188] Senthil Kumar, R.; Senthil Kumar, S.; Anbu Kulandainathan, M. Highly selective electrochemical reduction of carbon dioxide using Cu based metal organic framework as an electrocatalyst. *Electrochem. Commun.* **2012**, *25*, 70–73.

[189] Tu, W. G.; Xu, Y.; Yin, S. M.; Xu, R. Rational design of catalytic centers in crystalline frameworks. *Adv. Mater.* **2018**, *30*, 1707582.

[190] Ahrenholtz, S. R.; Epley, C. C.; Morris, A. J. Solvothermal preparation of an electrocatalytic metalloporphyrin MOF thin film and its redox hopping charge-transfer mechanism. *J. Am. Chem. Soc.* **2014**, *136*, 2464–2472.

[191] Hod, I.; Bury, W.; Gardner, D. M.; Deria, P.; Roznyatovskiy, V.; Wasielewski, M. R.; Farha, O. K.; Hupp, J. T. Bias-switchable permselectivity and redox catalytic activity of a ferrocene-functionalized, thin-film metal–organic framework compound. *J. Phys. Chem. Lett.* **2015**, *6*, 586–591.

[192] Huang, N.; Wang, P.; Jiang, D. L. Covalent organic frameworks: A materials platform for structural and functional designs. *Nat. Rev. Mater.* **2016**, *1*, 16068.

[193] Feng, X.; Ding, X. S.; Jiang, D. L. Covalent organic frameworks. *Chem. Soc. Rev.* **2012**, *41*, 6010–6022.

[194] Diercks, C. S.; Lin, S.; Kornienko, N.; Kapustin, E. A.; Nichols, E. M.; Zhu, C. H.; Zhao, Y. B.; Chang, C. J.; Yaghi, O. M. Reticular electronic tuning of porphyrin active sites in covalent organic frameworks for electrocatalytic carbon dioxide reduction. *J. Am. Chem. Soc.* **2018**, *140*, 1116–1122.

[195] Johnson, E. M.; Haiges, R.; Marinescu, S. C. Covalent-organic frameworks composed of rhenium bipyridine and metal porphyrins: Designing heterobimetallic frameworks with two distinct metal sites. *ACS Appl. Mater. Interfaces* **2018**, *10*, 37919–37927.

[196] Zagal, J. H. Metallophthalocyanines as catalysts in electrochemical reactions. *Coord. Chem. Rev.* **1992**, *119*, 89–136.

[197] Popov, D. A.; Luna, J. M.; Orchanian, N. M.; Haiges, R.; Downes, C. A.; Marinescu, S. C. A 2,2'-bipyridine-containing covalent organic framework bearing rhenium(I) tricarbonyl moieties for CO_2 reduction. *Dalton Trans.* **2018**, *47*, 17450–17460.

[198] Liu, H. Y.; Chu, J.; Yin, Z. L.; Cai, X.; Zhuang, L.; Deng, H. X. Covalent organic frameworks linked by amine bonding for concerted electrochemical reduction of CO_2. *Chem* **2018**, *4*, 1696–1709.

[199] Chen, X.; Addicoat, M.; Irle, S.; Nagai, A.; Jiang, D. L. Control of crystallinity and porosity of covalent organic frameworks by managing interlayer interactions based on self-complementary π-electronic force. *J. Am. Chem. Soc.* **2013**, *135*, 546–549.

[200] Peng, P.; Zhou, Z. H.; Guo, J. N.; Xiang, Z. H. Well-defined 2D covalent organic polymers for energy electrocatalysis. *ACS Energy Lett.* **2017**, *2*, 1308–1314.

[201] Li, H. W.; Guarr, T. F. Formation of electronically conductive thin films of metal phthalocyanines via electropolymerization. *J. Chem. Soc. Chem. Commun.* **1989**, 832–834.

[202] Bettelheim, A.; White, B. A.; Murray, R. W. Electrocatalysis of dioxygen reduction in aqueous acid and base by multimolecular layer films of electropolymerized cobalt tetra(o-aminophenyl)porphyrin. *J. Electroanal. Chem.* **1987**, *217*, 271–286.

[203] Magdesieva, T. V.; Zhukov, I. V.; Kravchuk, D. N.; Semenikhin, O. A.; Tomilova, L. G.; Butin, K. P. Electrocatalytic CO_2 reduction in methanol catalyzed by mono-, di-, and electropolymerized phthalocyanine complexes. *Russ. Chem. Bull.* **2002**, *51*, 805–812.

[204] Quezada, D.; Honores, J.; Aguirre M. J.; Isaacs, M. Electrocatalytic reduction of carbon dioxide on conducting glass electrode modified with polymeric porphyrin films containing transition metals in ionic liquid medium. *J. Coord. Chem.* **2014**, *67*, 4090–4100.

[205] Isaacs, M.; Armijo, F.; Ramírez, G.; Trollund, E.; Biaggio, S. R.; Costamagna, J.; Aguirre, M. J. Electrochemical reduction of CO_2 mediated by poly-M-aminophthalocyanines (M = Co, Ni, Fe): Poly-Co-tetraaminophthalocyanine, a selective catalyst. *J. Mol. Catal. A Chem.* **2005**, *229*, 249–257.

[206] Boeva, Z. A.; Sergeyev, V. G. Polyaniline: Synthesis, properties, and application. *Polym. Sci. Ser. C* **2014**, *56*, 144–153.

[207] Wu, H. H.; Zeng, M.; Zhu, X.; Tian, C. C.; Mei, B. B.; Song, Y.; Du, X. L.; Jiang, Z.; He, L.; Xia, C. G. et al. Defect engineering in polymeric cobalt phthalocyanine networks for enhanced electrochemical CO_2 reduction. *ChemElectroChem* **2018**, *5*, 2717–2721.

[208] Smith, P. T.; Benke, B. P.; Cao, Z.; Kim, Y.; Nichols, E. M.; Kim, K.; Chang, C. J. Iron porphyrins embedded into a supramolecular porous organic cage for electrochemical CO_2 reduction in water. *Angew. Chem., Int. Ed.* **2018**, *57*, 9684–9688.

[209] Choi, J.; Kim, J.; Wagner, P.; Gambhir, S.; Jalili, R.; Byun, S.; Sayyar, S.; Lee, Y. M.; MacFarlane, D. R.; Wallace, G. G. et al. Energy efficient electrochemical reduction of CO_2 to CO using a three-dimensional porphyrin/graphene hydrogel. *Energy Environ. Sci.* **2019**, *12*, 747–755.

[210] Portenkirchner, E.; Gasiorowski, J.; Oppelt, K.; Schlager, S.; Schwarzinger, C.; Neugebauer, H.; Knör, G.; Sariciftci, N. S. Electrocatalytic reduction of carbon dioxide to carbon monoxide by a polymerized film of an alkynyl-substituted rhenium(I) complex. *ChemCatChem* **2013**, *5*, 1790–1796.

[211] Collomb-Dunand-Sauthier, M. N.; Deronzier, A.; Ziessel, R. Electrocatalytic reduction of carbon dioxide with mono(bipyridine)carbonylruthenium complexes in solution or as polymeric thin films. *Inorg. Chem.* **1994**, *33*, 2961–2967.

[212] O'Toole, T. R.; Margerum, L. D.; Westmoreland, T. D.; Vining, W. J.; Murray, R. W.; Meyer, T. J. Electrocatalytic reduction of CO_2 at a chemically modified electrode. *J. Chem. Soc. Chem. Commun.* **1985**, 1416–1417.

[213] Cabrera, C. R.; Abruña, H. D. Electrocatalysis of CO_2 reduction at surface modified metallic and semiconducting electrodes. *J. Electroanal. Chem. Interfacial Electrochem.* **1986**, *209*, 101–107.

[214] Mackintosh, H. J.; Budd, P. M.; McKeown, N. B. Catalysis by microporous phthalocyanine and porphyrin network polymers. *J. Mater. Chem.* **2008**, *18*, 573–578.
[215] McCrory, C. C. L.; Jung, S.; Ferrer, I. M.; Chatman, S. M.; Peters, J. C.; Jaramillo, T. F. Benchmarking hydrogen evolving reaction and oxygen evolving reaction electrocatalysts for solar water splitting devices. *J. Am. Chem. Soc.* **2015**, *137*, 4347–4357.
[216] Artero, V.; Saveant, J. M. Toward the rational benchmarking of homogeneous H_2-evolving catalysts. *Energy Environ. Sci.* **2014**, *7*, 3808–3814.
[217] Costentin, C.; Drouet, S.; Robert, M.; Savéant, J. M. Turnover numbers, turnover frequencies, and overpotential in molecular catalysis of electrochemical reactions. Cyclic voltammetry and preparative-scale electrolysis. *J. Am. Chem. Soc.* **2012**, *134*, 11235–11242.
[218] Gupta, N.; Gattrell, M.; MacDougall, B. Calculation for the cathode surface concentrations in the electrochemical reduction of CO_2 in $KHCO_3$ solutions. *J. Appl. Electrochem*. **2006**, *36*, 161–172.
[219] Weng, L. C.; Bell, A. T.; Weber, A. Z. Modeling gas-diffusion electrodes for CO_2 reduction. Phys. Chem. Chem. Phys. **2018**, 20, 16973–16984.
[220] Burdyny, T.; Graham, P. J.; Pang, Y. J.; Dinh, C. T.; Liu, M.; Sargent, E. H.; Sinton, D. Nanomorphology-enhanced gas-evolution intensifies CO_2 reduction electrochemistry. *ACS Sustainable Chem. Eng*. **2017**, *5*, 4031–4040.
[221] Pidko, E. A. Toward the balance between the reductionist and systems approaches in computational catalysis: Model versus method accuracy for the description of catalytic systems. *ACS Catal*. **2017**, *7*, 4230–4234.
[222] Singh, M. R.; Goodpaster, J. D.; Weber, A. Z.; Head-Gordon, M.; Bell, A. T. Mechanistic insights into electrochemical reduction of CO_2 over Ag using density functional theory and transport models. *Proc. Natl. Acad. Sci. USA* **2017**, *114*, E8812–E8821.
[223] Shi, C.; Chan, K.; Yoo, J. S.; Norskov, J. K. Barriers of electrochemical CO_2 reduction on transition metals. *Org. Process Res. Dev.* **2016**, *20*, 1424–1430.
[224] Kastlunger, G.; Lindgren, P.; Peterson, A. A. Controlled-potential simulation of elementary electrochemical reactions: Proton discharge on metal surfaces. *J. Phys. Chem. C* **2018**, *122*, 12771–12781.
[225] Lu, X.; Wu, Y. S.; Yuan, X. L.; Huang, L.; Wu, Z. S.; Xuan, J.; Wang, Y. F.; Wang, H. L. High-performance electrochemical CO_2 reduction cells based on non-noble metal catalysts. *ACS Energy Lett.* **2018**, *3*, 2527–2532.
[226] Haas, T.; Krause, R.; Weber, R.; Demler, M.; Schmid, G. Technical photosynthesis involving CO_2 electrolysis and fermentation. *Nat. Catal.* **2018**, *1*, 32–39.
[227] Verma, S.; Lu, X.; Ma, S. C.; Masel, R. I.; Kenis, P. J. A. The effect of electrolyte composition on the electroreduction of CO_2 to CO on Ag based gas diffusion electrodes. *Phys. Chem. Chem. Phys.* **2016**, *18*, 7075–7084.
[228] Dinh, C. T.; Garcia de Arquer, F. P.; Sinton, D.; Sargent, E. H. High rate, selective, and stable electroreduction of CO_2 to CO in basic and neutral media. *ACS Energy Lett.* **2018**, *3*, 2835–2840.
[229] Bushuyev, O. S.; De Luna, P.; Dinh, C. T.; Tao, L.; Saur, G.; van de Lagemaat, J.; Kelley, S. O.; Sargent, E. H. What should we make with CO_2 and how can we make it? *Joule* **2018**, *2*, 825–832.
[230] House, K. Z.; Baclig, A. C.; Ranjan, M.; van Nierop, E. A.; Wilcox, J.; Herzog, H. J. Economic and energetic analysis of capturing CO_2 from ambient air. *Proc. Natl. Acad. Sci. USA* **2011**, *108*, 20428–20433.
[231] Keith, D. W.; Holmes, G.; St. Angelo, D.; Heidel, K. A process for capturing CO_2 from the atmosphere. *Joule* **2018**, *2*, 1573–1594.
[232] Wakerley, D. W.; Reisner, E. Oxygen-tolerant proton reduction catalysis: Much O_2 about nothing? *Energy Environ. Sci.* **2015**, *8*, 2283–2295.
[233] Williams, K.; Corbin, N.; Zeng, J.; Lazouski, N.; Yang, D. T.; Manthiram, K. Protecting effect of mass transport during electrochemical reduction of oxygenated carbon dioxide feedstocks. *Sustainable Energy Fuels*, in press, DOI: 10.1039/C9SE00024K.
[234] Kumagai, H.; Nishikawa, T.; Koizumi, H.; Yatsu, T.; Sahara, G.; Yamazaki, Y.; Tamaki, Y.; Ishitani, O. Electrocatalytic reduction of low concentration CO_2. *Chem. Sci.* **2019**, *10*, 1597–1606.